GLOBAL RIVER DELTA MORPHOLOGY RESPONSE TO FLUVIAL SEDIMENT CHANGE AND ANTHROPOGENIC STRESS

by

DINUKE S. NANAYAKKARA MUNASINGHE

SAGY COHEN, COMMITTEE CHAIR

DAVID J. KEELLINGS
VENKATARAMAN LAKSHMI
HONGXING LIU
JAAP NIENHUIS

A DISSERTATION

Submitted in partial fulfillment of the requirements
for the degree of Doctor of Philosophy
in the Department of Geography
in the Graduate School of
The University of Alabama

TUSCALOOSA, ALABAMA

2021

ABSTRACT

River deltas, home to almost half a billion people around the world, are important coastal depositional systems. Valuable natural resources, fertile grounds, and convenient locations for trade have proven deltaic land to become hot spots for urbanization, industrialization, and food production over the last few decades.

In this Dissertation the following research questions are investigated: (1) what remote sensing-based algorithms are most efficient in river delta shoreline detection? (2) what changes do we observe of shorelines of individual deltas historically? (3) how is human modification on river delta plains contributing to delta plain erosion? (4) are changes in fluvial sediment flux to the delta are directly linked to decadal changes in delta morphology? A novel multifaceted research approach is used that combines (1) remote sensing analysis of past delta morphology changes, (2) numerical modeling of fluvial sediment fluxes, and (3) GIS/Statistical analysis of shoreline migration rates to answer the intricacies of the aforesaid spatio-temporal questions.

This study (a) provides recommendations on different shoreline extraction techniques and make the transfer of knowledge to lesser studied deltaic systems done informatively, (b) provides quantitative understandings of historical shoreline change rates of deltas, (c) quantitative understandings of delta plain erosion from humans having modified delta plains from their pristine conditions, and (d) how shoreline mobility is informed based on riverine fluvial sediment, overall, at a global scale.

The outcomes of this study yield several novel insights and scientific advancements of delta morphology changes of the last four decades, and not only transforms our analytical capabilities for studying human influences on river deltas, globally, but also provide a predictive platform that could assist decision makers to make better informed decisions for long-term sustainability of deltas.

DEDICATION

To the hardworking, taxpaying citizens of the world.

ACKNOWLEDGEMENTS

I wish to express my sincere gratitude to my adviser and mentor, Dr. Sagy Cohen, for his guidance, encouragement, and provision of a warm, relaxed atmosphere for me to carry out my research, successfully. The memories at the Surface Dynamics Modeling Lab at UA will always be deeply etched in the mind, and fondly remembered throughout my life.

I would also like to extend my appreciation to my committee members Drs. David Keellings, Venkat Lakshmi, Hongxing Liu, and Jaap Nienhuis for providing me advice and guidance to during my proposal defense and later on with data needs, helping me overcome methodological challenges and better argue a scientific premise.

Most of all I would like to thank my wife, Nishani, for unconditionally supporting me throughout the years of my PhD journey, and my mother who was the cornerstone of my life but waved goodbye too soon. All success, I dedicate to these two trailblazing women.

Sincere thanks also go out to my brother and father, who have been massive pillars of support, all my lab-mates who have come and gone throughout the many years I've been here, and friends from my undergraduate and school days who have helped me become a better version of myself. I regret not being able to mention the names of each and every one individually, but your contribution is highly cherished and prized in the successful completion of this research.

CONTENTS

LIST OF TABLES

LIST OF FIGURES

CHAPTER 1

INTRODUCTION

A river delta is defined as a discrete shoreline protuberance formed from deposition of sediment where rivers enter oceans, semi-enclosed seas (coastal embayments), lakes, or lagoons (adapted from Elliott (1986)). Home to almost half a billion people across the world (Syvitski and Saito, 2007), these coastal depositional systems not only act as central locations for agricultural production (Syvitski & Saito, 2007), fisheries (Woodroffe et al., 2006), and hydrocarbon production (Syvitski et al., 2009), but are also biodiversity hotspots, and carry a vast cultural heritage (Hutchings & Campbell, 2005; Lentz et al., 2016).

Many deltas around the world are undergoing rapid changes in response to alterations in riverine fluxes of sediment, and coastal changes (Ericson et al., 2006; Syvitski et al., 2009). Fluvial fluxes into deltas have altered dramatically in most deltas in the last several decades due to river engineering (e.g. dams) and land use changes (Dunn et al., 2019; Wang et al., 2011; Syvitski et al., 2005). One of the major casualties of the afore-mentioned processes is the changes to the river delta shoreline governing the effective deltaic landmass for human habitation, quantified by the change in the river delta shoreline position.

Shoreline positions are important for constructing engineering structures (e.g. breakwaters, weirs) to mitigate flooding, construction of dams, erosion-accretion studies,

regional sediment budget calculations, ecological assessments of nearshore wildlife populations, and conceptual or predictive modeling of coastal morphodynamics (Al Bakri, 1996, Maiti and Bhattacharya, 2009; Masria et al., 2015, Cenci et al., 2018). Thus, understanding impacts of fluvial sediment fluxes on river delta shoreline positions and the ability to predict their evolution is of utmost importance for the sustainable planning of deltaic communities (Yang et al., 2015).

During the past four decades, satellite remote sensing technologies have emerged as a viable alternative to in-situ observations of river deltas and associated delta plain morphology changes. mainly attributed to their availability over large geographical regions, the effectiveness of the delta change mapping techniques, the temporal coverage of a given location, and the relatively low cost for large aerial extents (Mathers and Zalasiewicz, 1999; Munasinghe et al., 2018; Zhang et al., 2015; Zhao et al., 2008). Remotely sensed data can be seamlessly used as a stand-alone tool, or in tandem with complementary numerical modeling and statistical efforts. Numerical models for predicting global sediment dynamics are an attractive solution to observational data gaps, for developing and testing mechanistic hypotheses and for developing future predictive frameworks. Riverine modelling frameworks provide us with capabilities of simulating spatially and temporally explicit sediment fluxes taking into account anthropogenic land-use effects on sediment (Syvitski 2005, Cohen et al, 2013, 2014).

The overarching goal of this dissertation was to elucidate morphological responses of large global river deltas to temporal variations in fluvial sediment fluxes and anthropogenic modifications of the environment. This dissertation directly addressed four limitations in our

understanding of delta morphology changes and flux relationships that are consistently highlighted in the literature.

First, we critically review literature on satellite remote sensing techniques that were used to study delta morphology changes. In total, we offer a review of 18 techniques with example studies, and strengths and caveats of each and propose four pathways for future advancement delta morphological remote sensing. Second, a gap in literature is recognized where there is no understanding of the most effective shoreline extraction method for a delta. We evaluated the performance of 5 different remote sensing techniques. We propose a new metric (Robustness: R) to evaluate the performance of a given technique. Recommendations are made for the application of techniques in different types of deltas and unknown deltaic territories worldwide. Third, we investigate the anthropogenic stress on river delta plains. We identify dominant anthropogenic stressors on river delta plains and intensities of modification and quantify how much sediment is eroding from river delta plains. Fourth, we explore how delta shoreline mobility is governed by variations in incoming fluvial fluxes from feeder rivers.

Overall, this dissertation provides a framework for understanding the interconnectivity between fluvial fluxes, deltaic morphology, and anthropogenic dynamics in large global deltas. We envision outcomes of this study helping better understand shoreline mobility in delta systems, predicting future behavior of these depositional environments, and from a policy standpoint, helping improve delta management affecting human and ecological presences on deltas.

CHAPTER 2

A REVIEW OF SATELLITE REMOTE SENSING TECHNIQUES OF RIVER DELTA MORPHOLOGY CHANGE

Abstract

River deltas are important coastal depositional systems that are home to almost half a billion people worldwide. Understanding morphology changes in deltas is important in identifying vulnerabilities to natural disasters and improving sustainable planning and management. In this paper, we critically review literature on satellite remote sensing techniques that were used to study delta morphology changes.

We identify and categorize these techniques into 3 major classes: 1) One-step change detection, 2) Two-step change detection, and 3) Ensemble Classifications. In total we offer a review of 18 techniques with example studies, and strengths and caveats of each. Synthesis of literature reveals that sub-pixel-based algorithms perform better than pixel-based ones. Machine learning techniques rank second to sub-pixel techniques although an ensemble of techniques can be used just as effectively to achieve high feature detection accuracies. We also evaluate the performance of the 7 most commonly used techniques in literature on a sample of global deltas. Findings show the Unsupervised Classification significantly outperforms the others, and is recommended as a first order delta morphological feature extraction technique in previously unknown, or, data sparse deltaic territories.

We propose four pathways for future advancement delta morphological remote sensing: 1) utilizing high-resolution imagery and development of more efficient data mining techniques,

2) moving toward universal applicability of algorithms and their transferability across satellite platforms, 3) use of ancillary data in image processing algorithms, and 4) development of a global-scale repository of deltaic data for the sharing of scientific knowledge across disciplines.

1. Introduction

1.1 The River Delta and its Importance

A river delta is defined as a discrete shoreline protuberance formed from deposition of sediment where rivers enter oceans, semi enclosed seas (coastal embayments), lakes or lagoons (adapted from Elliott, 1986). Deltaic regions are home to more than 490 million people, including several megacities (Syvitski & Saito, 2007). These hubs act as major centers for agriculture (Syvitski & Saito, 2007), fisheries (Woodroffe *et al.*, 2006), and hydrocarbon production (Syvitski *et al*., 2009), offering employment opportunities for millions, and consequently making deltaic regions some of the most economically productive systems in the world (Woodroffe *et al*., 2006). The ecological significance of river deltas lies in the fact that they act as coastal storm surge protectors, biodiversity hotspots, provide habitats for many animal and plant species, provide pathways for migratory species and carry with them a cultural heritage which is a high revenue generation mechanism for local communities (Hutchings & Campbell, 2005; Lentz *et al*., 2016).

1.2 The Morphology of a Delta

Morphology, in the simplest of terms, is the configuration or form of a river delta in its natural environment. The morphology of modern deltaic systems (so named because their formation/progradation began during the late Holocene period, subsequent to the last glacial

period; Allison *et al.*, 2003) is controlled by the complex interaction between boundary conditions and forcing factors (Coleman and Wright, 1975; Orton and Reading, 1993; Postma, 1995; Syvitski and Saito, 2007). These forcing factors include (1) supply of bedload and suspended sediment load: reflecting drainage basin characteristics, water discharge, sediment yield and grain size; (2) deposition/accommodation space: reflecting sea-level fluctuations, offshore bathymetry, tectonics, subsidence, compaction, and isostasy; (3) coastal energy: reflecting waves and tides, longshore and cross-shelf transport; and (4) density differences between effluent and receiving waters defining the dynamics of sediment plumes. The complex interaction among these factors result in the formation of different features (e.g. main delta landmass governed by the delta shoreline, sandbars/barrier islands, beach spits). These features, which are component environments of the delta, collectively describe the morphology of the delta, reflect the status quo of the river delta, and can be used to monitor changes to the delta through time.

1.3 Importance of Delta Morphology Change Studies

Most modern deltas serve societal needs such as protecting residents, resources, and infrastructure, or preserving biodiversity and ecosystem services. Human settlements and infrastructure in low-lying deltaic regions are particularly vulnerable to floods induced by intense precipitation and storm surges (Motsholapheko *et al.*, 2011; Sanchez-Arcilla *et al.*, 2012). Floods disrupt cultivation in delta plains, livestock farming, destroy property leading to displacement of households, interrupt water reticulation systems, and curtail transport systems, thereby impacting a country's economic growth significantly (Bendsen and Meyer, 2002; Motsholapheko *et al*., 2011). Therefore, knowledge on morphology change is important to plan engineering works such

as identification of vulnerable areas, installation of coastal defense structures (e.g. breakwaters, weirs), confinement or widening of river channels, dredging, sand extraction, dam construction, development of setback planning and hazard zoning.

In addition to mitigate against flooding, delta morphology change information is also important for constructing engineering structures for transport, land reclamation and urbanization, erosion-accretion studies, regional sediment budgets, restoration activities for extensively altered deltas, and for conceptual or predictive modeling of coastal morphodynamics (Sherman and Bauer, 1993, Al Bakri, 1996, Zuzek *et al*., 2003; see Maiti and Bhattacharya (2009); Masria *et al*., 2015; Le *et al*., 2007). Therefore, understanding and predicting these morphology change dynamics is of utmost importance for sustainable planning of deltaic communities.

1.4 Satellite Remote Sensing of Deltaic Morphology Dynamics

During the past four decades, satellite remote sensing technologies have emerged as a viable alternative to in-situ observations of river deltas and associated deltaplain morphology changes (Figure 1: evolution of the Yellow river delta during the satellite era). This is mainly attributed to their availability over large geographical regions, the effectiveness of the delta-change mapping techniques, the temporal coverage of a given location, and the relatively low cost for large aerial extents (Mathers and Zalasiewicz, 1999; Zhao *et al.,* 2008; Zhang *et al.,* 2015; Munasinghe *et al.,* 2018). Although delta morphology mapping based on ground surveys and aerial observations (e.g. aerial photography, drone footage) is a viable and useful option, such methods are time-consuming, expensive and, in most cases, cannot provide data on time scales commensurate with

delta morphology change. Remotely sensed data can be seamlessly used as a stand-alone tool, or in tandem with complementary numerical modeling and statistical efforts.

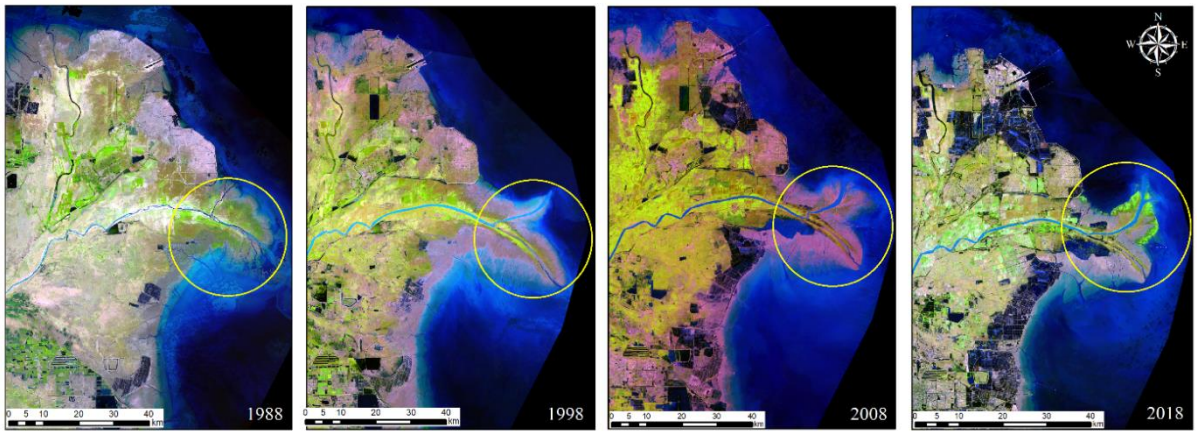

Figure 2.1. Landsat satellite imagery showing the evolution of the Yellow River Delta, China from 1988 to 2018. The circled area shows the downward development of the Qingshuigou Lobe, and the more prominent upward development of the Qing8 Lobe of the delta.

1.5 Motivation for this Review

The impetus for this review comes from the non-availability of a single robust document in the literature which portrays past and current research efforts in identifying river delta morphology changes using satellite remote sensing techniques. The need for such a summation stems from several reasons. Morphology detection techniques that work well for one particular river delta might not be ideal for another: This could be due to complications of geometries of river deltas (e.g. influenced by islands, sandbars), sediment plumes transported by rivers (gradational deposition at the river mouth) making the identification of the delta boundaries difficult, geographical location of river delta (governs the type and density of vegetation that grows at the land-sea margin), and tidal forces (determines formation of islands close to the main delta body due to breakage) which all act in varying degrees in determining the performance

accuracy of algorithms. This has led to morphology detection algorithms to mostly be location specific. A summation of knowledge as such also aids in morphology detection algorithm selection and application to lesser studied deltaic systems globally, done informatively. The transfer of knowledge from prior use cases could be done informatively (by relative comparison of similar delta forms and geographical regions) and with caution (prior understanding of limitations of detection algorithms). Thus, for current research frontiers in deltaic research to expand, a need arises for a comprehensive, organized summary of historical and emerging techniques of delta change mapping of key deltaic environments.

We also perform a comparison of remote sensing techniques on an array of delta types (river-, tide-, wave-dominated) from a global sample of deltas to understand the performance of techniques under varying fluvial and marine conditions. Elucidating which technique(s) work best in delta morphological feature extraction would allow us to infer why particular techniques underperform in different regions of the world. This will also highlight some of the inherent problems of particular techniques and will offer a pathway for improving existing algorithms and development of new ones to monitor river delta morphological change.

This document reviews the content of 146 articles/book chapters which used remote sensing technologies to detect deltaic features and their changes, and a further 38 articles/book chapters to gather supplementary information on river delta research and technological advances in computational algorithm development. Every effort has been taken to cover the breadth of remote sensing techniques that were used in delta morphology research from 1980 until present day.

2. Indicators of Delta Morphology Change

A river delta is a collection of different component environments (as described in section 1.2). Changes to these components result in the changes in geometries, sediment facies and depositional architecture of the delta. Thus, these components can be used as 'indicators' to assess changes to the morphology and can be quantitatively used to derive delta evolution. For example, a decrease in sediment fluxes to the delta can move it from a condition of active growth to a destructive phase portrayed by the recession of the land-sea margin (i.e. the delta shoreline). In a second example, strong wave climates effectively diffuse fluvial sediment, thereby limiting mouth bar growth and make the delta mainland more erosion prone, and vice versa. Therefore, as per the above two examples, the delta shoreline and presence/absence of mouth bars can be used as indicators to assess changes to river delta morphology.

Although there exist a plethora of morphology change indicators, it has to be noted that the focus of this review will only be on, a) indicators that can be identified using satellite remote sensing (e.g. shelf depth, (water depth reached by the submerged delta), although a factor governing delta morphology, cannot be assessed using satellite remote sensing), and b) indicators that directly reflect morphology-change of a delta (e.g. indicators reflecting changes to the effective deltaic landmass (i.e. the shoreline)) as opposed to indicators of forcing factors which act as causal factors of morphology change (e.g. drainage basin-averaged climate, which in turn can have an effect on erosion of delta plain and sediment loading into feeder river).

Based on above selection criteria, we categorize all satellite-detectable indicators which reflect morphology change into 5 classes summarized from studies conducted by Syvitski and Saito (2007), Mathers and Zalasiewicz, (1999), Ulrich *et al.* (2009), Passalacqua, (2017). Table 1

provides an overview of these indicators, and the role they play in structuring the overall morphology of the delta.

Table 2.1. Change indicators and their representation of delta morphology

Class	Indicator	Role of Indicator in Delta Morphology Change Representation	Can be Remotely Sensed? (Y/N)	Included in Review? (Y/N)
1	Shoreline	Governs the land-sea margin, determines the effective landmass available for human consumption, and determines subaerial view (plan view) of the delta.	Y	Y
2	Crevasse Splays and Channel Avulsions	Channel avulsions in deltaic areas start with the formation of a crevasse splay. Crevasse splays (deposits of sediment in the shape of a fan or lobe formed by river channels as a result of point failures of a levee) help better understand how rivers naturally distribute water and sediment across floodplains, local rates of sediment accumulation and sediment delivery to coastal regions, and influences on floodplain topography and alluvial architecture, and help make informed decisions on land-management solutions such as engineered diversions (Nienhuis et al., 2018).	Y	Y
3	Number and Size of Distributary Channels, and Meander belts	Avulsions and other channels on the delta make up the distributary network. Proper understanding of the size of the distributary channels and the ways in which they migrate through time is critical to many geomorphological and river management problems on a delta (Seker et al., 2005; Yang et al., 1999). Channel erosion and bank failure cause obstruction of navigation routes, changes to channel geomorphology, and most importantly changes to flood levels which can have adverse impacts on the infrastructure of the delta plain.	Y	Y
4	Barrier Islands, Beach Spits, and Mouth Bars	These are deltaic features that result from the dynamic interaction of fluvial sediment supply and the redistribution of sediment by marine processes at the river mouth-sea interface. Rapid deposition on river-mouth bars can cause their seaward progradation, which, through the control of upstream siltation in the main	Y	Y

		river channel, can serve as a stimulus to river channel migration. Heavy sedimentation in the lower reaches of the river channel can also cause the riverbed to aggrade and increases the flood risk on the floodplain, making the river channel avulsion-prone. Beach spits and barrier islands function more in the capacity of coastal storm surge attenuation and wave and tidal erosion control which impact the shoreface.		
5	Gradient of Delta Plain	Measured from the apex of the delta to the coast along the main channel (Syvitski and Saito, 2007), the gradient of the delta plain is a vertical measure of morphology. This in addition to the sediment supply to sediment retention on the delta plain, can be significantly impacted by subsidence of the delta plain itself. Subsidence related morphological changes to the gradient might not be reflected by the land-sea boundary but can be reflective in flood extents during extreme events which impact floodplain architecture.	Y	*N

* studies pertaining to the gradient of the delta plain will not be discussed in this review for two reasons. Firstly, the majority of the studies related to the gradient in the literature are from a geological perspective without any substantial remote sensing component to them. Thus, they do not scope well within the constraints of this review. Secondly, even the studies that did discuss remotely sensed changes in river delta gradient, were done so as secondary derivatives of changes in land subsidence of the delta. Subsidence mapping is an entirely vast and different field of remote sensing which would constitute a separate review of its own.

The change in deltaic shoreline can be regarded as the most important environmental descriptor of delta morphology, as it is the only parameter that reflects the 'quantity' of landmass available for human consumption indicating how the delta front prograded or degraded over the years. In comparison, other indicators detect morphology changes 'on' the deltaic landmass and thus has garnered a lesser importance in literature (over 90% of the studies reviewed for morphology change were based on the shoreline). Delta shoreline changes are described in section 3, and studies discussing all other indicators are summarized in section 4.

3. Delta Shoreline Change Detection Techniques

Delta progradation/degradation determination through remote sensing relies on the varied spectral response of the land-water boundary (i.e. the shoreline) at different wavelengths. Different landforms produce characteristic surface spectral responses as products of the combination of the terrain color and surface moisture linked with composite materials, texture and structure properties of the exposed portions, terrain geometry and land cover. A large number of techniques for delta progradation detection from satellite imagery have been developed over the years and can be classified into three broad categories of change detection methods (Figure 2): 1) Two-step Change Detection: use of a remote sensing technique(s) to delineate morphology for a particular time step, use the same or different set of technique(s) to retrieve morphology at a different time step and compare between them; 15 such techniques will be discussed, 2) One-step change detection: The use of a remote sensing technique(s) on multidate imagery to detect change in one step; two such techniques will be discussed: a) Layer Arithmetic: use of band mathematics on the reflectance values to compare between multi-date imagery, b) Change Vector Analysis: use of the radiometric properties of multi-date imagery to

yield both magnitude and direction of change, and 3) Ensemble Classification: use of a mixed methods approach.

It is important to note, and user applications need to pay attention to the fact that, the location of a shoreline on a satellite image might not be the topographical boundary between land and water as it is an instantaneous one influenced by seawater level fluctuations caused by waves, tides and local seasonal sea level changes. Therefore, it would be erroneous to apply said shoreline detection techniques to a single image representative of a time step, as these external forces can substantially affect water levels (Walker and Hammack, 2000) and consequently the boundary, without necessarily indicating a morphological change. There are statistical methods to correct for the shoreline position (Zhang *et al.*, 2018) if changes of shorter time steps are desired (e.g. change every year during a 5-year period). For longer time scale analysis (e.g. change every 5 years for a 30-year period), a composite, representative of the deltaic region, using imagery over a few consecutive months (e.g. 6 months), is created, and the averaged raster is used as a single time step.

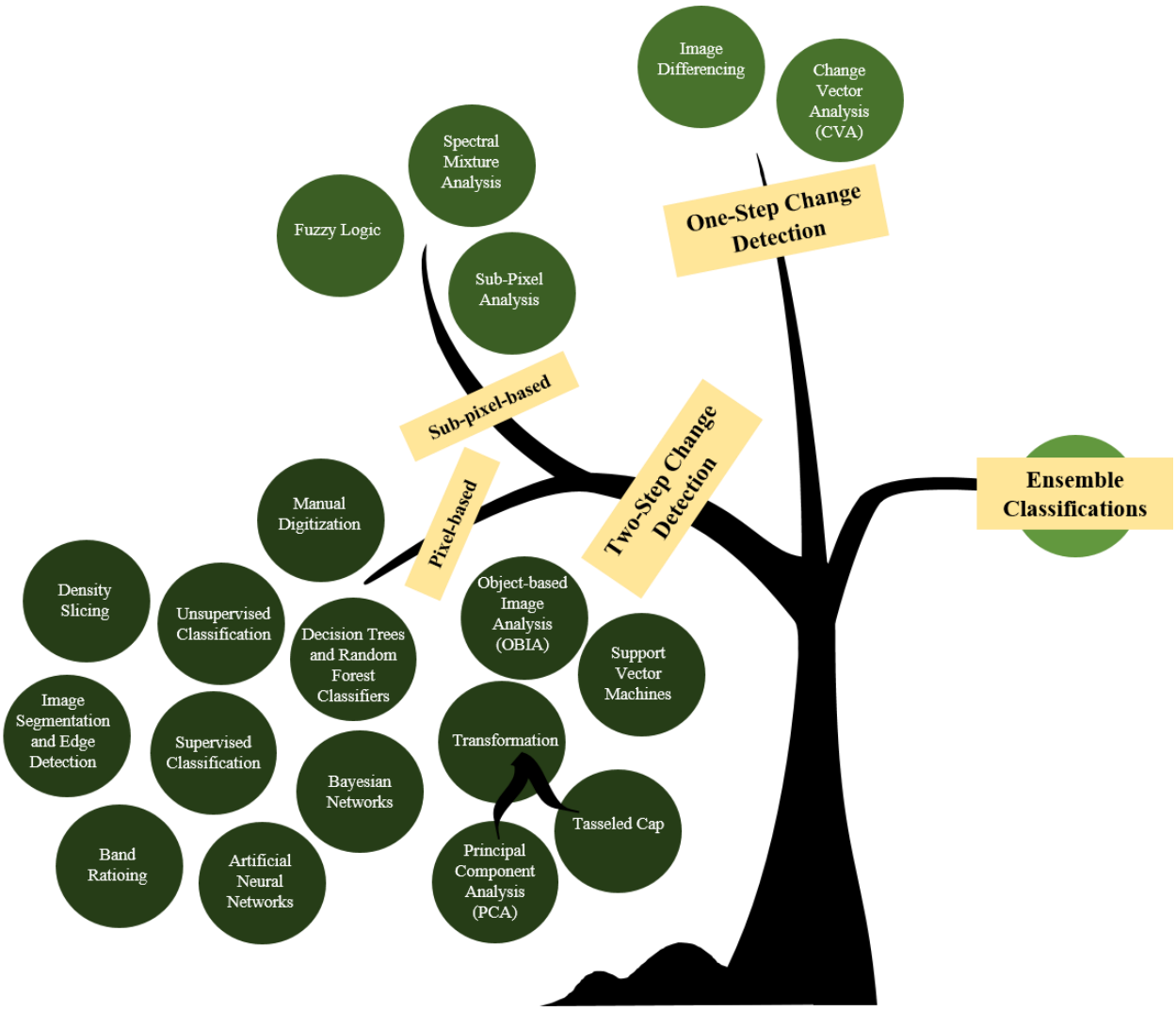

Figure 2.2. Classification of remote sensing techniques used for river delta morphology change detection.

The discussion of each technique is framed on the conceptual background of the technique, how and why it is applied to deltaic feature detection, the technical merit of application, and its caveats informed by the conclusions and recommendations of the literature reviewed. We present a summary of all techniques reviewed in this paper along with example studies in Table 2 below for the readership to revert to, during the length of the document, as a quick reference guide.

Table 2.2. A summary of remote sensing techniques of river delta morphology change identification

Technique	**Example Studies**	**River Delta (Country)**	**Satellite Platform**
Manual Digitization	Yang (1996)	Yellow (China)	Landsat MSS, Landsat TM
	Yang *et al.* (1999)	Yellow (China)	Landsat MSS, Landsat TM
	Chu *et al.* (2006)	Yellow (China)	Landsat MSS, Landsat TM
	Zhao *et al.* (2008)	Yangtze (China)	Landsat TM, Landsat ETM+
	Marghany *et al.* (2010)	Kuala Terengganu (Malaysia)	ERS-1, RADARSAT-1
	El Asmar and Hereher (2011)	Nile (Egypt)	Landsat MSS, Landsat TM, SPOT-4
	Kuenzer *et al.* (2014)	Yellow (China)	Landsat MSS, Landsat TM
	Duţu *et al.* (2014)	Danube (Romania/Ukraine)	Landsat TM, Landsat ETM+
	Ahmed *et al.* (2018)	Ganges-Brahmaputra-Meghna (India)	Landsat TM, Landsat ETM+
Density Slicing	Mouchot *et al.* (1991)	Mackenzie (Canada)	Landsat TM
	Mathers and Zalasiewicz (1999)	Red (Vietnam)	Landsat TM
	Ryu *et al.* (2002)	Gosmo Bay (Korea)	Landsat TM, ASTER
	Maiti and Bhattacharya (2009)	Subarnarekha and Rasulpur (India)	Landsat MSS, Landsat TM, Landsat ETM+, ASTER
	Mallinis *et al.* (2011)	Nestos (Greece)	Quickbird
	Allen *et al.* (2012)	Wax Lake (USA)	Landsat TM, Landsat ETM+
	Kong *et al.* (2015)	Yellow (China)	Landsat MSS, Landsat TM, Landsat ETM+
	Ghoneim *et al.* (2015)	Nile (Egypt)	Landsat MSS, Landsat TM, Landsat ETM+
	Dada *et al.* (2018)	Niger (Nigeria)	Landsat TM, Landsat ETM+
Image Segmentation and Edge Detection	Lee and Jurkevich (1990)	Chesapeake Bay (USA)	Saesat, Shuttle Imaging Radar (SIR)
	Mason and Davenport (1996)	Wash delta/estuary (UK)	ERS-1
	Niedermeier *et al.* (2000)	Elbe (Germany)	ERS-1 and ERS-2
	Bayram *et al.* (2008)	Bhosporous (Turkey)	Corona, IRS-1D, Landsat ETM+
	Al Fugura *et al.* (2011)	Kuala Terrenganu (Malaysia)	RADARSAT-1
Band Ratioing	Yang *et al.* (1999)	Yellow (China)	Landsat MSS, Landsat TM
	El-Raey *et al.* (1999)	Nile (Egypt)	Landsat MSS
	Ryu *et al.* (2002)	Gosmo Bay (Korea)	Landsat TM, ASTER

	Guariglia *et al.* (2006)	Ionian coast (Italy) inclusive of deltas	Landsat TM, Landsat ETM+, SPOT XS, Corona
	Ekercin (2007)	nothern coast of Turkey including deltas	Landsat MSS, Landsat TM, Landsat ETM+
	Kuleli (2010)	Cukurova (Turkey)	Landsat TM
	Cui and Li (2011)	Yellow (China)	Landsat MSS, Landsat TM, Landsat ETM+
	Mukhopadhyay *et al.* (2012)	Puri coast and Mahanadi (India)	Landsat TM
	Niya *et al.* (2013)	Dalaki (Iran)	Landsat TM
	Kundu *et al.* (2014)	Sagar Island, GBM (India)	Landsat TM
	Louati *et al.* (2015)	Medjerda (Tunisia)	Landsat TM, Landsat ETM+, Landsat OLI
	Nitze and Grosse (2016)	Lena (Russia)	Landsat TM, Landsat ETM+, Landsat OLI
	Sun *et al.* (2018)	Yangtze (China)	Landsat MSS, TM, OLI, GF-1 PMS, SPOT-7
	Wang *et al.* (2019)	Yellow (China)	Landsat TM, Landsat OLI
	Da Silva *et al.* (2019)	Parnaíba (Brazil)	Landsat MSS, TM, ETM+, OLI
	Viaña-Borja and Ortega-Sánchez (2019)	Guadalfeo, Adra, and Ebro (Spain)	Landsat TM, Landsat ETM+, Landsat OLI
Unsupervised Classification	Wilson (1997)	Fitzroy (Australia)	Corona
	Frihy *et al.* (1998)	Nile (Egypt)	Landsat MSS, Landsat TM
	Guariglia *et al.* (2006)	Ionian coast (Italy) inclusive of deltas	Landsat-TM, Landsat ETM+, SPOT-PX/XS, Corona
	Ekercin (2007)	nothern coast of Turkey including deltas	Landsat MSS, Landsat TM, Landsat ETM+
	Nath and Deb (2010)	Okavango Delta (Botswana)	AVHRR
	Mukhopadhyay *et al.* (2012)	Puri coast and Mahanadi (India)	Landsat TM
	Muster *et al.* (2012)	Lena (Russia)	Proba -1
	Kundu *et al.* (2014)	Sagar Island of the GBM (India)	Landsat TM
	Buono *et al.* (2017)	Yellow (China)	RADARSAT-2
Supervised Classification	Sgavetti and Ferrari (1988)	Po and Adige (Italy)	Landsat TM
	Ciavola *et al.* (1999)	Shkumbini, Semani and Vjosë (Albania)	Landsat TM
	Seker *et al.* (2003)	Riva (Turkey)	Landsat MSS, Landsat TM, Landsat ETM+
	El-Kawya *et al*. (2011)	Nile (Egypt)	Landsat TM, Landsat ETM+
	Masria *et al.* (2015)	Nile (Egypt)	Landsat TM, Landsat ETM+

Transformation Methods			
Principal Component Analysis (PCA)	El Raey *et al*. (1995)	Nile (Egypt)	Landsat MSS, Landsat TM
	Li and Yeh (1998)	Pearl (China)	Landsat TM
	Kushwaha *et al.* (2000)	West Bengal coast inclusive of deltas (India)	ERS-1
	Seto *et al*. (2002)	Pearl (China)	Landsat TM
	Li and Yeh (2004)	Pearl (China)	Landsat TM
	Ghanavati *et al*. (2008)	Hendijan (Iran)	Landsat TM, Landsat ETM+
	Ghoneim *et al*. (2015)	Nile (Egypt)	Quickbird, Worldview-2
Tasseled Cap Transformation	Nandi *et al.* (2016)	Sagar Island, GBM (India)	Landsat MSS, Landsat TM, Landsat ETM+
	Chen *et al.* (2019)	Yangtze (China)	Landsat OLI
Artificial Neural Networks (ANN)	Berberoglu *et al.* (2000)	Cukurova (Turkey)	Landsat TM
	Zhu (2001)	Pearl (China)	Landsat MSS, Landsat TM
	Del Frate *et al.* (2012)	Italian coastline inclusive of deltas	COSMO-SkyMed
	Ding (2013)	Yellow (China)	Landsat TM, Landsat ETM+
Decision Trees and Random Forest Classifiers	Ottinger *et al.* (2013)	Yellow (China)	Landsat TM
	Kuenzer *et al.* (2014)	Niger (Nigeria)	Landsat TM, Landsat ETM+
	Haas and Bun (2014)	Yellow, Pearl (China)	Landsat TM, HJ-1A/B satellites
	Banks *et al.* (2015)	Kitikmeot region (Canada) inclusive of deltas	RADARSAT-2, Landsat TM
	Berhane *et al.* (2018)	Selenga (Russia)	Worldview-2
Bayesian Networks	Gutierrez *et al.* (2011)	U.S. Atlantic Coast inclusive of deltas	
	Yates and Cozannet (2012)	European coasts inclusive of deltas	Areal observations used as input
Support Vector Machines	Xu *et al.* (2012)	Yellow (China)	RADARSAT-2
	Masria *et al.* (2015)	Nile (Egypt)	Landsat TM, Landsat ETM+
	Petropoulos *et al.* (2015)	Axios and Aliakmonas (Greece)	Landsat TM
	Gou *et al.* (2016)	Yellow (China)	ALOS-2

Object-based Image Analysis	Cao *et al.* (2007)	Yellow (China)	SPOT 5
	Liu *et al.* (2014)	Yellow (China)	Landsat TM, Landsat ETM+, HJ-1A/B satellites
	Demers *et al.* (2015)	Islands of Mackenzie Delta (Canada)	RADARSAT-2
	Zhu *et al.* (2018)	Yellow (China)	Landsat MSS, Landsat TM, Landsat OLI
Fuzzy Logic	Dellepiane *et al.* (2004)	coastline in Genova (Italy) inclusive of deltas	ERS-1, ERS-2
	Foody *et al.* (2005)	coast in Terengganu (Malaysia) inclusive of deltas	IKONOS
	Ghanavati *et al.* (2008)	Hendijan (Iran)	Landsat TM, Landsat ETM+
	Dewi *et al.* (2016)	deltaic region in the Sayung District (Indonesia)	Landsat TM, Landsat ETM+, Landsat OLI
Spectral Mixture Analysis	Liu *et al.* (2016)	Yellow (China)	Landsat OLI
	Liu *et al.* (2017)	Pearl (China)	Landsat OLI
Sub-Pixel Analysis	Wei *et al.* (2008)	Yellow (China)	ASTER
Image Differencing	Yeh and Li (1997)	Pearl (China)	Landsat MSS, Landsat TM
	Xia (1998)	Pearl (China)	Landsat TM
	El-Raey *et al.* (1999)	Nile (Egypt)	Landsat MSS
	Adegoke (2010)	Niger (Nigeria)	Landsat TM, Landsat ETM+
Change Vector Analysis	El-Raey *et al.* (1999)	Nile (Egypt)	Landsat MSS
	Seto *et al.* (2002)	Pearl (China)	Landsat TM

3.1 Classification Techniques used in Two-Step Change Detection

3.1 (A) Pixel-Based Methods

3.1.1 Manual Digitization

Deltaic coastlines are delineated manually based on the delineator's/digitizer's knowledge of the morphological features, vegetation and sediment characteristics of the delta. Compared to computer aided classification techniques, manual operation takes advantage of the judgment skills and interpretation of humans in defining what and where the boundary is between land and water.

The combination of digitization and automatic boundary detection algorithms (discussed later) to detect the land–ocean shoreline boundaries were proven to be successful (Kong *et al*., 2015). However, this technique has several inherent problems. In addition to the inaccuracies induced through the monotonous nature of digitization, it is also challenging for the human eye to interpret the boundary (based largely on digitizer's experience) since, mainly in low-resolution images, color shades may decay gradually (Niedermeier *et al*., 2005). Presence of water saturated zones in the vicinity of the land water boundary could complicate the issue. Therefore, calculations have to be performed in order to recognize if the inaccuracies constitute a significant source of error in comparison to the magnitude of the overall changes in the delta (Chu *et al*., 2006). This approach is also highly time-consuming and tedious. It is therefore expensive (labor cost) and ineffective when a large number of images need to be analyzed.

3.1.2 Density Slicing

The concept of density slicing involves classifying the remotely-sensed image into land and sea, often by identifying a threshold value for a single spectral band. In order to determine this critical threshold without bias, a histogram analysis is often performed (Figure 3). Ryu *et al.* (2002) and Shen *et al*. (2008) showed that in tidal flat zones, thermal-infrared (TIR) band is the most sensitive to the location of waterline through density slicing. Work on Landsat has shown that mid-infrared bands (band 5 in the case of Landsat TM) is the most suitable for extracting the land water interface because it exhibits a strong contrast between land and water features due to the high degree of absorption of the mid-infrared wavelength by water (Manavalan *et al*., 1993; Kelly *et al*., 1998; Frazier and Page, 2000; Lee *et al*., 2001; Alesheikh *et al*., 2007).

While overall successful, this method carries with it certain caveats. Although land and water generally appear to be spectrally separable, the accuracy of waterline prediction is sometimes low due to the dynamic and complex land-water interactions in coastal deltaic regions. This could be due to spectral confusion, arising from effects such as variable depth and turbidity, together with the spatial resolution of the imagery, which influences the clarity of boundaries and proportion of mixed pixels, limiting the accuracy of shoreline mapping (Frazier and Page, 2000; Ryu *et al*., 2002; Malthus and Mumby, 2003). Also, the use of one spectral band usually does not allow every type of change to be detected (Gong, 1993). Density slicing alone is not sufficient in determining the shoreline and, therefore, typically used in conjunction with other methods to obtain higher delta shoreline classification accuracies (Marghany *et al*., 2010).

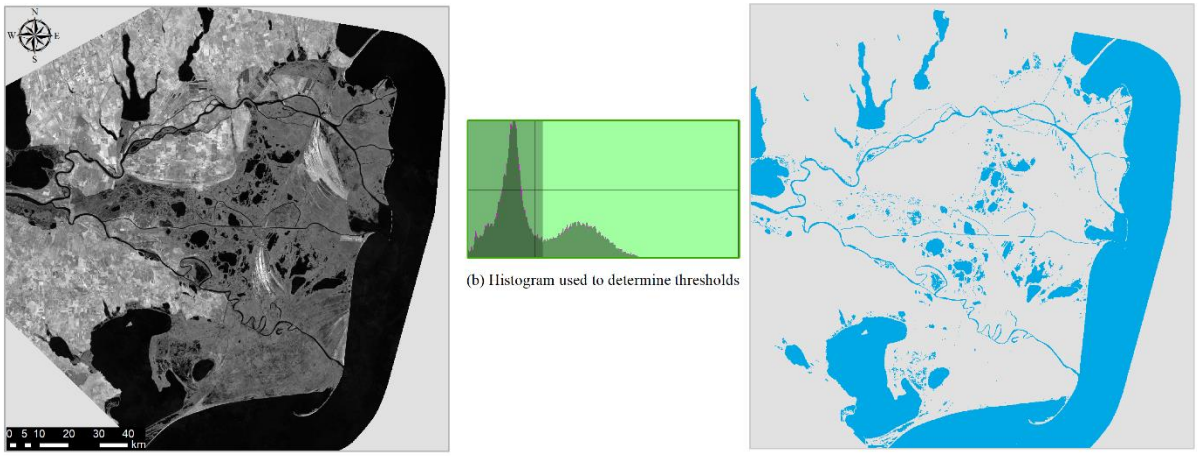

(a) Landsat TM 5 band

(b) Histogram used to determine thresholds

(b) Density-sliced raster with water features in blue

Figure 2.3. Density Slicing of band 5 (Landsat TM) of the Danube delta region to obtain a land-water raster. The shoreline was subsequently extracted using GIS methods.

3.1.3 Image Segmentation and Edge Detection

Image segmentation and edge detection algorithms follow the process of manual digitization more closely by dividing an image into different regions where sharp intensity alterations occur. The “alternative connective approach”, one of two major image segmentation and edge detection algorithms is used in deltaic research where it seeks to grow homogeneous regions by merging pixels or sub-regions on the basis of some similarity criterion (Lemoigne and Tilton, 1995). This approach is based on ‘guiding’ the remote sensing software by manually identifying points along the shoreline of the original image. The software then examines the edges of the image following these points. The parameters by which the shoreline is identified are determined by the analyst. This heuristic search is found to be faster and more reliable than entirely automated approaches (Loos and Niemann, 2002) due to the input of previously gathered information by the analyst.

Albeit its success, this method also has its limitations in possible inclusion of different earth feature classes into the same region, making spectral separation and subsequent

identification of thematic information classes difficult. As White and El Asmar (1999) and Heimann *et al.* (2004) stated, since the classical region growing methods (classifying neighboring pixels outward from a point of origin based on similarity of reflectance of the originating pixel) yield outcomes in accordance with the contrast of the image, contrast similarities between land and water zones impedes the extraction of coastline from other existing constituents and could result in irregularities of coastline extractions.

3.1.4 Band Ratioing

This method exploits the near infrared (NIR) and short-wave infrared (SWIR) bands whose wavelengths are absorbed by water, resulting in surface water rendered as black color in the processed image. A combination of these spectral bands ((NIR-SWIR)/(NIR+SWIR)) is used to reduce the effect of suspended sediment near shorelines (Lohani & Mason, 1999; Lodhi *et al*., 1997) and accentuate higher reflectance characteristics from soil and healthy vegetation, providing a context for the land/water interface (Braud and Feng, 1998; Fraizer and Page, 2000; Guariglia *et al*., 2006). In comparison to other methods, ratioing is a relatively rapid means of identifying areas of change.

However, there are certain downsides to this method. The Band 2/Band 5 ratio has a value greater than one for water and less than one for land in large areas of the coastal zone (Alesheikh *et al*., 2007). Image processing software use this ratio as an algorithm for separating water from land from TM or ETM+ imagery. This ratio works well in coastal zones covered by soil, but not in land with vegetative cover. This can lead to mistakenly classifying other land use types as water (Alesheikh *et al*., 2007). Therefore, this is a readily go-to method if the aim is to rapidly extract the coastline. However, if the goal is accurate coastline extraction, then this might

not be the most suitable. Figure 4 below shows an example application we conducted on the Irrawaddy delta in the shoreline extraction process using Landsat-8 imagery.

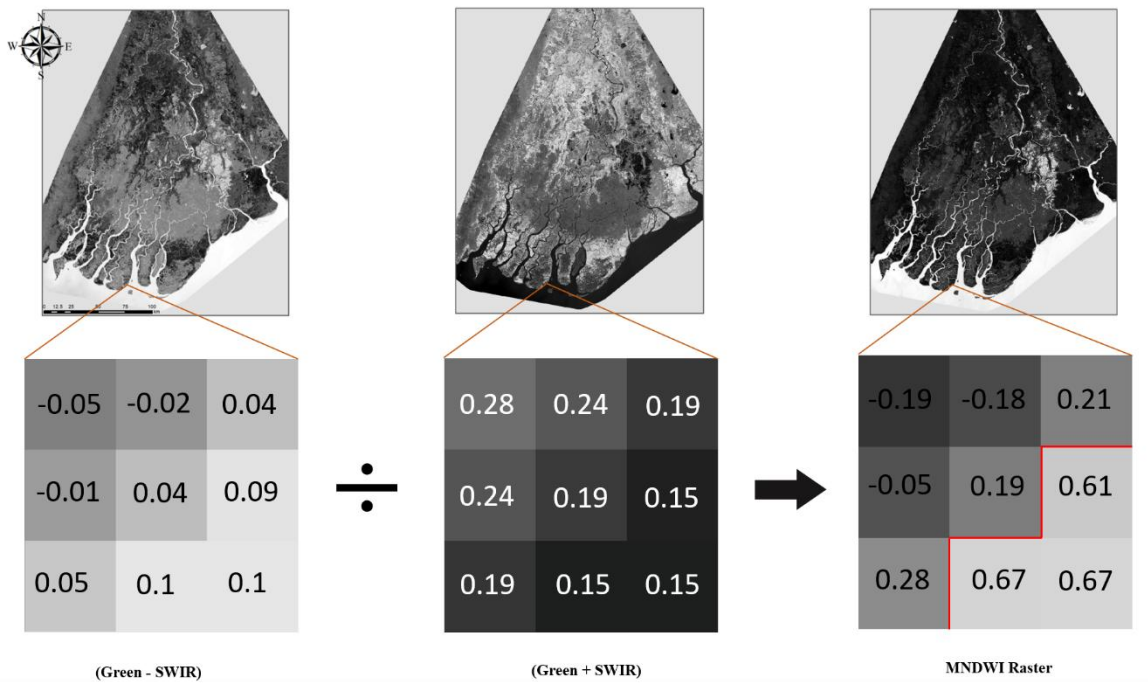

Figure 2.4. Band ratioing of Landsat-OLI imagery of the Irrawaddy river delta to produce a land-water raster after which the shoreline is extracted using GIS methods. The combination and ratio used here is the Modified Normalized Water Index (MNDWI; Xu, 2006) used to accentuate water features. *left:* A subtracted difference raster of Band 6 (SWIR) and Band 3 (Green) is generated (the blow-up denotes raster values of the selected region). *Middle:* An added difference raster of Band 6 (SWIR) and Band 3 (Green) is generated. *Right:* The difference-rasters are ratioed to produce the MNDWI feature-accentuated raster.

3.1.5 Unsupervised Classification

Unsupervised classification is an effective method of natural clustering and extracting land-cover information of remotely sensed image data based on spectral properties of pixels. Compared to supervised classification (discussed in 3.1.6), unsupervised classification requires minimal initial input from the analyst (determining the clustering algorithm and desired number of classes) as it does not require training data. The clustering process results in a classification

map consisting of *n* spectral classes. The analyst then attempts to assign or transform the spectral classes into thematic information classes of interest (e.g., forest, agriculture). Many clustering algorithms have been developed to date (e.g. ISODATA Clustering, K-Means).

Unsupervised methods, although not completely exempt from the user's interaction, require less inputs than their supervised counterparts and is computationally efficient. However, the user must have knowledge of the area and understand the spectral characteristics of the terrain in order to relate the classes to actual land cover types (such as water features, wetlands, developed areas, coniferous forests, etc.). Difficulties in obtaining consistent classes from images taken at different times, owing to variability in illumination, atmospheric effects, and instrumental response, have been reported (Adams *et al*., 1995). Also, some spectral clusters may be meaningless because they represent mixed classes of earth surface materials. It has been noted in the literature that although the use of unsupervised classification is nearly a labor-independent analysis, this technique does not lead to the most detailed analysis and cannot produce the highest classification accuracy (Congalton, 1991; Xia, 1998; Enderle and Weih, 2005).

3.1.6 Supervised Classification

In supervised classification, the analyst selects sample pixels in an image that are representative of land cover classes, and then directs the image processing software to use these end-member pixels (training pixels) as references for the classification of all other pixels in the image (determination of maximum likelihood of image pixels of a land use class based on training data). Training sites are selected based on the analyst’s knowledge and experience of image interpretation. The analyst also designates the number of classes that the image is classified into.

Since supervised classification is based on prior knowledge about the land cover and their typical spectral characteristics by the analyst, this method is deemed one of the more successful methods of delta morphology detection and is commonly used as a benchmark to test other algorithms (Khatami *et al.*, 2016). Higher classification accuracies resulting from supervised classification motivated researchers to combine this technique with other methods. Shalaby and Tateishi (2007), for example, concluded that the use of a combination of supervised classification and visual interpretation analysis increased the overall classification accuracy by approximately 10%. However, because the training sites are selected based on the knowledge and experience of the analyst, there is always the possibility that the sample pixels that one selects for a given information class (e.g. shoreline) will not be homogenous across the entire study domain (i.e. training areas will not encompass unique spectral signatures of a particular land feature). In addition, since this is a user driven method, it can be a time consuming and an exhaustive one, if done for multiple time steps over different study domains.

3.1.7 Transformation methods

When multispectral images are used to detect change of delta morphology, a reduction of the number of bands is often warranted in order to identify dominant patterns in the imagery (i.e. enhance the original classification feature space) without compromising the variance. Although simple band mathematics can be used and is straightforward (e.g. density slicing, band ratioing), it can be inefficient when the number of spectral bands of the image exceeds three. To overcome these difficulties the process of image transformation was introduced. Different transformation methods have been developed over the years, and two of those have been reported in delta morphological studies: Principal Component Analysis (PCA) and Tasseled Cap Analysis (TCA).

The central concept of a PCA is to reduce the dimensionality of a dataset consisting of many interrelated variables, while retaining as much variation present in the dataset as possible. This is achieved by transforming the data to a new set of variables (principal components) which are uncorrelated and ordered so that the first few retain most of the variation present in all the original variables (Deng *et al.,* 2008). The procedure works as such that subsequent to performing a PCA on multi temporal imagery, conventional clustering methods (e.g. unsupervised) can be applied to the first few principal components to produce thematic maps representative of different earth features. This method was shown to improve accuracy gains when utilized with other techniques in the image classification process (Khatami *et al.,* 2016).

Although comparatively PCA analysis has advantages over simple band mathematics techniques (i.e. band ratioing, band differencing), it introduces difficulties in interpreting and labeling each component image (to associate physical scene characteristics with the individual components). This type of analysis is also scene dependent and is difficult to obtain the 'from-to change' class information (change in pixel information from an earlier time step to a later one) when detecting change over multiple time steps. Moreover, it was found that the application of PCA for multiple time step analysis is subject to the condition that the areas of change must be a small proportion of the entire study area (Gong, 1993; Seto *et al.,* 2002).

TCA transformation rotates multispectral data and creates three planes: Brightness (B), Greenness (G) and Wetness (W) (Crist, 1985). The Brightness band is a weighted sum of all reflective bands and can be interpreted as the overall brightness or albedo at the earth's surface. The Greenness band primarily measures the contrast between the visible bands and near-infrared bands and is similar to a vegetation index. The wetness band measures the difference between the weighted sum of the visible and near-infrared bands and the mid-infrared bands and is a

proxy of plant and/or soil moisture (Seto *et al.*, 2002). In TCA, the brightness, greenness, wetness bands are directly associated with physical scene attributes and therefore easily interpreted (Figure 5). TCA analyses to detect delta morphological change is seldom carried out alone and is used as a data reduction technique prior to the data being analyzed by another technique(s). Examples of the usage of TCA is given in section 4.3.

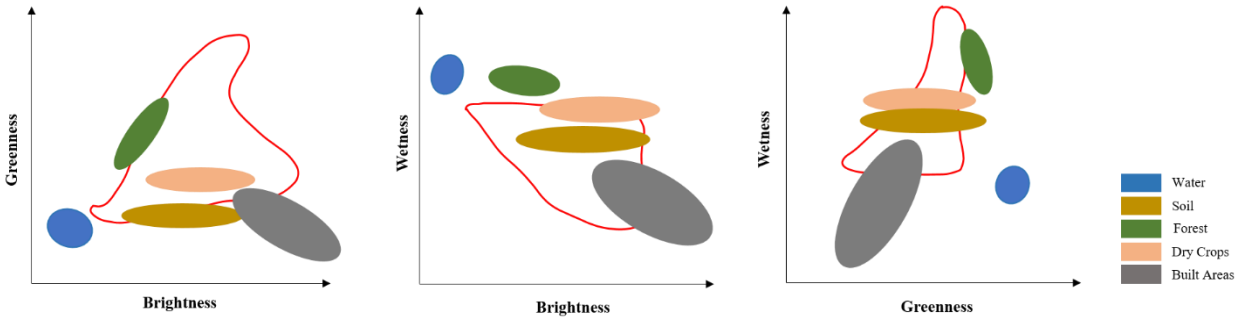

Figure 2.5. A typical representation of earth features between correlations of the three transformed bands.

3.1.8 Artificial Neural Networks (ANN)

Artificial Neural Networks (ANN), a form of Artificial Intelligence (AI), can be used to semi-automate image classification, and has become a common alternative to conventional band statistical approaches. The development of ANNs was inspired from human brain recognition and brain learning mechanisms (Berberoglu *et al.*, 2000). Neural networks consist of input and output layers, as well as (in most cases) a hidden layer consisting of units that transform the input into something that the output layer can use (Foody *et al.*, 1995). They are excellent tools for finding patterns which are far too complex or numerous for a human programmer to extract and train the machine to recognize (Samarasinghe, 2016).

The backpropagation algorithm (Paola and Schowengerdt, 1995) is the most common method of training multi-layer networks to date (Samarasinghe, 2016), with an emphasis on its

application to pattern recognition in multispectral imagery. It allows networks to adjust their hidden layers of neurons in situations where the outcome does not match what the user is hoping for (Samarasinghe, 2016), similar to a network designed to recognize muddy shores, and misidentifies them as turbid waters.

As delta evolution is a very intricate non-linear process influenced by many factors such as water and sediment discharges and coastal dynamics, neural networks possess great robustness over traditional classifiers in that they are inherently nonparametric nature. The strengths of a neural network lie in arbitrary decision boundary capabilities (the ability to partition the data set into separate classes effectively), easy adaptation to different types of data and input structures, possibility of fuzzy output values (probability of a pixel belonging to a certain information class type) that can enhance classification accuracies (classification accuracies of fuzzy outputs are discussed in the Fuzzy logic section), and good generalization for use with multiple images. Land/water rasters created using neural networks are later used with GIS methods to extract deltaic shorelines. The disadvantages of the method are inconsistent results due to random initial weights, the requirement of obscure initialization values (e.g., learning rate and hidden layer size: the "black box," phenomenon in which the user feeds in data and receives answers, and no access to the exact decision making process), slow training time of the network, and heavy computational demand to train the network for large datasets (Xie *et al*. 2008). For a detailed analysis of advantages and disadvantages of neural networks for remote sensing applications, the readers are referred to Jarvis and Stuart (1996) and Mas and Flores (2008). We can conclude from the literature that although the neural network method has several unique capabilities, it will become a useful tool in remote sensing only if it is made faster, more predictable, and easier to implement.

3.1.9 Decision Trees and Random Forest Classifiers

A Decision Tree is a tree-structure like flowchart (Friedl and Brodley, 1997; Figure 6). There are many different types of decision tree algorithms, e.g. Classification and Regression Tree Algorithm (CART; Denison *et al.,* 1998), C4.5 (Mazid *et al.,* 2010).

Decision Trees are easy to interpret, their internal workings are capable of being observed, making it possible to reproduce work, while making no statistical assumptions regarding the distribution of data (Hass and Bun, 2014). They are also computationally efficient (Friedl and Brodley, 1997), and perform well on large multispectral datasets (Zhang *et al.,* 2017).

One of the major problems with using decision trees is overfitting, especially when a tree is particularly deep (Friedl and Brodley, 1997; Pal and Mather, 2003). Over-fitting occurs when the tree is designed so as to perfectly fit all samples in the training data set, resulting in branches with strict rules of sparse data. This affects the accuracy when predicting samples that are not part of the training set (i.e. yields highly accurate output for the training data but low accuracy for test data).

Random Forest (RF) classifiers mitigate this problem well. First proposed by Breiman (2001), a RF is simply a collection of decision trees whose results are aggregated into one final result. Their ability to limit over-fitting without substantially increasing error due to bias makes them a powerful model. In a random forest, the number of trees in the forest (n estimators), and the maximum number of features to be used in each tree can be specified. However, one cannot control the randomness over which feature is part of which tree in the forest, and there is no control on which data point is part of which tree. Accuracy keeps increasing as the number of trees is increased but becomes constant at a certain point.

RFs can handle both high dimensional data and use a large number of trees where the key issue is correlation reduction between the random classification variables (ability to handle thousands of input variables without variable deletion) and they can be run efficiently on large databases. The RF algorithm can also detect outliers, which can be very useful when some of the cases may be mislabeled.

Random forests have been extensively applied to deltaic image classification and has resulted in improved classification accuracy compared to traditional methods, such as maximum likelihood (ML) and artificial neural network (ANN) methods (Adam *et al.,* 2012; Akar and Güngör, 2015). RFs outperform single decision tree algorithms (Gislason *et al.,* 2006; Khatami *et al.,* 2016). With this combination of efficiency and accuracy, along with very useful analytical tools, the RF classifier is considered very desirable for multisource classification of remote sensing and geographic data. That said, RFs are not immune to caveats; they can be time-consuming, difficult to construct and require greater computational resources in comparison to decision trees. In addition, since RFs deal with a number of decision trees, and the randomness of features within decision trees is uncontrollable, there is no way for the user to have a qualitative understanding of the behavior of the dataset to have an educated guess of the outputs, and therefore, has to take the output decision of the algorithm at face value.

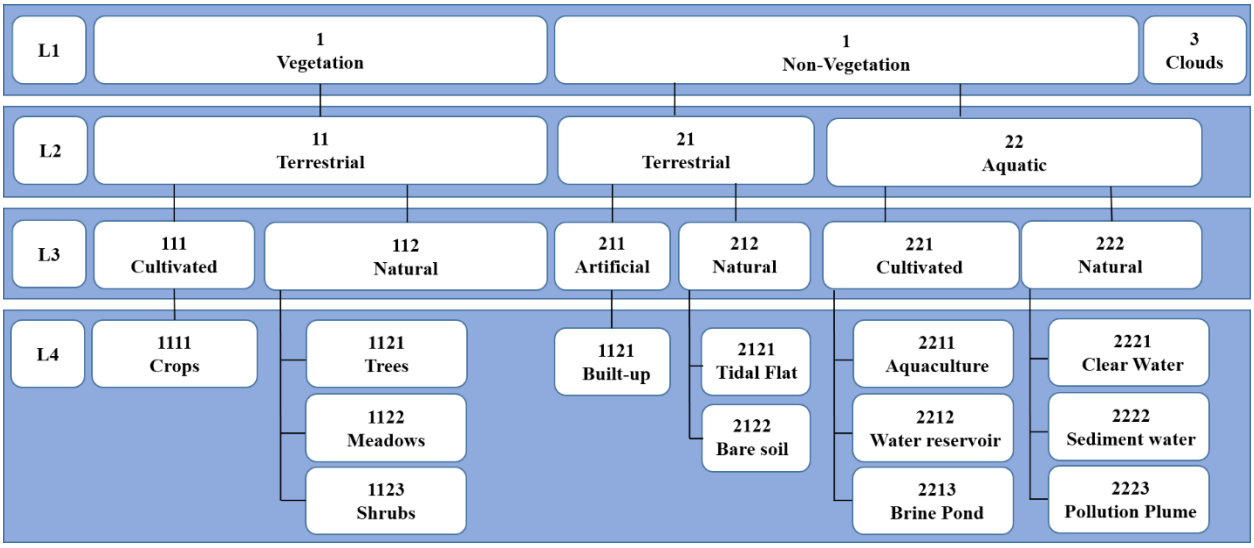

Figure 2.6. A decision tree to characterize different coastal features and isolate the shoreline

3.1.10 Bayesian Networks

Bayesian networks (BNs), also known as belief networks (or Bayes nets for short), are directed acyclic graphs (DAGs) belonging to the family of graphical models (Jensen, 1996). These graphical structures include nodes representing the various quantities, variables, or parameters that serve as input information, and edges between the nodes (the arrows connecting the nodes) representing probabilistic dependencies among the corresponding random variables. A node that is not connected shows a variable that is independent by other variables represented by nodes in the graph. In comparison to others, this is a relatively new method in deltaic-feature identification using remotely sensed imagery. Remotely sensed imagery can be used as input information (in contrast to the conventional field collected/modeled databases), and the conditional dependencies in the graph are often estimated by using known statistical and computational methods. The structure of a DAG in relation to evolution of a delta shoreline is illustrated in Figure 7.

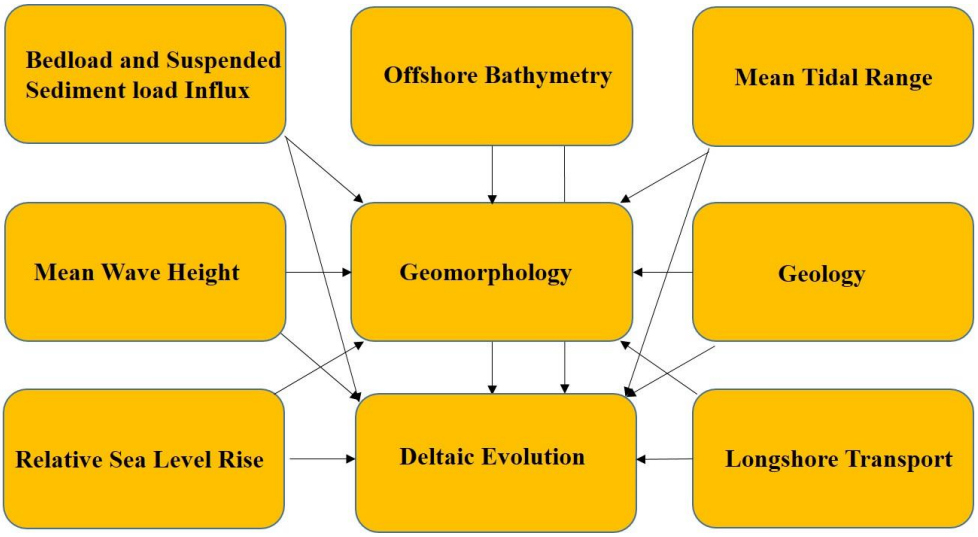

Figure 2.7. Bayesian Network to detect deltaic evolution. Black arrows indicate causal relationships linking the forcing factors and the response variable (deltaic evolution)

In Figure 7, the nodes represent random variables and are drawn as boxes labeled by the variable names. The edges represent direct dependence among the variables and are drawn by arrows between nodes. In particular, an edge from node “Mean Tidal Range” to node “[Deltaic] Geomorphology” represents a statistical dependence between the corresponding variables. Thus, the arrow indicates that a value given to variable “Geomorphology” depends on the value of variable “Mean Tidal Range”. Given the conditional dependencies, BNs can be effectively used to represent knowledge about an uncertain domain (e.g. “Deltaic evolution”) and algorithms can be created that allow for learning and inference through the use of a Bayesian network.

Often ANNs are compared to BNs due to their similarities in using directed graphs methods and are both used as classifier algorithms in problem solving. However, unlike ANNs the BN structure itself provides valuable information about conditional dependence between the variables. It is a visual representation of graph where its vertices and edges have meaning in comparison the ANNs where the network structure does not offer direct interpretations between

nodes and can be difficult to interpret. Not many studies are found in literature which use BNs exclusively for deltaic feature detection (Table 2), primarily due to the large amount of supplementary data needed to setup such networks.

3.1.11 Support Vector Machines

A Support Vector Machine (SVM) is a machine-learning technique that is useful for multispectral and hyperspectral remotely-sensed classifications in which spectral separability between coastal land and water is difficult to ascertain due to lack of clear zonation between vegetation species, and mixed pixel effects. SVM differs from traditional classification approaches by identifying the boundary between classes in n-dimensional spectral-space rather than assigning points to a class based on mean values of class clusters (Heumann, 2011).

SVM creates a hyperplane through n-dimensional spectral-space that separates classes based on a user defined kernel function and parameters that are optimized using machine-learning (Figure 8). In other words, given labeled training data, the algorithm outputs an optimal hyperplane which categorizes new feature classes (Figure 8). In two-dimensional space this hyperplane is a line dividing a plane in two parts where each class lays either side of the hyperplane. By identifying the hyperplane that separates two classes rather than using the distance between class spectral means, SVM can produce a more accurate classification.

Several studies have demonstrated the great potential of SVM. Pal and Mather (2005) found that SVM outperforms maximum likelihood and artificial neural network using Landsat TM and is well suited for small training sets and high-dimensional data. Foody and Mathur (2006) found SVM outperforms discriminate analysis and decision-tree algorithms for airborne sensor data. Li *et al.* (2010) applied SVM to an Object-based Image Analysis (OBIA) with better

results than standard fuzzy logic classification. Elhag *et al.* (2013) used Landsat TM and ETM+ imagery to map landcover in the Nile River Delta using SVM and Supervised classification approaches and showed that SVM showed higher classification accuracies. Thanh Noi and Kappas (2018) concluded that the SVM classifier on average outperformed the Random forest and kNN (K-nearest neighbor (unsupervised)) classifiers. Given the success in the literature (see examples in Table 2), we can conclude that SVM is the best individual classification technique for morphology change detection amongst pixel-based classification techniques.

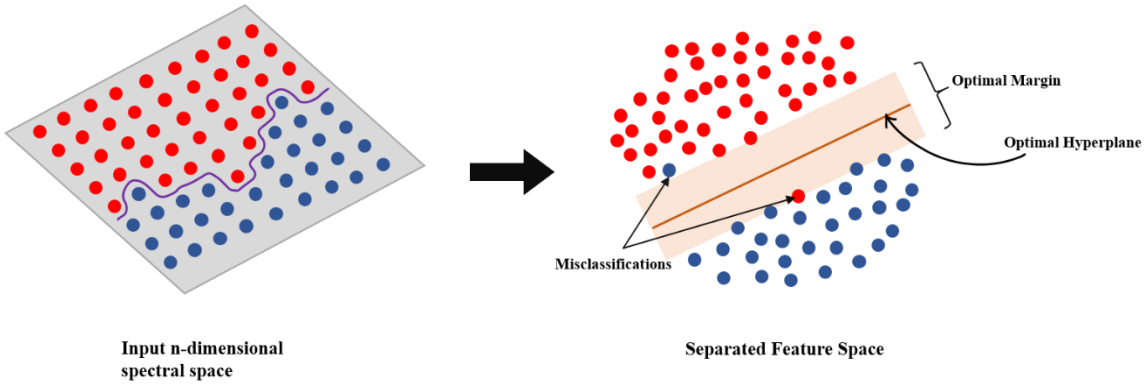

Figure 2.8. An Illustration of the SVM concept

3.1.12 Object-based Image Analysis (OBIA)

Traditional pixel-based image classification assigns a land cover class per pixel. All pixels are the same size, same shape and do not have any implicit connectivity with of their neighboring cells. OBIA, on the other hand, segments an image by grouping small pixels together into vector objects. The OBIA is a two–step process: segmentation and classification. Segmentation breaks up the image into objects representing land-based features. These segmented objects become the unit of analysis, from which spectral statistics, such as spectral band means and standard deviation, or spatial information, such as image texture, can be used in

the second process; image classification. In image classification, according to the spectral, temporal and spatial response of land cover types in the objects, the corresponding bands and band combinations are selected, and their sensitivity is trained.

Object Based Image Analysis is conceptually simple and generic across sensors (Blaschke, 2010). The key benefits of OBIA relative to pixel-based methods include: (1) the possibility to incorporate user-defined scale, shape, and compactness parameters useful for creating objects with heterogeneous pixels (in the process of creating objects, scale determines the occurrence or absence of an object class, and the size of an object affects a classification result), in addition to spectral values of the input image layers (Blaschke, 2010); (2) smoothing some of the local variation within objects, which may reduce the salt-and-pepper noise and enhance classification accuracy (Kamal and Phinn, 2011; Kim *et al.*, 2011); and (3) accounting for the landscape hierarchy of patch, cover type and ecosystem structure by working with multiple object layers nested within each other at different spatial scales (Krause *et al.*, 2004). The approximation of ground entities and patches by image objects makes them more ecologically relevant and potentially more resilient to minor geospatial positioning and image registration error than pixel units (Yoshino *et al.*, 2014).

Drawbacks include spectral similarity of diverse classes due to homogenizing effects of moisture or dead vegetation signals, and dilution of fine morphological features which may reduce classification accuracy and the effectiveness of class discrimination (Kamal and Phinn, 2011; Yoshino *et al.*, 2014).

3.1 (B) Sub-pixel-based methods

Most classification approaches, as discussed above, are based on per-pixel information, in which each pixel is classified into one category and the land-cover classes are mutually exclusive. However, in the highly turbid coastal zone, waters are mixed with various materials including suspended particles, sediments and phytoplankton, and can often be classified as "land" in many conventional algorithms. In addition, classification accuracies decrease when there is more than one land cover type within a given pixel (Figure 9), making it a challenging task to correctly classify new land growth and shorefront with shoal waters.

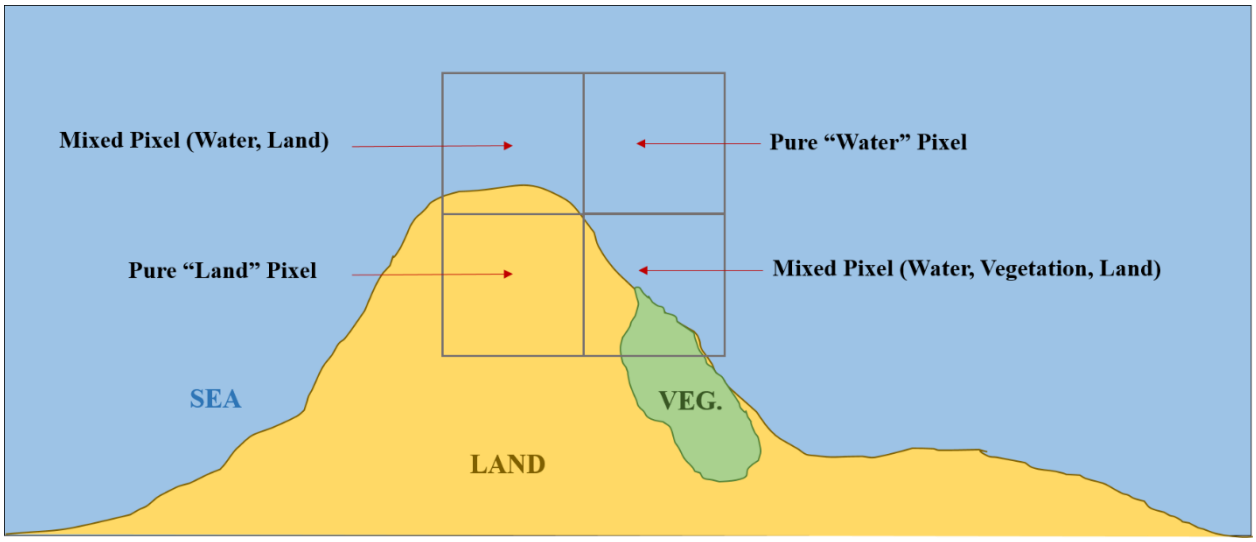

Figure 2.9. The case of the 'mixed pixel'

A relatively young field in image analysis, and one that has gained traction over the past decade or so, Sub-pixel representations, provide the opportunity to extract information about the fraction of different classes within a mixed pixel (soft classification). Soft Classification approaches in general were shown to result in improved cartographic representations of transitional zones and heterogeneous landscapes (Frohn *et al.*, 2012; Wei *et al.*, 2008; Zhang, 2009). There are three main types of soft classification approaches used in delta morphology studies currently: Fuzzy Logic, Spectral Mixture Analysis, and Sub-Pixel Analysis.

3.1.13 Fuzzy Logic

A fuzzy classification technique is a probability-based classification rather than a hard classification. It was shown to be an extremely useful classification technique in deltaic regions where the identification of the shoreline is challenging due to the shallowness and turbidity of water, vegetative gradients, and dynamically changing waterline (Zhu, 2001). A fuzzy classification allows a pixel to have multiple and partial class memberships to accommodate the effects of mixed pixels. The conventional output of a fuzzy classification is a set of fraction images which indicate the relative coverage of the classes in the area represented by the pixel. If these predicted class covers could be located geographically within the area represented by the pixel, it would allow the boundary between classes to be plotted at a subpixel scale.

Fuzzy classification has advantages over conventional methods and improves drastically on the classification accuracies by fuzzy partitioning as the spectral space and retaining information otherwise would have been lost due to conventional partitioning and classifier training. Ghanavati *et al.* (2008) showed a better performance of fuzzy classification over maximum likelihood classification and also showed better discrimination of mixed and unmixed land use/land cover categories. It is also more feasible in integrating remotely sensed data and ancillary data (Zhang & Foody, 1998; Sha *et al*., 2008) such as digital elevation models, channel networks and climate data (Lu and Weng, 2007). However, fuzzy classifications can be very slow with long run-times during feature classifications when higher accuracies are sought after. This is because additional fuzzy rules have to be incorporated into the system, and algorithms need to be tweaked (since they do not use training data) to solve for complex deltaic environments.

3.1.14 Spectral Mixture Analysis

Spectral mixture analysis (SMA) enables the extraction of information about the surface materials present in a pixel. This is done by calculating the least-squares best fit for each pixel along mixing lines bounded by spectra of end-members and in this way accounts for each pixel's variation in the mixture composition (Ozesmi and Bauer, 2002). An end-member ideally represents a pure component of the mixtures present in the pixels.

The output of SMA is typically presented in the form of fraction images, with one image for each end-member spectrum, representing the area proportions of the end-members within the pixel. End-member selection is one of the most important aspects in SMA, and much previous research has explored selection/identification approaches (Mustard and Sunshine, 1999; Theseira *et al.,* 2003; Small, 2004).

Previous research has demonstrated that SMA is helpful for improving classification accuracy (Shimabukuro *et al.,* 1998; Lu *et al.,* 2003) and is especially important for improving area estimation of land-cover classes based on coarse spatial resolution data. Albeit its increased accuracy over other methods, SMA suffers from two major caveats of 1) not having potential end-members occurring in patches larger than the image resolution; there could exist earth features in smaller patches smaller than pixel dimensions. This makes the identification of an end-member for classification impossible and consequently be classified erroneously. 2) end-members not being truly constant within an image; there always exist a range of reflectance values for a particular end-member class that could result in overlap between different end-member classes. This could create a mismatch between the defined end-member and ground truth and yield misclassification results.

3.1.15 Sub-Pixel Analysis

Sub-pixel processing is defined as the search for specific materials of interest from within a pixel's mixed multispectral image digital number spectrum. This method has advantages over SMA and fuzzy classifications, because the overall composition of each pixel is not limited to a combination of already defined image classes (end-members). The steps in sub-pixel processing include signature derivation for a material of interest and classification of each pixel identifying the fraction of material of interest present. Therefore, for each material a separate classification must be done. The fraction image pixel values vary from 0.0 to 1.0 (Ozesmi and Bauer, 2002). This specific technique of sub-pixel analysis in deltaic environments was the least used technique in the reviewed literature.

3.1.16 General Concerns about Techniques used in Two-Step Change Detection

The 15 techniques used in Two-Step Change Detection for delta morphology analysis described above, although commonly used, share some inherent limitations. One limitation is that since separate classifications are carried out on two different satellite images before detecting the deltaic change, the accuracy of the change map typically will be at best the multiplication of the accuracies of each individual classification for each date (Serra *et al.*, 2003). This is a concerning problem as this error can be significant at times, especially when multiple time steps are compared. Also, when the analyses include utilization of imagery from longer archives (i.e. use of different satellites even in the same constellation; e.g. Landsat MSS, TM etc.), it is inevitable that different data extraction and classification algorithms needed to be used to infer deltaic features (due to the variability of spectral resolution of bands). This process, in addition to the caveat mentioned above, carries the distinct disadvantage of having

uncertainties occurring due to differing classification/extraction algorithms. Thus, the two-step detection will incur an additional step of quantifying of uncertainties.

Furthermore, Two-Step Change Detection, since it requires the production of at least two different maps, can be operationally complex and computationally intensive (especially on high resolution multispectral imagery covering large areas). Therefore, the use of said methods to produce time series of change-maps can be difficult and expensive. Multi-temporal image comparison techniques/One-step change detection techniques (discussed below) were, in part, developed to alleviate these limitations.

3.2 Classification Techniques used in One-Step Change Detection

3.2.1 Image Differencing/Layer Arithmetic

In this technique, spatially registered images from different times are subtracted, pixel by pixel, to produce a layer which represents the change between the two. This procedure yields a difference distribution for each band (i.e. a histogram). In such a distribution, pixels of small radiance change are distributed around the mean, while pixels of large radiance change are distributed in the tails of the distribution (Mas, 1999). A critical element of the image differencing method is deciding where to place the threshold boundaries between change and no-change pixels displayed in this distribution.

Although Image Differencing is a widely used technique for change detection and has been used in river deltas of different geographical environments (Table 2), interpreting the difference image can be difficult because different input values can have similar output results after subtraction (e.g. input pixel values of 190 and 150 can have the same result of 40, as inputs of 100 and 60, after subtraction), and also since the original pixel value information is not

retained for further investigations (Cohen *et al.*, 1998). The mathematics of typical image differencing is shown in Figure 10 below.

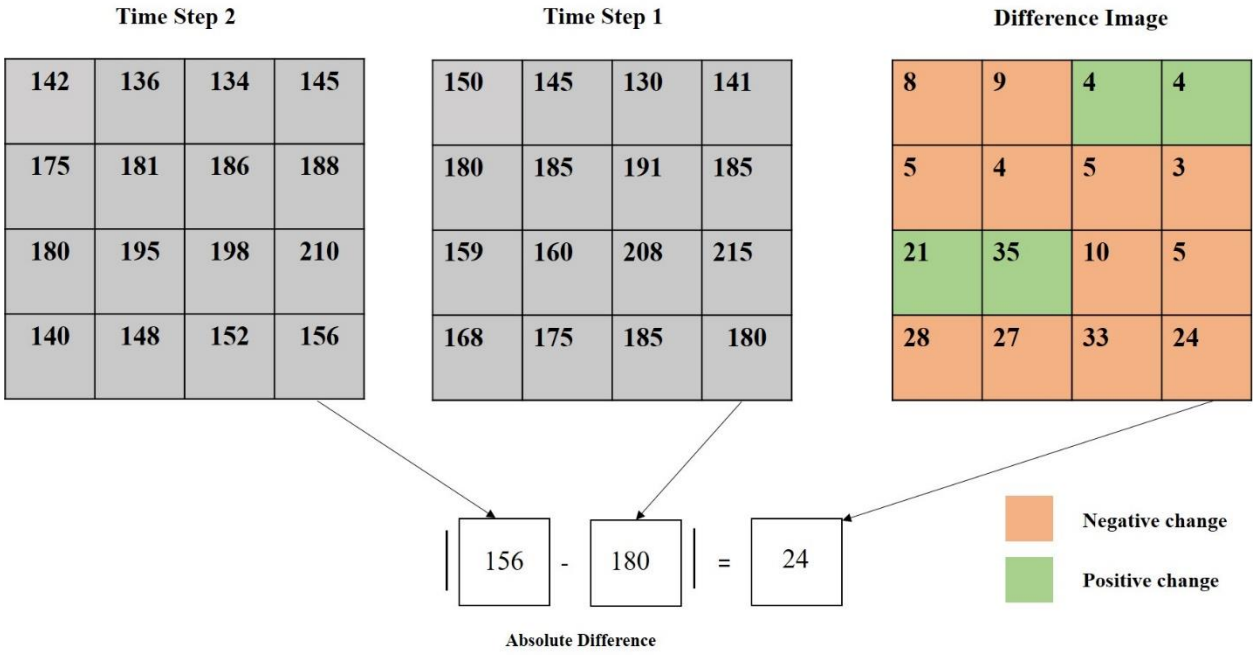

Figure 2.10. Image differencing workflow between typical rasters. The values are arbitrary values used for illustration purposes.

3.2.2 Change Vector Analysis

Change Vector Analysis (CVA) is an enhanced version of band differencing. It detects changes above a selected threshold value to generate a binary image of change and no-change pixels (Singh and Talwar, 2013). A change vector can be described as an angle (vector direction) and a magnitude of change between two different time instances from multi-spectral satellite data (Civco *et al.*, 2002). A decision on change is made based on whether the change magnitude exceeds a specific threshold. Once a pixel is identified as changed, the direction can be examined further to determine the type of change. The type of change is often identified using the angle of

the vector in two spectral dimensions (Chen *et al.,* 2003). Although initially developed for only two spectral bands, modifications to CVA enable its use to any number of spectral bands (Bayarjargal *et al.,* 2006).

In addition to providing the direction of change, which is unparalleled to other techniques discussed, CVA also has the capability of avoiding cumulative error in image classification of an individual date and processing any number of spectral bands simultaneously to retrieve maximum "from-to" type information. However, like other radiometric change approaches, CVA also has several drawbacks that limit its use. These include a strict requirement for reliable image radiometry. CVA is based on pixel-wise radiometric comparison and so the accuracy of image radiometric correction (for alleviating the impacts caused by disturbing factors such as different atmospheric conditions, solar angle, soil moisture and vegetation phenology, etc.) is more critical for CVA than for spectral classification approaches. Another drawback is a lack of automatic or semiautomatic methods to effectively determine the threshold of change magnitude between change and no-change pixels (Chen *et al.,* 2003).

3.3 Ensemble Classifications

Different image classification methods, such as parametric classifiers (e.g. maximum likelihood) and non-parametric classifiers (e.g. neural networks, decision trees), have their own strengths and limitations (Tso and Mather, 2001). For example, when sufficient training samples are available and the features in a dataset are normally distributed (distribution in space; among pixels), a maximum likelihood classifier (MLC) may yield an accurate classification result. In contrast, when image data are anomalously distributed, neural network and decision tree classifiers may demonstrate a better classification result (Lu *et al.,* 2004).

Ensemble (Hybrid) classification methods combine the strengths of multiple classification approaches. They can be valuable for river delta studies because of how they effectively address the complex variability in spectral responses of shoreline environments. Ensemble classifications can be classified into two approaches: 1) classifying a single image of a particular time step and then comparing it with an image of a different time step (classified using the same techniques or otherwise), or 2) directly comparing between two timestamps. The direct comparison between time steps is often expressed as a layer arithmetic operation to identify changed elements (locating change through e.g. CVA), followed by a supervised or unsupervised direct classification of the changed features (Lu *et al.,* 2004). Previous research has indicated that the integration of two or more classifiers provides improved classification accuracy compared to the use of a single classifier (Warrender and Augusteihn, 1999; Steele, 2000; Huang and Lees, 2004; Khatami *et al.,* 2016). In an effort to not duplicate studies and maintain the succinctness of the document, the readership is reverted to sections discussed above (3.1.1 – 3.1.15; 3.2.1 and 3.2.2) where instances of ensemble classifications can also be found. A note of caution when applying ensemble classifications is that the uncertainties occurring from different techniques have to be quantified and factored into accuracy calculations of feature extractions, as they can be significant depending on the methods used and the number of time steps of satellite imagery processed.

As evident from the discussion in sections 3.1-3.3, sub-pixel-based classifications tend to yield better results than pixel-based classifications. However, sub-pixel-based methods can be computationally expensive, and algorithm development can be time consuming. Thus, the choice of a sub-pixel-based algorithm is a trade-off between how complex the deltaic environment is, how big the river delta is (i.e. is the value of a pixel significant in comparison to the size of the

delta?), and what is the time span of the delta change analysis (are multiple image time steps involved which could compound uncertainties). In addition, since there is also the problem of compounding error resulting from classification techniques of different time steps, development of algorithms to detect sub-pixel heterogeneity can be worthwhile if a one-step change detection method, even pixel-based (e.g. image differencing. CVA), can achieve comparable results as sub-pixel algorithms.

4. Other Delta Morphology Change Indicators

Section 3 of the manuscript focused on one delta morphology change indicator: the shoreline. The discussion of all other environmental indicators in one section is due to that fact that the number of studies pertaining to every other environmental indicator was markedly less than those for deltaic shoreline change studies. We attribute this to two reasons 1) research interest: more attention is given to how deltaic landmass available for humans evolve over time (governed by the shoreline), and 2) methodological challenges: difficulty for classification algorithms to distinguish between spectral characteristics of these specific deltaic features and the surrounding terrain features. The shoreline, on the other hand, even with its own complexities at the land-sea margin, is relatively easier to detect, as changes in spectral characteristic between land and sea are comparatively prominent. Possible pathways to address these less-researched environmental indicators are discussed as future directions in section 5. The following sub-sections will discuss studies with regard to other deltaic morphology change indicators. The importance and role of these indicators in delta morphology change detection is summarized in Table 1.

4.1 Meander Belts

Lateral migration as a response to variations in river flow and sediment discharges is associated with erosion of the stream bed or channel bank and can cause many geomorphological and river management problems on a delta (Le *et al.*, 2006). Mathers and Zalasiewicz (1999) used a combination of filtration and contrast stretching on Landsat TM imagery to map and classify Meander Belts of the Red River in the Red River Delta in Vietnam. Yang (1996) and Yang *et al.* (1999) used Manual Digitization and Band Ratioing/Manual digitization on Landsat MSS and TM imagery to identify channel shifting change (Channel Migrations), channel geometric change (Channel length and width) and channel pattern change (braiding, straight, slight meandering) of the Yellow River in the Yellow River Delta. Seker *et al.* (2005) studied meander migrations of the Filyos River in and upstream of the Filyos delta, Turkey (Figure 11) and Ghanavati *et al*. (2007) used topographic maps and Landsat TM and ETM+ imagery to detect channel migrations in the Hendijan River delta, Iran.

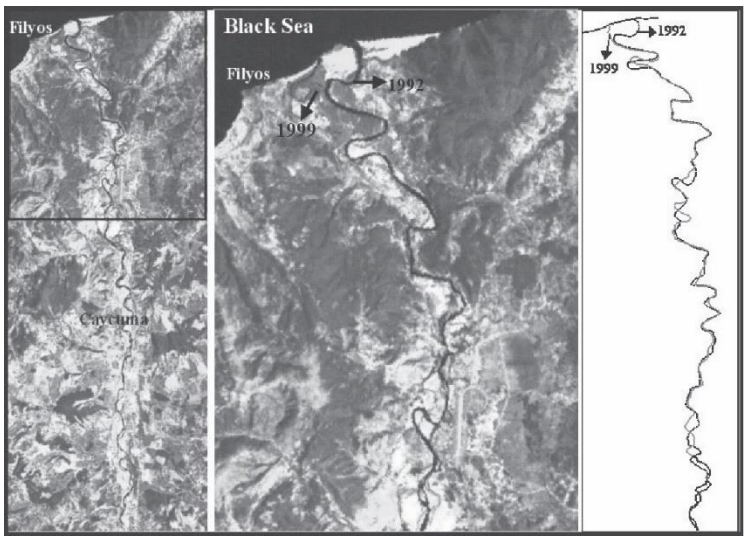

Figure 2.11. The meandering of the Filyos River through time observed using satellite imagery. Source: Seker *et al.* (2005).

4.2 Crevasse Splays, Channel Avulsions and Distributary Networks

A crevasse splay is a deposit of sediment in the shape of a fan or lobe formed by river channels (crevasse channels) as a result of point failures of a levee induced by a trigger event such as a major flood (adapted from Kargel et al., 1994; Mohrig et al., 2000). Many channel avulsions in deltaic areas start with the formation of a crevasse splay (Stouthamer, 2001). The development, evolution and finally stabilization of splays leads to the formation of avulsions, and progradation of avulsion deposits into the floodbasin. Such avulsions and other channels on the delta make up the distributary network.

Syvitski *et al.* (2012) used SRTM (Shuttle Radar Topography Mission) interferometric synthetic aperture radar (InSAR) data to study zones of nodal avulsions in 33 lowland floodplains (inclusive of deltas). Li *et al.* (2014) used Landsat MSS and TM imagery, and Li and Bristow (2015) used QuickBird-2 and WorldView-2 imagery to monitor flood-induced river morphology changes and to study splay development morphology respectively in the Río Colorado river delta in Salar de Uyuni, Bolivia (Figure 12). Mathers and Zalasiewicz (1999) used Landsat TM with the integration of geological data to study tidal creeks, channels, anastomosing rivers in the Red River Delta, Vietnam. Isikdogan *et al.* (2015) proposed an algorithm to automatically extract the channel networks from satellite imagery where water and non-water pixels have the greatest spectral contrast, and in an innovative use of high resolution google earth imagery, Gugliotta *et al.* (2019) obtained channel network widths and sinuosity of five deltas (Fly, Yangtze, GBM, Irrawaddy, and Mekong).

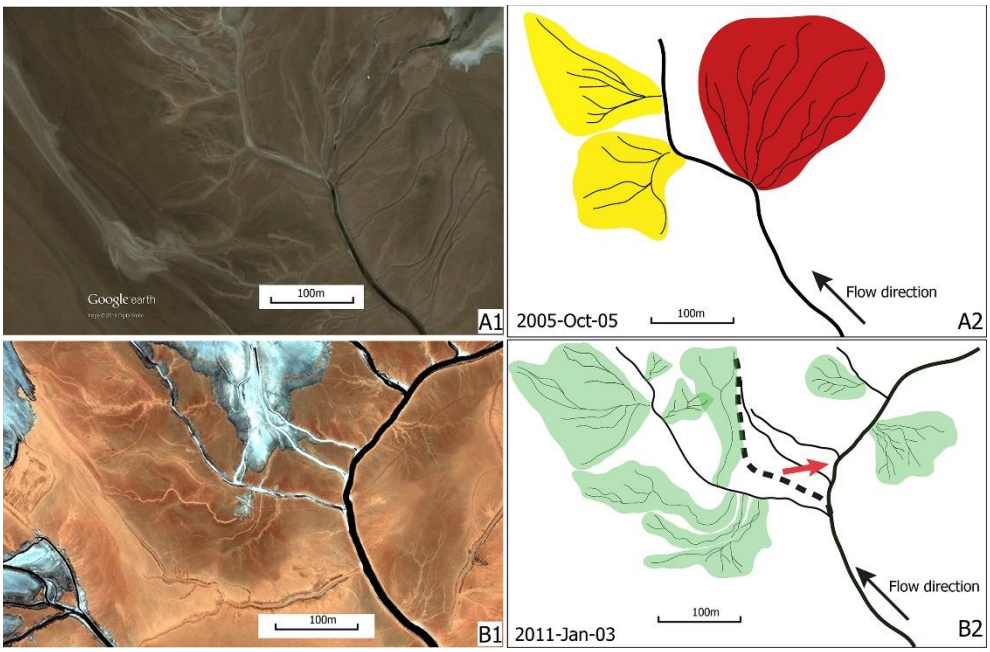

Figure 2.12. Crevasse splay-led avulsion in the Salar de Uyuni, Bolivia. A1 and B1: The same region observed from Quickbird (A1) and Worldview-2 (B1) satellites at two different times; A2 and B2: Line drawings, main river channel is demarcated by the thick black line. A2: yellow splays represent Inactive Crevasse Splays; red splay demarcates the site where avulsion occurs. B2: green splays represent new crevasse splays. Dashed line indicates river channel before avulsion. The arrow shows the channel shift after avulsion. Source: Li and Bristow (2015).

Studies of splays, avulsions and channel networks is particularly challenging in coastal deltas due to low topographic gradients, the presence of features such as sediment plumes, and the wide range of scales over which channel features are present. Channel networks identified in most of the studies were as good as the moderate resolution of the satellite imagery used. In addition, robust channel extraction methods would ease monitoring coastal areas and analyzing deltaic response to anthropogenic and natural forcing over large spatial areas and long temporal intervals. The role of higher resolution satellite imagery in better identifying these deltaic features and the need for more robust deltaic feature extraction methods based on these better platforms is discussed in section 7.

4.3 Barrier Islands, Beach Spits, and Mouth Bars

There are several deltaic features that result from the dynamic interaction of fluvial sediment supply and the redistribution of sediment by marine processes at the river mouth-sea interface. Barrier islands are shore-parallel elongated accumulations of the out-flowing effluents of the feeder river, formed mainly by the wave action at the river mouth, and build vertically by the accumulation of sand from wind transport (Van Maren, 2005). A Beach Spit also stems from an identical formation principle except that it is a stretch of sorted and reworked sediment deposited by the waves which has a connection to the mainland at one end, unlike barrier islands. A mouth bar is different in that it is created typically in the middle of the main feeder river of the delta. As the flow diverges near the ocean, sediment settles out in the channel and creates an incipient mouth bar. As flow is routed around the incipient bar, additional sediment is deposited on the incipient bar. This continued process results in the formation of a full-fledged mouth bar, which causes the channel to bifurcate. There can be hundreds of mouth bars in a large feeder river (e.g. Ganges-Brahmaputra-Meghna River System).

Frihy *et al.* (1998) used Landsat satellite data to assess the evolution of the coastal spit and changes in the lagoon margin and contiguous barrier islands in the Damietta Promontary of the Nile River Delta. Nandi *et al.* (2016) used Tasseled Cap Transformation on Landsat MSS, TM, ETM+ while Gopinath and Seralathan (2005) used image differencing on satellite data of the Indian Remote Sensing Satellite-IC to monitor changes of Sagar Island, the largest mouth bar of the Ganga-Brahmaputra-Meghna (GBM) delta. Demers *et al.* (2015) used RADARSAT-2 C–band and optical satellite data to map the shoreline of islands of the outer Mackenzie Delta using Object Based Image Analysis. A common problematic are highlighted in these studies was detecting these morphological features using medium to coarse resolution imagery. Better pixel

resolutions in comparison to the scale of deltaic features (Figure 13) were shown to be an area of improvement for better feature detection. In addition, the detections were heavily impaired by the sediment plume in the delta nearshore environment. The necessity of data mining and sub-pixel analyses was apparent. We discuss these shortcomings and possible pathways forward in detail in section 7; Future Directions.

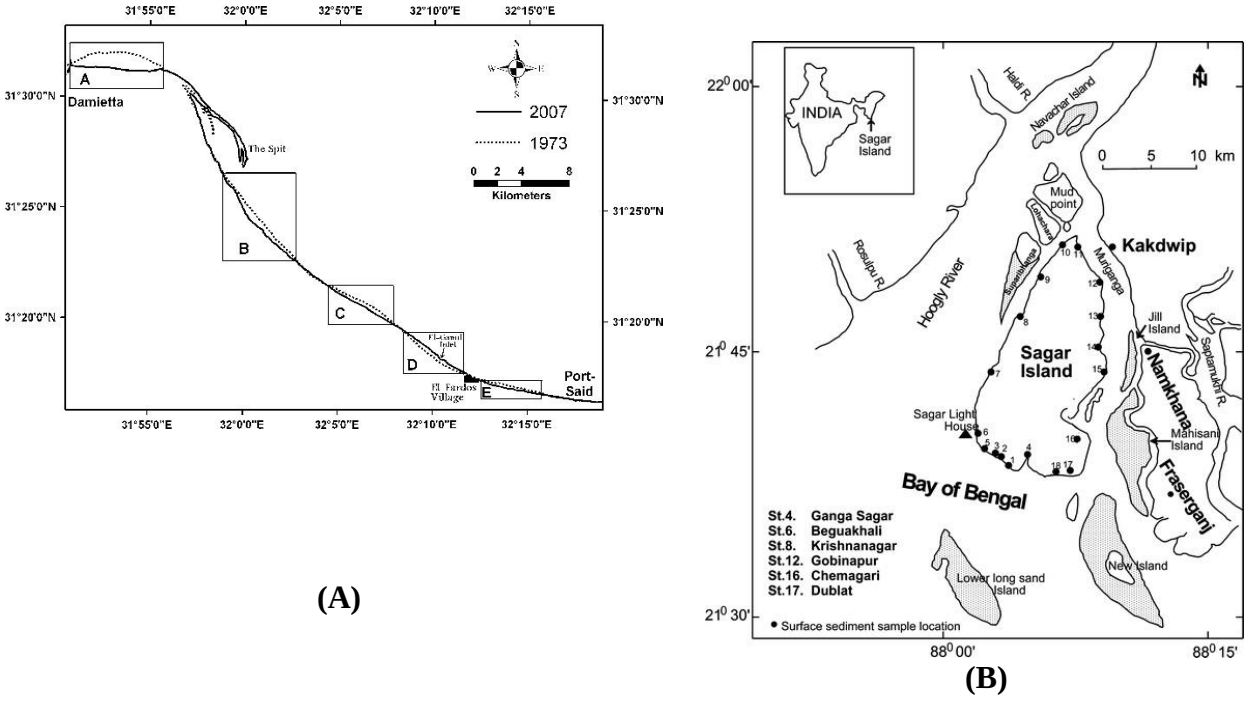

Figure 2.13. (A) The shoreline position change through time (1973 and 2007) between Damietta and Port-Said of the Nile River Delta. A prominent beach spit is visible between locations A and B. Source: El-Asmar and Hereher (2011). (B) Location of The Sagar Island, the largest barrier Island in the Ganges-Brahmaputra-Meghna Delta. Ground control points were collected at each sampling station to calibrate satellite data. Source: Gopinath and Seralathan (2005).

5. Synthesis and Applications

5.1 Machine Learning

One of the major insights stemming from this literature review is that sub-pixel-based methods tend to yield the highest accuracies among all the discussed methods in morphology change detection, while machine learning (ML) techniques perform relatively better (contingent upon good training data, and knowledge and skill of the algorithm developer) than conventional pixel-based techniques (band ratioing, density slicing). The former is a straightforward conclusion given that sub-pixel-based methods inspect details within the constraints of a pixel to elucidate information about the land surface which is otherwise impossible through pixel-based methods; higher level of inspection within a pixel will yield greater amounts of detail.

Perhaps more interesting is the insight that ML techniques (e.g. ANNs, Bayesian networks etc.) perform better than conventional methods, given that they both work at a pixel-level. It is also found that using a combination of ML techniques with others (another ML technique or other conventional ones) was shown to yield very high accuracy and utility in morphological feature classification. Thus, it is worthwhile examining why ML techniques perform well in deltaic environments, so we could better understand and harness their strengths to develop data mining algorithms in under-studied deltaic regions of the world.

The reasons for the success of ML techniques in case studies in the studied literature lie in the complexity of the deltaic system itself. One of the fundamental characteristics of a complex system is that classification results are non-linear stemming from the heterogeneity in the system (a spectral reflectance of x denoting water at one location, might be a mixture of mud, water and vegetation debris, at another). A conventional algorithm is designed to classify the system using a simple succession of steps subject to simple conditions. ML algorithms, on the other hand, have the ability to identify complex relationships through the testing of a very large number of possibilities. Typically, the algorithm runs multiple experiments of classification on

the primary image data before arriving at a final decision output. The outcome of the second experiment will not be the same as the first, and the final result is thus an ensemble of the two. ML algorithms work on the principle that it generally approximates the truth instead of aiming to find it exactly, in comparison to conventional methods, which in a complex domain such as a delta, can lead to lowered accuracies due to misclassification. The approximation of the truth of ML techniques, thus, also provide a measure of uncertainty, and can act as platforms for other types of research to build up on, which can later-on be incorporated into the decision-making process. Secondly, in a ML algorithm, many other factors related to morphology change are considered before assigning a label to a particular image pixel (e.g. see Figure 7 of how a Bayesian network solves for a deltaic evolution). This provides ancillary data (remotely sensed or not) of the deltaic environment, which improves the classification accuracy of the algorithm.

We understand that not every researcher engaged in remote sensing possesses the skills of developing complex ML algorithms. Therefore, we would also like to make a point that although ML algorithms are favorable, a combination of conventional methods in an ensemble could also lead to good classification accuracies.

What type of algorithm should one use for delta morphology detection? Is it worth the effort of going the entire distance of developing highly accurate, complex ML algorithms when, comparable results can be achieved through already existing conventional remote sensing techniques? The answer to these questions, in our opinion, depends on several factors. The most important is the study domain of interest. For example, the Damietta and Rosetta Promontaries of the Nile River Delta, Egypt (which are made of the Damietta and Rosetta branches of the Nile River, respectively) are cuspate shaped, with straight forward land-sea margins (Figure 14a). Due to the clear difference in spectral signatures the deltaic land can be clearly distinguishable

from the ocean. On the contrary, the Ganges-Brahmaputra-Meghna (GBM) delta in India/Bangladesh has intricate coastal features on the land-sea margin (Figure 14b). The extensive anastomosis of channels, huge volume of sediment output, complex vegetation gradient, presence of barrier islands, mouth bars and lagoons at the land-sea interface complicates the detection of morphological features.

Figure 2.14. The comparisons of shorelines between the (a) Damietta Promontary of the Nile River Delta and the (b) Ganges-Brahmaputra-Meghna Delta

Therefore, it would be prudent to use a combination of conventional techniques to monitor the Nile, in order to utilize available resources (time, user-skills) effectively rather than going the extra step of deep algorithm development, which might be very well the case for the GBM delta. It is therefore of utmost importance to have an understanding of the complexity of the study domains prior to the development of research methodology. It is also important to be informed of how much validation data is needed to train these algorithms (data intensive nature of algorithm) and the run-time (computational cost). For example, a Bayesian network might be significantly better than a simple band ratio, but is it worth the trade-off of time that one would invest to develop the algorithm and the amount of ancillary data (which might need to be

purchased and pre-conditioned) that is required to arrive at a relatively uncomplicated feature extraction?

5.2 Radar Imagery

Literature about the use of radar imagery for deltaic morphological feature detection was minimal compared to optical platforms. This is likely due to a combination of factors. The first is the premium access that was needed for almost all radar archives until very recently. Research proposals on intended projects had to be submitted to data providing agencies, and on most occasions, imagery had to be purchased. Secondly, unlike the lengthy activation periods of optical platforms (e.g. Landsat, since 1972) the discontinuation of radar platforms within a short period of time has led to short archival length of radar imagery which consequently resulted in difficulty in monitoring deltaic changes over time. Thirdly, skilled photogrammetric operators are needed to process and analyze radar imagery, and these skills are not ubiquitous. Fourthly, and most importantly is the utility in distinguishing on-land deltaic features such as crevasse splays and avulsions, especially in complex deltaic regions. Although radar imagery is well utilized in shoreline delineation (see examples in Table 2), there is no conclusive evidence that suggests that radar imagery performs well in comparison to optical imagery in recognizing on-land deltaic features. Thus, given the choice between optical and radar platforms, the rational selection seemed to be optical imagery over the years in most cases. However, with open accessibility policies to radar archives through the Copernicus Program of the European Union, Alaska Satellite Facility and the Japan Aerospace Exploration Agency (JAXA), and training programs/Webinars offered by NASA, European Space Agency and other private institutions, opportunities in relation to feature detection are expected to open into the future.

6. Intercomparison of Delta Morphology Feature Extraction Techniques

One of the more important insights that we draw from the summation of studies is that the review of literature revealed no clear clustering of a particular set of technique(s) that could be used for feature extraction for a particular type of delta (e.g. river-dominated vs. tide-dominated). One or two given techniques which were used to extract a particular morphological feature (e.g. shoreline) of a particular type of delta (e.g. river-dominated delta) was not necessarily ideal for a river dominated delta elsewhere on the earth. This is understandable as deltaic morphology dynamics are driven by many other location/climate related factors (e.g. inherent variability in rainfall, soil minerals, growing cycle phases of vegetation) that make the identification of morphological features even using the same technique complex. We noted that there were not enough comparison studies which 1) compared multiple techniques at a given case study, nor 2) comparisons of even one or two techniques across multiple case studies in different geographical regions of the world. The notion of which technique(s) would be the most appropriate for a given deltaic region would be immensely important for potential future research as these could be used to infer on how to fine tune algorithms to compensate for environmental noise, and subsequently accurately detect deltaic landmass evolution over time. This will help us infer why particular techniques underperform in differentiating earth features in different geographic regions of the world, enabling deeper investigation into some of the inherent problems of particular techniques and provide a platform for their improvement. In addressing this niche, we evaluated seven techniques on ten different river deltas (Amazon, Chao Phraya, Burdekin, Brahmani, Po, Danube, Ebro, Han, Irrawaddy, Colorado) globally, belonging to different river delta types (i.e. river-dominated, tide-dominated, wave-dominated) and representing the different Köppen climate classes.

Five conventional and two ML methods were compared. The conventional methods are: 1) Modified Normalized Difference Water Index (MNDWI), 2) Normalized Difference Water Index (NDWI), 3) PCA analysis, 4) Unsupervised Classification, and 5) Supervised Classification)]. The ML techniques used are: 6) Random Forest Classifier, and 7) Support Vector Machine)]. These seven techniques were selected as they were the most used as per our review. All were compared against hand-digitized vectors (used as a reference baseline) of Landsat-OLI 2018 imagery for the 10 case study deltas (the number of case studies were constrained by the availability of sufficient training data for ML techniques). The accuracy of different indicators of morphology (shoreline, beach spits, mouth bars etc.) were evaluated against the hand-digitizations based on two parameters: a) the continuity of the technique-derived vector to the reference baseline, and b) Proximity of technique-derived vector to the reference baseline. A new robustness index (R) was developed which joins both metrices:

$$R = \frac{L_E * 100 / L_R}{D_{EA}} \quad (1)$$

where L_E is the length of the extracted shoreline, L_R is the length of the real shoreline, and D_{EA} is the averaged perpendicular distance between the extracted and real shoreline. The R index value increases as the shoreline extracted by a given method is closer to the real shoreline in length, whereas robustness decreases as the extracted shoreline is farther away from the real shoreline. Best and worst performing techniques of each delta are summarized in Figure 15 below.

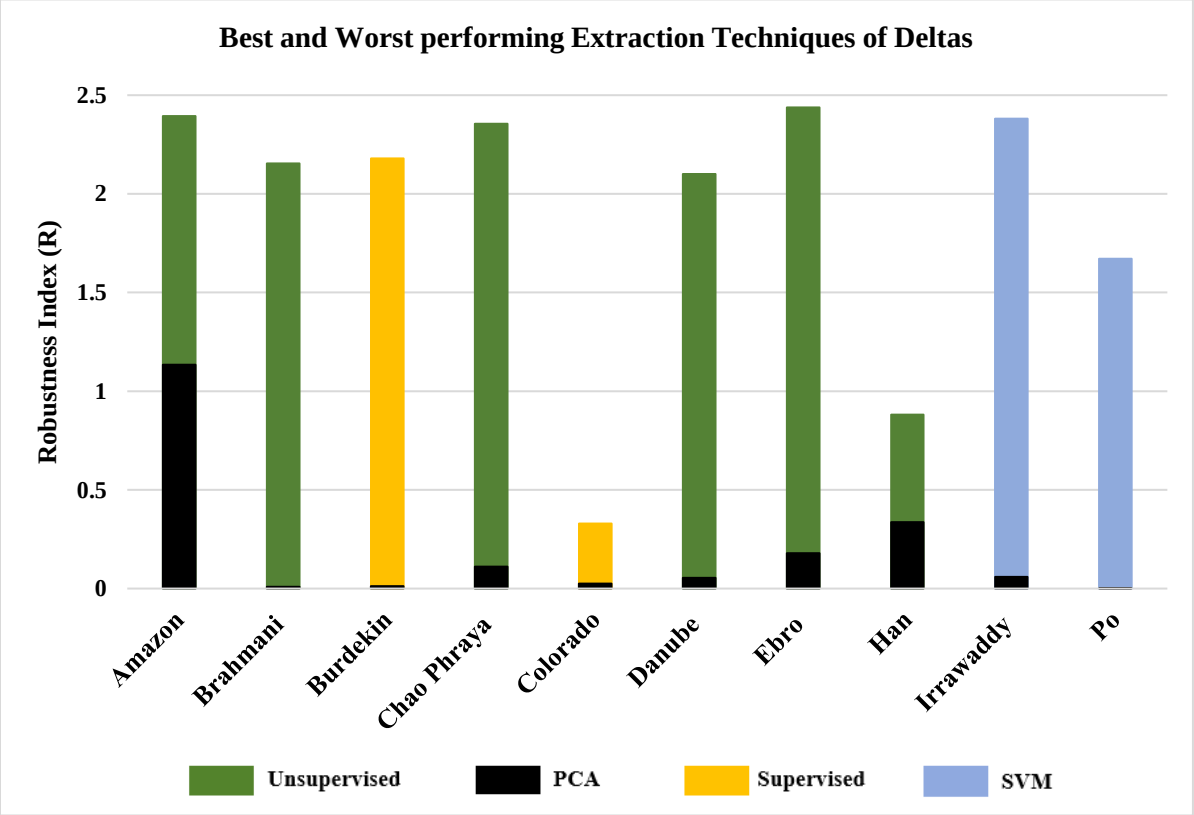

Figure 2.15. A summary of the best and worst performing techniques of the sample deltas.

Analyses show that, except for two cases (the Po and Irrawaddy Deltas), Unsupervised and Supervised Classifications performed the best across all morphology indicators (e.g. beach spits, tombolos, shoreline) (Figure 16). For the Po and Irrawaddy Deltas, the Support Vector Machine algorithm performed the best. PCA ranked the lowest among the techniques for all the deltas, and we attribute these low PCA scores to the non-capture of boundary line land-sea pixels as ‘noise’, from the first few principal components during the transformation process.

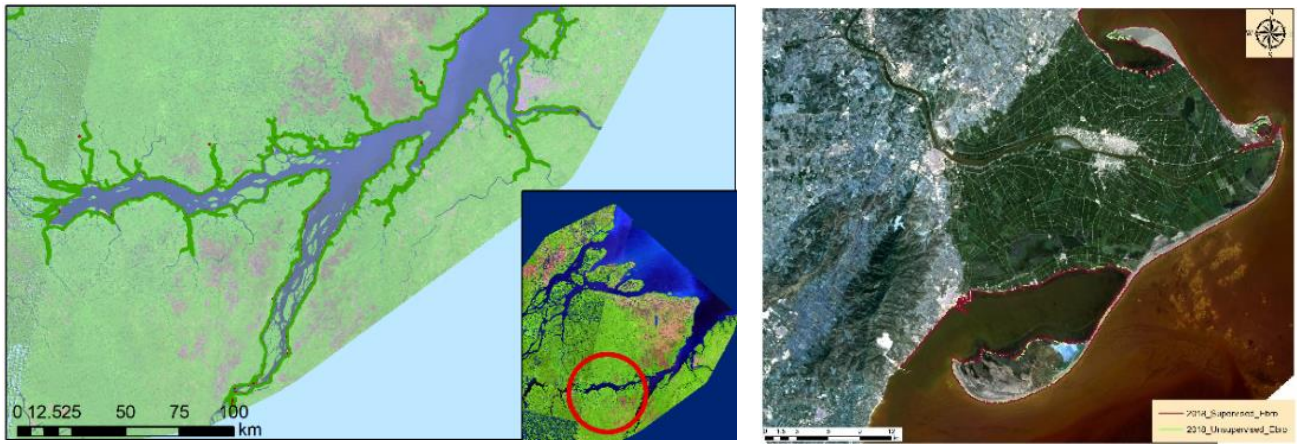

Figure 2.16. Algorithm performance on delta morphology indicators. *left*: the detailed extraction of extensive channel networks of the Amazon river subsequent to unsupervised classification. *Right:* A comparison of vectors of shoreline and beach spit extractions between unsupervised (green) and supervised (red) of the Ebro delta.

However, when the performance of all the techniques were summarized (Table 1) and analyzed for robustness, we find that Unsupervised Classification yielded the best performance on average. A nonparametric ANOVA showed that when all river deltas were considered, Robustness (*R)* values of Unsupervised Classifications were significantly outperforming all the other techniques. SVM, Supervised Classifications, and Random Forest Classifications did not show a significant difference ($\alpha = 0.05$) between each other. The two ratioing techniques' performance also did not have a significant difference between each other ($P=0.79$; $\alpha = 0.05$). All other techniques had significant differences with PCA (Table 1).

Table 2.3. The ranges of the percentage lengths of extracted shorelines, their average distances from the real shoreline and mean robustness values for each technique, for the entire suit of deltas (10) analyzed.

Technique	*Range of L_E (%) (Median in parenthesis)*	*Range of D_{EA} (m) (Median in parenthesis)*	*R* mean
Unsupervised	78-100 (98)	40-239 (45)	1.72
SVM	36-99 (79)	42-340 (60)	1.17
Supervised	56-99 (87)	45-246 (87)	1.14
Random Forest	45-97 (76)	45-471 (78)	0.95
MNDWI	23-79 (50)	78-587 (229)	0.32
NDVI	29-70 (52)	105-623 (172)	0.31
PCA	4-84 (24)	75-2668 (427)	0.19

We did not observe clustering of techniques around delta types, nor between deltas in specific Köppen climate classes. However, it must be noted that these are only a small sample of deltas from each delta type and Köppen category. It was interesting to note how although past literature showed that support vector machines (SVMs) as the best among pixel-based classifications, our comparisons yield mixed outcomes (SVM performing best in only 2 cases out of the 10, and second ranked in all other cases). We attribute this to two reasons: 1) classification algorithm accuracies depend vastly on the resolution of the satellites, and 2) the training data that we used for the SVMs were derived from other satellite products (of higher resolutions than Landsat). The literature review reflects a variety of resolutions and sources as opposed to our use of 30 m Landsat imagery for all the case studies. On the other hand, some studies used in-situ field measurements as training data which likely led to higher classification accuracy. However, given the almost similar accuracies of unsupervised classification and SVM, we recommend the prior (because SVMs require good training data and takes time for algorithm development) for deltaic feature detection based on Landsat imagery.

In a synergistic study, Munasinghe et al. (under review) evaluated five conventional remote sensing techniques (the same as used in this study) on 44 global river deltas worldwide in an attempt to infer on the performance of techniques in shoreline extraction in different types of deltas (River, Tide, Wave-dominated) in different geographic/climatic regions. A major goal of that study was to draw common generalizations and working behaviors of techniques around well-known types of deltas and apply them to lesser studied, data sparse regions. Results showed that unsupervised classification yielded the best performance for the majority of the deltas (35 of 44) whilst supervised classification yielded the best for the remainders (9 of 44). They also found that extraction accuracies were higher in wave dominated deltas, lower for tide-dominated deltas, and moderate for river-dominated deltas. Reasons were attributed to the alongshore sediment transport processes of the wave-dominated deltas, resulting in sandy shorelines which has higher contrast with the less-muddied ocean making it easier for land-water boundary identification. In comparison, sediment-rich murky waters in the nearshore environment governed by the intertidal oscillations in tide-dominated deltas provided less contrast with land. Hence reduced extraction accuracies. Based on results of both these studies, we recommend the use of unsupervised classification as a first order extraction technique for data sparse deltas or previously unstudied deltaic regions.

7. Future Directions

Based on our evaluation of the literature, we see four areas which we deem most opportune for future development:

Direction 1: Utilization of higher resolution imagery and developing better sub-pixel data mining techniques

An important aspect that we recognized earlier was that, compared to shoreline changes, there was a dearth in the number of studies that focused on other environmental indicators of delta morphology change. This was explained by the fact that the shoreline governs the effective landmass that is suitable for human use and is prudent to know the progradation and degradation of a delta against sea level rise and fast changing climatic conditions. Consequently, shoreline change studies, evidently, seem to have greater weightage and research merit than other indicators. We, however, would like to bring out a different perspective to the problem in recognizing that technological limitation is also an important governing factor of these disparate numbers: specifically, the spatial resolutions of earth observing satellites that are used to detect environmental indicators of river delta morphology change.

Detecting the shoreline of a delta, although as described earlier is quite complicated, can be performed relatively well with imagery with moderate spatial resolution (in the range of 30 – 250 m). On the other hand, detecting crevasse splays, channel avulsions and anastomosis of channels with a high level of accuracy, especially in smaller channels and topographically challenging regions, require very high-resolution satellite imagery (below 10 m). The problem is exacerbated if these changes are required to be detected in particularly small deltas, as the background noise from surrounding, non-deltaic, features can heavily influence these analyses.

In the last decade, we experienced a great increase in the availability of higher resolution satellite imagery, primarily through commercial space programs (e.g. Planet Labs, Airbus Defense and Space, Inc.). These sub-meter resolution platforms could be instrumental in detecting intricate deltaic features. Striving for higher resolutions, however, comes at a cost. With an exception of programs that provide conditional access to high resolution satellite archives (e.g. Planet labs), most of these platforms are payment-based, and imagery acquisition

could be a significant proponent of the project budget. Costs also include data storage and purchase and maintenance of high-powered computational systems. Due to exorbitant costs, and also due to limited archival length (since most of these platforms are new, the length of their archives is not sufficient for delta change studies), the usage of higher resolution platforms is still limited in deltaic research. However, it can be expected that, as time progresses, the use of these platforms will increase dramatically.

In the meantime, fusion of high and medium resolution imagery for detecting fine resolution deltaic features is one promising way forward. Image fusion and the consequent overall increase in resolution presents a solution to another problem: presence of mixed pixels in shoreline classification. As described earlier, this issue has been recognized as a major problem influencing the accuracy of remote-sensing image classification (Liu *et al.*, 2016). Theoretically, with improvements in imagery spatial resolution, the number of mixed pixels will be greatly decreased (Wu, 2009).

There is also great potential in developing novel data mining algorithms, especially sub-pixel algorithms (which have historically shown success in the literature) that can be used with already existing moderate spatial resolution platforms. Examples of such algorithms, which were recently applied to delta morphology studies, include the grid-based colocation pattern mining technique (Sainju and Zhang, 2017), Spectral Unmixing Algorithm Based on Distance Geometry (Pu *et al.*, 2013), and the use of colorimetry to estimate the proportion of classes in mixed pixels (Suresh and Jain, 2018). Finding solutions to sub-pixel information will not only help advance morphological science forward but could also provide great impetus to the studies that will be forthcoming using high resolution satellite imagery.

Direction 2: Use of automated pattern recognition techniques, universal applicability and algorithm transferability across platforms

Although there exist several manual/semi-automated methods to extract information from satellite imagery as discussed in the sections above, we see great advantages in extraction of information though automated techniques for change detection which could reduce the errors due to operator bias and more efficiently partition and recognize patterns and relationships in datasets.

In this context, we think that "Smart Data Discovery - the idea of automating the identification of patterns and trends in large data sets" (Sallam *et al.,* 2017) - can play an important role in feature extraction from satellite big data. Smart data discovery is currently used increasingly in the business intelligence sector in making informed market decisions (Sallam *et al.,* 2017). We think however, that there is great potential for this technique in the domain of satellite remote sensing to prepare and cleanse data more intelligently, automatically find hidden patterns and correlations in data, especially where traditional and even semi-automatic machine learning techniques are expensive, difficult and time intensive to implement.

Algorithms that we develop also need to be near-universally applicable. Localized algorithms which work perfectly in one particular region or for a particular size and type of delta often do not perform well in other locations and is thus of relatively limited use elsewhere. For the holistic study of Earth's geomorphology and its evolution, continental deltaic dynamics is warranted. There is importance of looking at how these landforms change at large scales prompting the need for universal techniques. Such techniques are unfortunately yet to be developed.

It is to be expected that the number of remote sensing applications of delta morphology analysis will increase in the near future due to continued extensions of freely-available satellite imagery archives (e.g. Landsat, MODIS), and increased availability of higher resolution imagery via commercial and government platforms. It is therefore important to promote algorithm developments with the capability to be transferred across platforms (e.g. to efficiently upscale and downscale information from different spatial resolutions). This will enhance their longevity and utility to the entire constellation of satellites.

Direction 3: Improvement of ancillary data

In our and others' view, inclusion of additional explanatory variables that can differentiate spectral classes is more promising than enhancement of the image processing technique alone (Khatami *et al.,* 2016). Common examples include topographic data such as digital elevation models, slope, aspect layers, geological layers, data from active sensors such as synthetic aperture radar or LiDAR, data from passive sensors, data from different temporal rates of phenological changes in vegetation mapping, and anisotropy of land surface reflectance. The inclusion of such data gives additional data layers of information that can be utilized in the problem-solving framework (e.g. Figure 7: The additional information that contributes to the understanding of deltaic evolution) to solve for the complexities of the deltaic environment more easily.

There exist challenges, however, in collecting ancillary data. Firstly, there is a regional disparity in the quantity of data collected. Although data is abundantly collected and housed in most of the economically developed countries of the world, data collection is sparse in developing countries. Second is the bureaucracy of organizations which own these data. The lack of open data policies makes it difficult for researchers to access them. Thirdly, the culture of data

sharing among researchers. Research culture should orient itself in a direction of openly sharing data subsequent to your own research for other interested parties to build up on. This culture is gathering momentum through public platforms like GitHub, researchgate, HydroShare, and stack exchanges. We envision the need for more subject-specific research repositories.

Direction 4: A Global Information System of deltaic data

One of the major challenges for researchers working in the domain of deltaic remote sensing is that there is a lack of ground truth data to validate their observations against. On the other hand, field geomorphologists, who base their research efforts on identifying changes in deltaic features on a local scale, would immensely benefit from the "bigger picture" of the deltaic domain from the remote sensing community. One of the major challenges has been to build a data sharing bridge between these two communities. There currently exists no portal/database/repository which offers different types of data in relation to deltaic research. A repository for river deltaic research similar to, for example, HydroShare should be established. HydroShare (Tarboton *et al.*, 2014), operated by the Consortium of Universities for the Advancement of Hydrologic Science, Inc. (CUAHSI), is an online collaboration environment for sharing data, models, and code related to hydrology. A delta repository could (conceptually) include field data (e.g. soil types, point climate data, different land use types) collected by field researchers, remotely sensed data (e.g. locations and extents of deltaic features, land use class delineations, temporal change of features), different numerical models which model deltaic features (e.g. crevasse splays, avulsions, shoreline changes), and publicly volunteered and vetted geographic information. We believe that such a repository will foster collaborative and interdisciplinary research and help to propel deltaic research to the next level.

8. Conclusions

River deltas are important landforms that serve many societal and ecological functions. Assessing changes to delta morphology is important to identify vulnerable areas and sustainably manage deltaic land. Satellite remote sensing provides an effective way of detecting delta morphology change over time.

This review focused on Remote Sensing Techniques that are used in detecting delta morphology change. We discussed 18 such techniques, their strengths and their caveats with regard to deltaic feature extraction and change detection. The review of literature suggests that sub-pixel algorithms such as spectral mixture analysis and fuzzy logic yield very high accuracies, while machine learning techniques ranked second. Support Vector Machines rank as the best individual machine learning technique across reviewed literature. We also found that the use of an ensemble of techniques (a machine learning technique ensemble, or a mix of machine learning and conventional ones) yields high accuracies.

The choice of the technique(s) that one should preferably use to extract features of a river delta is governed primarily by the complexity of the delta. Simple deltas can be analyzed using relatively simple techniques and vice versa. We also found that the choice of technique depends on how data intensive the algorithm is, the availability of resources (time and computational resource), and the skill level of the user (e.g. machine learning applications requires specific skillsets). A comparison study performed between ten deltas using seven algorithms yielded unsupervised classification as the go-to method for quick and robust delta-morphology-indicator detection.

We discuss the pathway forward for future research by recognizing the utility of using different delta morphology remote sensing techniques on one particular river delta to gain a

better understanding of its landmass evolution, and also of the importance of comparison studies across deltas to infer on the similarities/dissimilarities of morphological changes and identify strengths limitations of remote sensing techniques themselves in different geographic/climatic conditions.

Four directions in which how future research will benefit are presented. The importance of higher spatial resolutions and the need for the development of more robust sub-pixel detection algorithms to mine data from moderate resolution imagery to more accurately infer on deltaic features such as smaller channel avulsions and formation of splays, is highlighted. The importance of automated pattern recognition techniques, universal applicability of algorithms, and algorithm-transferability across platforms are discussed. Thirdly, the effective use of ancillary data to make better judgement calls during the deltaic feature extraction process are brought forth, and finally, the concept of a repository which houses different types of data and models pertaining to deltaic research which is envisioned to foster interdisciplinary collaboration are opined.

9. References for Chapter 2

Adams, J.B., Sabol, D.E., Kapos, V., Almeida Filho, R., Roberts, D.A., Smith, M.O., Gillespie, A.R., 1995. Classification of multispectral images based on fractions of endmembers: Application to land-cover change in the Brazilian Amazon. Remote sensing of Environment, 52(2), 137-154. https://doi.org/10.1016/0034-4257(94)00098-8

Adam, E M., Mutanga, O., Rugege, D., Ismail, R., 2012. Discriminating the papyrus vegetation (Cyperus papyrus L.) and its co-existent species using random forest and hyperspectral data resampled to HYMAP. International Journal of Remote Sensing, 33(2), 552-569. https://doi.org/10.1080/01431161.2010.543182

Adegoke, J.O., Fageja, M., James, G., Agbaje, G., Ologunorisa, T.E., 2010. An assessment of recent changes in the Niger Delta coastline using satellite imagery. Journal of Sustainable Development, 3(4), 277. https://doi.org/10.5539/jsd.v3n4p277

Ahmed, A., Drake, F., Nawaz, R., Woulds, C., 2018. Where is the coast? Monitoring coastal land dynamics in Bangladesh: An integrated management approach using GIS and remote sensing techniques. Ocean & Coastal Management, 151, 10-24. https://doi.org/10.1016/j.ocecoaman.2017.10.030

Akar, Ö., and Güngör, O., 2015. Integrating Multiple Texture Methods and NDVI to the Random Forest Classification Algorithm to Detect Tea and Hazelnut Plantation Areas in Northeast Turkey. International Journal of Remote Sensing 36(2): 442–464. https://doi.org/10.1080/01431161.2014.995276

Alesheikh, A.A., Ghorbanali, A., Nouri, N., 2007. Coastline change detection using remote sensing. International Journal of Environmental Science & Technology, 4(1), 61-66. https://doi.org/10.1007/BF03325962

Al Fugura, A., Billa, L., Pradhan, B., 2011. Semi-automated procedures for shoreline extraction using single RADARSAT-1 SAR image. Estuarine, Coastal and Shelf Science, 95(4), 395-400. https://doi.org/10.1016/j.ecss.2011.10.009

Allen, Y. C., Couvillion, B. R., Barras, J. A., 2012. Using multitemporal remote sensing imagery and inundation measures to improve land change estimates in coastal wetlands. Estuaries and Coasts, 35(1), 190-200. https://doi.org/10.1007/s12237-011-9437-z

Allison, M.A., Khan, S.R., Goodbred Jr, S.L., Kuehl, S.A., 2003. Stratigraphic evolution of the late Holocene Ganges–Brahmaputra lower delta plain. Sedimentary Geology, 155(3-4), 317-342. https://doi.org/10.1016/S0037-0738(02)00185-9

Banks, S., Millard, K., Pasher, J., Richardson, M., Wang, H., Duffe, J., 2015. Assessing the potential to operationalize shoreline sensitivity mapping: Classifying multiple Wide Fine Quadrature Polarized RADARSAT-2 and Landsat 5 scenes with a single Random Forest model. Remote Sensing, 7(10), 13528-13563. https://doi.org/10.3390/rs71013528

Bayarjargal, Y., Karnieli, A., Bayasgalan, M., Khudulmur, S., Gandush, C., Tucker, C.J., 2006. A comparative study of NOAA–AVHRR derived drought indices using change vector analysis. Remote Sensing of Environment, 105(1), 9-22. https://doi.org/10.1016/j.rse.2006.06.003

Bayram, B., Acar, U., Seker, D., Ari, A., 2008. A novel algorithm for coastline fitting through a case study over the Bosphorus. Journal of Coastal Research, 983-991. https://doi.org/10.2112/07-0825.1

Bendsen, H., Meyer, T., 2002. The dynamics of land use systems in Ngamiland: Changing livelihood options and strategies. In: Environmental Monitoring of Tropical Wetlands, Proceedings of a Wetland Conference, Maun, Botswana (pp. 278-304).

Berberoglu, S., Lloyd, C.D., Atkinson, P.M., Curran, P.J., 2000. The integration of spectral and textural information using neural networks for land cover mapping in the Mediterranean. Computers & Geosciences, 26(4), 385-396. https://doi.org/10.1016/S0098-3004(99)00119-3

Berhane, T., Lane, C., Wu, Q., Autrey, B., Anenkhonov, O., Chepinoga, V., Liu, H., 2018. Decision-tree, rule-based, and random forest classification of high-resolution multispectral imagery for wetland mapping and inventory. Remote sensing, 10(4), 580. https://doi.org/10.3390/rs10040580

Blaschke, T., 2010. Object based image analysis for remote sensing. ISPRS Journal of Photogrammetry and Remote Sensing, 65(1), 2–16. https://doi.org/10.1016/j.isprsjprs.2009.06.004

Braud, D.H., Feng, W., 1998. Semi-automated construction of the Louisiana coastline digital land/water boundary using Landsat Thematic Mapper satellite imagery (Department of Geography and Anthropology, Louisiana State University, Louisiana Applied Oil Spill Research and Development Program), OSRAPD Technical Report. 97-002.

Breiman, L., 2001. Random forests. Machine learning, 45(1), 5-32. https://doi.org/10.1023/A:1010933404324

Buono, A., Nunziata, F., Migliaccio, M., Yang, X., Li, X., 2017. Classification of the Yellow River delta area using fully polarimetric SAR measurements. International journal of remote sensing, 38(23), 6714-6734. https://doi.org/10.1080/01431161.2017.1363437

Cao, M., Liu, G., Zhang, X., 2007. An object-oriented approach to map wetland vegetation: a case study of yellow river delta. In 2007 IEEE International Geoscience and Remote Sensing Symposium. pp 4585-4587.

Chen, J., Gong, P., He, C., Pu, R., Shi, P., 2003. Land-use/land-cover change detection using improved change-vector analysis. Photogrammetric Engineering & Remote Sensing, 69(4), 369-379. https://doi.org/10.14358/PERS.69.4.369

Chen, C., Fu, J., Zhang, S., Zhao, X., 2019. Coastline information extraction based on the tasseled cap transformation of Landsat-8 OLI images. Estuarine, Coastal and Shelf Science, 217, 281-291. https://doi.org/10.1016/j.ecss.2018.10.021

Chu, Z.X., Sun, X.G., Zhai, S.K., Xu, K.H., 2006. Changing pattern of accretion/erosion of the modern Yellow River (Huanghe) subaerial delta, China: Based on remote sensing images. Marine Geology, 227(1-2), 13-30. https://doi.org/10.1016/j.margeo.2005.11.013

Ciavola, P., 1999. Relation between river dynamics and coastal changes in Albania: an assessment integrating satellite imagery with historical data. International Journal of Remote Sensing, 20(3), 561-584. https://doi.org/10.1080/014311699213343

Civco, D.L., Hurd, J.D., Wilson, E.H., Song, M., Zhang, Z., 2002. A comparison of land use and land cover change detection methods. In ASPRS-ACSM Annual Conference (Vol. 21).

Cohen, W.B., Fiorella, M., Gray, J., Helmer, E., Anderson, K., 1998. An efficient and accurate method for mapping forest clearcuts in the Pacific Northwest using Landsat imagery. Photogrammetric Engineering and Remote Sensing, 64(4), 293-299.

Coleman, J.M., Wright, L.D., 1975. Modern river deltas: variability of processes and sand bodies. In: Broussard M.L., Deltas: models for Exploration. Houston Geological Society. pp. 99-149.

Congalton, R.G., 1991. A review of assessing the accuracy of classifications of remotely sensed data. Remote sensing of environment, 37(1), 35-46.

Crist, E.P., 1985. A TM tasseled cap equivalent transformation for reflectance factor data. Remote Sensing of Environment, 17(3), 301-306.

Cui, B. L., Li, X. Y., 2011. Coastline change of the Yellow River estuary and its response to the sediment and runoff (1976–2005). Geomorphology, 127(1-2), 32-40. https://doi.org/10.1016/j.geomorph.2010.12.001

Dada, O. A., Li, G., Qiao, L., Asiwaju-Bello, Y. A., Anifowose, A. Y. B., 2018. Recent Niger Delta shoreline response to Niger River hydrology: Conflict between forces of Nature and Humans. Journal of African Earth Sciences, 139, 222-231. https://doi.org/10.1016/j.jafrearsci.2017.12.023

Da Silva, A. G. A., Stattegger, K., Vital, H., & Schwarzer, K. (2019). Coastline change and offshore suspended sediment dynamics in a naturally developing delta (Parnaíba Delta, NE Brazil). Marine Geology, 410, 1-15. https://doi.org/10.1016/j.margeo.2018.12.013

Del Frate, F., Latini, D., Minchella, A., Palazzo, F., 2012. A new automatic technique for coastline extraction from SAR images. In: SAR Image Analysis, Modeling, and Techniques XII (Vol. 8536, p. 85360R). International Society for Optics and Photonics.

Dellepiane, S., De Laurentiis, R., Giordano, F., 2004. Coastline extraction from SAR images and a method for the evaluation of the coastline precision. Pattern Recognition Letters, 25(13), 1461-1470. https://doi.org/10.1016/j.patrec.2004.05.022

Demers, A.M., Banks, S.N., Pasher, J., Duffe, J., Laforest, S., 2015. A comparative analysis of object-based and pixel-based classification of RADARSAT-2 C–band and optical satellite data for mapping shoreline types in the Canadian arctic. Canadian Journal of Remote Sensing, 41(1), 1-19. https://doi.org/10.1080/07038992.2015.1020361

Deng, J.S., Wang, K., Deng, Y.H., Qi, G.J., 2008. PCA-based land-use change detection and analysis using multitemporal and multisensor satellite data. International Journal of Remote Sensing, 29(16), 4823-4838. https://doi.org/10.1080/01431160801950162

Denison, D.G., Mallick, B.K., Smith, A.F., 1998. A bayesian CART algorithm. Biometrika, 85(2), 363-377. https://doi.org/10.1093/biomet/85.2.363

Dewi, R., Bijker, W., Stein, A., Marfai, M., 2016. Fuzzy classification for shoreline change monitoring in a part of the northern coastal area of Java, Indonesia. Remote sensing, 8(3), 190. https://doi.org/10.3390/rs8030190

Ding, W.J., Wang, R.Q., Wu, D.Q., Liu, J., 2013. Cellular automata model as an intuitive approach to simulate complex land-use changes: an evaluation of two multi-state land-use models in the Yellow River Delta. Stochastic Environmental Research and Risk Assessment, 27(4), 899-907. https://doi.org/10.1007/s00477-012-0624-7

Ekercin, S., 2007. Coastline change assessment at the Aegean Sea coasts in Turkey using multitemporal Landsat imagery. Journal of Coastal Research, 691-698. https://doi.org/10.2112/04-0398.1

El-Asmar, H.M., Hereher, M.E., 2011. Change detection of the coastal zone east of the Nile Delta using remote sensing. Environmental Earth Sciences, 62(4), 769-777. https://doi.org/10.1007/s12665-010-0564-9

Elhag, M., Psilovikos, A., Sakellariou-Makrantonaki, M., 2013. Land use changes and its impacts on water resources in Nile Delta region using remote sensing techniques. Environment, Development and Sustainability, 15(5), 1189-1204. https://doi.org/10.1007/s10668-013-9433-5

El-Kawya, O.A., Rød, J.K., Ismail, H.A., Suliman, A.S., 2011. Land use and land cover change detection in the western Nile delta of Egypt using remote sensing data. Applied Geography, 31(2), 483-494. https://doi.org/10.1016/j.apgeog.2010.10.012

El Raey, M., Nasr, S.M., Frihy, O.E., El Hattab, M.M., 1995. Change detection of Rosetta promontory over the last forty years. International Journal of Remote Sensing, 16, 825-834 https://doi.org/10.1080/01431169508954446

El-Raey, M., El-Din, S.S., Khafagy, A.A., Abo Zed, A.I., 1999. Remote sensing of beach erosion/accretion patterns along Damietta-Port Said shoreline, Egypt. International Journal of Remote Sensing, 20(6), 1087-1106. https://doi.org/10.1080/014311699212867

Elliott T., 1986. Deltas. In: Reading H.G. (Ed.) Sedimentary Environments and Facies, Blackwell Scientific Publications, Oxford, pp. 113-154.

Enderle, D.I., Weih Jr, R.C., 2005. Integrating supervised and unsupervised classification methods to develop a more accurate land cover classification. Journal of the Arkansas Academy of Science, 59(1), 65-73.

Foody, G.M., McCulloch, M.B., Yates, W.B., 1995. Classification of Remotely Sensed Data by an Artificial Neural Network: Issues Related to Training Data. Photogrammetric Engineering & Remote Sensing, 61(4), 391-401.

Foody, G.M., Mathur, A., 2006. The use of small training sets containing mixed pixels for accurate hard image classification: Training on mixed spectral responses for classification by a SVM. Remote sensing of Environment, 103(2), 179-189. https://doi.org/10.1016/j.rse.2006.04.001

Foody, G.M., Muslim, A.M., Atkinson, P.M., 2005. Super-resolution mapping of the waterline from remotely sensed data. International Journal of Remote Sensing, 26(24), 5381-5392. https://doi.org/10.1080/01431160500213292

Frazier, P.S., Page, K.J., 2000. Water body detection and delineation with Landsat TM data, Photogrammetric Engineering & Remote Sensing, 66 (2), 1461-1467.

Friedl, M.A., Brodley, C.E., 1997. Decision tree classification of land cover from remotely sensed data. Remote sensing of Environment, 61(3), 399-409. https://doi.org/10.1016/S0034-4257(97)00049-7

Frihy, O.E., Dewidar, K.M., Nasr, S.M., El Raey, M.M., 1998. Change detection of the northeastern Nile Delta of Egypt: shoreline changes, Spit evolution, margin changes of Manzala lagoon and its islands. International Journal of Remote Sensing, 19(10), 1901-1912. https://doi.org/10.1080/014311698215054

Frohn, R.C., D'Amico, E., Lane, C., Autrey, B., Rhodus, J., Liu , H., 2012. Multi-temporal sub-pixel Landsat ETM+ classification of isolated wetlands in Cuyahoga County, Ohio, USA. Wetlands, 32(2), 289-299. https://doi.org/10.1007/s13157-011-0254-8

Ghanavati, E., Firouzabadi, P.Z., Jangi, A.A., Khosravi, S., 2008. Monitoring geomorphologic changes using Landsat TM and ETM+ data in the Hendijan River delta, southwest Iran. International Journal of Remote Sensing, 29(4), 945-959. https://doi.org/10.1080/01431160701294679

Ghoneim, E., Mashaly, J., Gamble, D., Halls, J., AbuBakr, M., 2015. Nile Delta exhibited a spatial reversal in the rates of shoreline retreat on the Rosetta promontory comparing pre-

and post-beach protection. Geomorphology, 228, 1-14. https://doi.org/10.1016/j.geomorph.2014.08.021

Gislason, P.O., Benediktsson, J.A., Sveinsson, J.R., 2006. Random forests for land cover classification. Pattern Recognition Letters, 27(4), 294-300. https://doi.org/10.1016/j.patrec.2005.08.011

Gong, P., 1993. Change detection using Principal Component Analysis and Fuzzy set theory. Canadian Journal of Remote Sensing, 19(1), 22-29. https://doi.org/10.1080/07038992.1993.10855147

Gopinath, G., Seralathan, P., 2005. Rapid erosion of the coast of Sagar island, West Bengal-India. Environmental Geology, 48(8), 1058-1067. https://doi.org/10.1007/s00254-005-0044-9

Gou, S., Li, X., Yang, X., 2016. Coastal zone classification with fully polarimetric SAR imagery. IEEE Geoscience and Remote Sensing Letters, 13(11), 1616-1620. https://doi.org/10.1109/LGRS.2016.2597965

Guariglia, A., Buonamassa, A., Losurdo, A., Saladino, R., Trivigno, M.L., Zaccagnino, A., Colangelo, A., 2006. A multisource approach for coastline mapping and identification of shoreline changes. Annals of geophysics, 49(1).

Gugliotta, M., Saito, Y., 2019. Matching trends in channel width, sinuosity, and depth along the fluvial to marine transition zone of tide-dominated river deltas: The need for a revision of depositional and hydraulic models. Earth-science reviews. https://doi.org/10.1016/j.earscirev.2019.02.002

Gutierrez, B.T., Plant, N.G., Thieler, E.R., 2011. A Bayesian network to predict coastal vulnerability to sea level rise. Journal of Geophysical Research: Earth Surface, 116(F2). https://doi.org/10.1029/2010JF001891

Haas, J., Ban,Y., 2014. Urban growth and environmental impacts in Jing-Jin-Ji, the Yangtze, River Delta and the Pearl River Delta. International Journal of Applied Earth Observation and Geoinformation, 30, 42-55. https://doi.org/10.1016/j.jag.2013.12.012

Heimann, T., Thorn, M., Kunert, T., Meinzer, H.P., 2004. New methods for leak detection and contour correction in seeded region growing segmentation. In 20th ISPRS Congress, Istanbul (Vol. 35, pp. 317-322).

Heumann, B.W., 2011. An object-based classification of mangroves using a hybrid decision tree—Support vector machine approach. Remote Sensing, 3(11), 2440-2460. https://doi.org/10.3390/rs3112440

Huang, Z., Lees, B.G., 2004. Combining non-parametric models for multisource predictive forest mapping. Photogrammetric Engineering and Remote Sensing, 70(4), pp. 415–425. https://doi.org/10.14358/PERS.70.4.415

Hutchings, R.M., Campbell, S.K., 2005. The Importance of Deltaic Wetland Resources: A Perspective from the Nooksack River Delta, Washington State. Journal of Wetland Archaeology, 5(1): 17-34. https://doi.org/10.1179/jwa.2005.5.1.17

Isikdogan, F., Bovik, A., Passalacqua, P., 2015. Automatic channel network extraction from remotely sensed images by singularity analysis. IEEE Geoscience and Remote Sensing Letters, 12(11), 2218-2221. https://doi.org/10.1109/LGRS.2015.2458898

Jarvis, C.H., Stuart, N., 1996. The sensitivity of a neural network for classifying remotely sensed imagery. Computers & Geosciences, 22(9), 959-967. https://doi.org/10.1016/S0098-3004(96)00034-9

Jensen, J.R., 1996. Introductory Digital Image Processing: A Remote Sensing Perspective, 2nd Edition, Englewood Cliffs, NJ: Prentice-Hall.

Kamal, M., Phinn, S., 2011. Hyperspectral data for mangrove species mapping: A comparison of pixel-based and object-based approach. Remote Sensing, 3(10), 2222–2242. https://doi.org/10.3390/rs3102222

Kargel, J.S., Kirk, R.L., Fegley Jr, B., Treiman, A.H., 1994. Carbonate-sulfate volcanism on Venus?. Icarus, 112(1), 219-252. https://doi.org/10.1006/icar.1994.1179

Kelley, G.W., Hobgood, J.S., Bedford, K.W., Schwab D.J., 1998. Generation of three-dimensional lake model forecasts for Lake Erie, Weather and Forecasting, 13(3), 305-315. https://doi.org/10.1175/1520-0434(1998)013<0659:GOTDLM>2.0.CO;2

Khatami, R., Mountrakis, G., Stehman, S.V., 2016. A meta-analysis of remote sensing research on supervised pixel-based land-cover image classification processes: General guidelines for practitioners and future research. Remote Sensing of Environment, 177, 89-100. https://doi.org/10.1016/j.rse.2016.02.028

Kim, M., Warner, T.A., Madden, M., Atkinson, D.S., 2011. Multi-scale GEOBIA with very high spatial resolution digital aerial imagery: Scale, texture and image objects. International Journal of Remote Sensing, 32(10), 2825–2850. https://doi.org/10.1080/01431161003745608

Kong, D., Miao, C., Borthwick, A.G., Duan, Q., Liu, H., Sun, Q., Ye, A., Di, Z., Gong, W., 2015. Evolution of the Yellow River Delta and its relationship with runoff and sediment load from 1983 to 2011. Journal of Hydrology, 520, 157-167. https://doi.org/10.1016/j.jhydrol.2014.09.038

Krause, G., Bock, M., Weiers, S., Braun, G., 2004. Mapping land-cover and mangrove structures with remote sensing techniques: A contribution to a synoptic GIS in support of coastal management in North Brazil. Environ. Manage., 34(3), 429–440. https://doi.org/10.1007/s00267-004-0003-3

Kuenzer, C., van Beijma, S., Gessner, U., Dech, S., 2014. Land surface dynamics and environmental challenges of the Niger Delta, Africa: Remote sensing-based analyses

spanning three decades (1986–2013). Applied Geography, 53, 354-368. https://doi.org/10.1016/j.apgeog.2014.07.002

Kuleli, T., 2010. Quantitative analysis of shoreline changes at the Mediterranean Coast in Turkey. Environmental monitoring and assessment, 167(1-4), 387-397. https://doi.org/10.1007/s10661-009-1057-8

Kundu, S., Mondal, A., Khare, D., Mishra, P.K., Shukla, R., 2014. Shifting shoreline of Sagar Island Delta, India. Journal of maps, 10(4), 612-619. https://doi.org/10.1080/17445647.2014.922131

Kushwaha, S.P.S., Dwivedi, R.S., Rao, B.R.M., 2000. Evaluation of various digital image processing techniques for detection of coastal wetlands using ERS-1 SAR data. International Journal of Remote Sensing, 21(3), 565-579. https://doi.org/10.1080/014311600210759

Le, M. H., Hitoshi, T., Nguyen, T. T., Nguyen, T.V., 2006. Prediction of river bank erosion in the lower Mekong river delta. In Vietnam-Japan Estuary workshop, Hanoi, Vietnam. pp. 22-24.

Le Moigne, J., Tilton, J.C., 1995. Refining image segmentation by integration of edge and region data. IEEE Transactions on Geoscience and Remote Sensing, 33(3), 605-615. https://doi.org/10.1109/36.387576

Le, T.V.H., Nguyen, H. N., Wolanski, E., Tran, T.C., Haruyama, S., 2007. The combined impact on the flooding in Vietnam's Mekong River delta of local man-made structures, sea level rise, and dams upstream in the river catchment. Estuarine, Coastal and Shelf Science, 71(1-2), 110-116. https://doi.org/10.1016/j.ecss.2006.08.021

Lee, K.S., Kim, T.H., Yun, Y.S., Shin, S.M., 2001. Spectral characteristics of shallow turbid water near the shoreline on inter-tidal flat. Korean Journal of Remote Sensing, 17(2), 131–139.

Lee, J. S., Jurkevich, I., 1990. Coastline detection and tracing in SAR images. IEEE Transactions on Geoscience and Remote Sensing, 28(4), 662-668. https://doi.org/10.1109/TGRS.1990.572976

Lentz, E. E., Thieler, E.R., Plant, N.G., Stippa, S.R., Horton, R.M., Gesch, D.B., 2016. Evaluation of dynamic coastal response to sea-level rise modifies inundation likelihood. Nature Climate Change, 6(7), 696. https://doi.org/10.1038/nclimate2957

Li, H.T., Gu, H.Y., Han, Y.S., Yang, J., 2010. Object-oriented classification of high-resolution remote sensing imagery based on an improved colour structure code and a support vector machine. International Journal of Remote Sensing, 31(6), 1453-1470. https://doi.org/10.1080/01431160903475266

Li, J., Donselaar, M. E., Aria, S.E.H., Koenders, R., Oyen, A.M., 2014. Landsat imagery-based visualization of the geomorphological development at the terminus of a dryland river

system. Quaternary international, 352, 100-110. https://doi.org/10.1016/j.quaint.2014.06.041

Li, J., Bristow, C.S., 2015. Crevasse splay morphodynamics in a dryland river terminus: Río Colorado in Salar de Uyuni Bolivia. Quaternary International, 377, 71-82. https://doi.org/10.1016/j.quaint.2014.11.066

Li, X., Yeh, A.G.O., 1998. Principal component analysis of stacked multi-temporal images for the monitoring of rapid urban expansion in the Pearl River Delta. International Journal of Remote Sensing, 19(8), 1501-1518. https://doi.org/10.1080/014311698215315

Li, X., Yeh, A. G. O., 2004. Analyzing spatial restructuring of land use patterns in a fast growing region using remote sensing and GIS. Landscape and Urban planning, 69(4), 335-354. https://doi.org/10.1016/j.landurbplan.2003.10.033

Liu, G., Zhang, L., Zhang, Q., Musyimi, Z., Jiang, Q., 2014. Spatio–temporal dynamics of wetland landscape patterns based on remote sensing in Yellow River Delta, China. Wetlands, 34(4), 787-801. https://doi.org/10.1007/s13157-014-0542-1

Liu, J., Feng, Q., Gong, J., Zhou, J., Li, Y., 2016. Land-cover classification of the Yellow River Delta wetland based on multiple end-member spectral mixture analysis and a Random Forest classifier. International Journal of Remote Sensing, 37(8), 1845-1867. https://doi.org/10.1080/01431161.2016.1165888

Liu, X., Deng, R., Xu, J., Zhang, F., 2017. Coupling the modified linear spectral mixture analysis and pixel-swapping methods for improving subpixel water mapping: Application to the Pearl River Delta, China. Water, 9(9), 658. https://doi.org/10.3390/w9090658

Lohani B., Mason D.C., 1999. Construction of a digital elevation model of the Holderness Coast using the waterline method and Air-borne Thematic Mapper data. International Journal of Remote Sensing, 20(3): 593–607 https://doi.org/10.1080/014311699213361

Lodhi, M.A., Rundquist, D.C., Han, L., Juzila, M.S., 1997. The potential for remote sensing of loess soils suspended in surface water. Journal of the American Water Resources Association, 33(1), 111–127. https://doi.org/10.1111/j.1752-1688.1997.tb04087.x

Loos, E.A., Niemann, K.O., 2002. Shoreline feature extraction from remotely sensed imagery. In: International Geoscience and remote sensing symposium, 2002. IEEE Int. 6 (24–28), 3417–3419. https://doi.org/10.1109/IGARSS.2002.1027201

Louati, M., Saïdi, H., Zargouni, F., 2015. Shoreline change assessment using remote sensing and GIS techniques: a case study of the Medjerda delta coast, Tunisia. Arabian Journal of Geosciences, 8(6), 4239-4255. https://doi.org/10.1007/s12517-014-1472-1

Lu, D., Moran, E., Batistella, M., 2003. Linear mixture model applied to Amazonian vegetation classification. Remote Sensing of Environment, 87(4), 456–469. https://doi.org/10.1016/j.rse.2002.06.001

Lu, D., Mausel, P., Batistella, M., Moran, E., 2004. Comparison of land-cover classification methods in the Brazilian Amazon Basin. Photogrammetric Engineering and Remote Sensing, 70(6), 723–731. https://doi.org/10.14358/PERS.70.6.723

Maiti, S., Bhattacharya, A.K., 2009. Shoreline change analysis and its application to prediction: A remote sensing and statistics based approach. Marine Geology, 257(1-4), 11-23. https://doi.org/10.1016/j.margeo.2008.10.006

Mallinis, G., Emmanoloudis, D., Giannakopoulos, V., Maris, F., Koutsias, N., 2011. Mapping and interpreting historical land cover/land use changes in a Natura 2000 site using earth observational data: the case of Nestos delta, Greece. Applied Geography, 31(1), 312-320. https://doi.org/10.1016/j.apgeog.2010.07.002

Malthus, T.J., Mumby, P.J., 2003. Remote sensing of the coastal zone: an overview and priorities for future research. International Journal of Remote Sensing, 24, 2805–2815. https://doi.org/10.1080/0143116031000066954

Manavalan, P., Sathyanath, P., Rajegowda, G. L., 1993. Digital image analysis techniques to estimate waterspread for capacity evaluations of reservoirs. Photogrammetric Engineering and Remote Sensing, 59(9), 1389–1395.

Marghany, M., Sabu, Z., Hashim, M., 2010. Mapping coastal geomorphology changes using synthetic aperture radar data. International Journal of Physical Sciences, 5(12), 1890-1896.

Mas, J. F., 1999. Monitoring land-cover changes: a comparison of change detection techniques. International Journal of Remote Sensing, 20(1), 139-152. https://doi.org/10.1080/014311699213659

Mas, J. F., Flores, J. J., 2008. The application of artificial neural networks to the analysis of remotely sensed data. International Journal of Remote Sensing, 29(3), 617-663. https://doi.org/10.1080/01431160701352154

Mason, D. C., Davenport, I. J., 1996. Accurate and efficient determination of the shoreline in ERS-1 SAR images. IEEE Transactions on Geoscience and Remote Sensing, 34(5), 1243-1253. https://doi.org/10.1109/36.536540

Masria, A., Nadaoka, K., Negm, A., Iskander, M., 2015. Detection of shoreline and land cover changes around Rosetta promontory, Egypt, based on remote sensing analysis. Land, 4(1), 216-230. https://doi.org/10.3390/land4010216

Mathers, S., Zalasiewicz, J., 1999. Holocene sedimentary architecture of the Red River delta, Vietnam. Journal of Coastal Research, 314-325.

Mazid, M. M., Ali, S., Tickle, K.S., 2010. Improved C4. 5 algorithm for rule based classification. In Proceedings of the 9th WSEAS international conference on Artificial intelligence, knowledge engineering and data bases (pp. 296-301). World Scientific and Engineering Academy and Society (WSEAS).

Mohrig, D., Heller, P.L., Paola, C., Lyons, W.J., 2000. Interpreting avulsion process from ancient alluvial sequences: Guadalope-Matarranya system (northern Spain) and Wasatch Formation (western Colorado). Geological Society of America Bulletin, 112(12), 1787-1803. https://doi.org/10.1130/0016-7606(2000)112<1787:IAPFAA>2.0.CO;2

Motsholapheko, M. R., Kgathi, D. L., Vanderpost, C., 2011. Rural livelihoods and household adaptation to extreme flooding in the Okavango Delta, Botswana. Physics and Chemistry of the Earth, 36(14-15), 984–995. https://doi.org/10.1016/j.pce.2011.08.004

Mouchot, M. C., Alföldi, T., De Lisle, D., McCullough, G., 1991. Monitoring the water bodies of the Mackenzie Delta by remote sensing methods. Arctic, 21-28. https://doi.org/10.14430/arctic1566

Mukhopadhyay, A., Mukherjee, S., Mukherjee, S., Ghosh, S., Hazra, S., Mitra, D., 2012. Automatic shoreline detection and future prediction: A case study on Puri Coast, Bay of Bengal, India. European Journal of Remote Sensing, 45(1), 201-213. https://doi.org/10.5721/EuJRS20124519

Munasinghe, D., Cohen, S., Huang, Y. F., Tsang, Y. P., Zhang, J., Fang, Z., 2018. Intercomparison of Satellite Remote Sensing-Based Flood Inundation Mapping Techniques. JAWRA Journal of the American Water Resources Association, 54(4), 834-846. https://doi.org/10.1111/1752-1688.12626

Munasinghe, D.S.N., Cohen, S., Hand, B., (under review), A Review of Satellite Remote Sensing Techniques of River Delta Morphology Change.

Mustard, J. F., Sunshine, J. M., 1999. Spectral analysis for earth science: investigations using remote sensing data. Remote sensing for the earth sciences: Manual of remote sensing, 3, 251-307.

Nandi, S., Ghosh, M., Kundu, A., Dutta, D., Baksi, M., 2016. Shoreline shifting and its prediction using remote sensing and GIS techniques: a case study of Sagar Island, West Bengal (India). Journal of coastal conservation, 20(1), 61-80. https://doi.org/10.1007/s11852-015-0418-4

Nath, R. K., Deb, S. K., 2010. Water-body area extraction from high resolution satellite images-an introduction, review, and comparison. International Journal of Image Processing (IJIP), 3(6), 265-384.

Niedermeier, A., Hoja, D., Lehner, S., 2005. Topography and morphodynamics in the German Bight using SAR and optical remote sensing data. Ocean Dynamics 55(2), 100-109. https://doi.org/10.1007/s10236-005-0114-2

Niedermeier, A., Romaneessen, E., Lehner, S., 2000. Detection of coastlines in SAR images using wavelet methods. IEEE Transactions on Geoscience and Remote Sensing, 38(5), 2270-2281. https://doi.org/10.1109/36.868884

Nienhuis, J.H., Törnqvist, T.E., Esposito, C.R., 2018. Crevasse splays versus avulsions: A recipe for land building with levee breaches. Geophysical Research Letters, 45(9), 4058-4067. https://doi.org/10.1029/2018GL077933

Nitze, I., Grosse, G., 2016. Detection of landscape dynamics in the Arctic Lena Delta with temporally dense Landsat time-series stacks. Remote Sensing of Environment, 181, 27-41. https://doi.org/10.1016/j.rse.2016.03.038

Niya, A.K., Alesheikh, A.A., Soltanpor, M., Kheirkhahzarkesh, M.M., 2013. Shoreline change mapping using remote sensing and GIS. International Journal of Remote Sensing Applications, 3(3), 102-107.

Orton, G. J., Reading, H.G., 1993. Variability of deltaic processes in terms of sediment supply, with particular emphasis on grain size. Sedimentology, 40(3), 475-512. https://doi.org/10.1111/j.1365-3091.1993.tb01347.x

Ottinger, M., Kuenzer, C., Liu, G., Wang, S., Dech, S., 2013. Monitoring land cover dynamics in the Yellow River Delta from 1995 to 2010 based on Landsat 5 TM. Applied Geography, 44, 53-68. https://doi.org/10.1016/j.apgeog.2013.07.003

Ozesmi, S.L., Bauer, M.E., 2002. Satellite remote sensing of wetlands. Wetlands ecology and management, 10(5), 381-402. https://doi.org/10.1023/A:1020908432489

Pal, M., Mather, P.M., 2003. An assessment of the effectiveness of decision tree methods for land cover classification. Remote sensing of Environment, 86(4), 554-565. https://doi.org/10.1016/S0034-4257(03)00132-9

Pal, M., Mather, P.M., 2005. Support vector machines for classification in remote sensing. International Journal of Remote Sensing, 26(5), 1007-1011. https://doi.org/10.1080/01431160512331314083

Paola, J.D., Schowengerdt, R.A., 1995. A review and analysis of backpropagation neural networks for classification of remotely-sensed multi-spectral imagery. International Journal of Remote Sensing, 16(16), 3033-3058. https://doi.org/10.1080/01431169508954607

Passalacqua, P., 2017. The Delta Connectome: A network-based framework for studying connectivity in river deltas. Geomorphology, 277, 50-62. https://doi.org/10.1016/j.geomorph.2016.04.001

Petropoulos, G.P., Kalivas, D.P., Griffiths, H.M., Dimou, P.P., 2015. Remote sensing and GIS analysis for mapping spatio-temporal changes of erosion and deposition of two Mediterranean river deltas: The case of the Axios and Aliakmonas rivers, Greece. International Journal of Applied Earth Observation and Geoinformation, 35, 217-228. https://doi.org/10.1016/j.jag.2014.08.004

Postma, G., 1995. Sea-level-related architectural trends in coarse-grained delta complexes. Sedimentary Geology, 98(1-4), 3-12. https://doi.org/10.1016/0037-0738(95)00024-3

Pu, H., Xia, W., Wang, B., Jiang, G.M., 2013. A fully constrained linear spectral unmixing algorithm based on distance geometry. IEEE Transactions on Geoscience and Remote Sensing, 52(2), 1157-1176. https://doi.org/10.1109/TGRS.2013.2248013

Ryu, J.H., Won, J.S., Min, K.D., 2002. Waterline extraction from Landsat TM data in a tidal flat: a case study in Gomso Bay, Korea. Remote sensing of Environment, 83(3), 442-456. https://doi.org/10.1016/S0034-4257(02)00059-7

Sallam, R.L., Howson, C., Idoine, C.J., 2017. Augmented Analytics Is the Future of Data and Analytics. https://www.gartner.com/en/documents/3773164

Samarasinghe, S., 2016. Neural networks for applied sciences and engineering: from fundamentals to complex pattern recognition. Auerbach publications.

Sanchez-Arcilla, A., Jimenez, J.A., Valdemoro, H.I., 2012. The Ebro Delta: morphodynamics and vulnerability. Journal of Coastal Research, 14(3).

Sainju, A. M., Jiang, Z., 2017. Grid-based colocation mining algorithms on gpu for big spatial event data: A summary of results. In International Symposium on Spatial and Temporal Databases (pp. 263-280). Springer, Cham. https://doi.org/10.1007/978-3-319-64367-0_14

Seker, D.Z., Goksel, C., Kabdasli, S., Musaoglu, N., Kaya, S., 2003. Investigation of coastal morphological changes due to river basin characteristics by means of remote sensing and GIS techniques. Water Science and technology, 48(10), 135-142. https://doi.org/10.2166/wst.2003.0558

Seker, D.Z., Kaya, S., Musaoglu, N., Kabdasli, S., Yuasa, A., Duran, Z., 2005. Investigation of meandering in Filyos River by means of satellite sensor data. Hydrological Processes: An International Journal, 19(7), 1497-1508. https://doi.org/10.1002/hyp.5593

Serra, P., Pons, X., Sauri, D., 2003. Post-classification change detection with data from different sensors: Some accuracy considerations. International Journal of Remote Sensing, 24(16), 3311–3340. https://doi.org/10.1080/0143116021000021189

Seto, K.C., Woodcock, C.E., Song, C., Huang, X., Lu, J., Kaufmann, R.K., 2002. Monitoring land-use change in the Pearl River Delta using Landsat TM. International Journal of Remote Sensing, 23(10), 1985-2004. https://doi.org/10.1080/01431160110075532

Sgavetti, M., Ferrari, C., 1988. The use of TM data for the study of a modern deltaic depositional system. International Journal of Remote Sensing, 9(10-11), 1613-1627. https://doi.org/10.1080/01431168808954964

Sha, Z., Bai, Y., Xie, Y., Yu, M., Zhang, L., 2008. Using a hybrid fuzzy classifier (HFC) to map typical grassland vegetation in Xilin River Basin, Inner Mongolia, China. International Journal of Remote Sensing, 29(8), 2317-2337. https://doi.org/10.1080/01431160701408436

Shalaby, A., Tateishi, R., 2007. Remote sensing and GIS for mapping and monitoring land cover and land-use changes in the Northwestern coastal zone of Egypt. Applied Geography, 27(1), 28-41. https://doi.org/10.1016/j.apgeog.2006.09.004

Shen, F., Gao, A., Wu, J.P., Zhou, Y.X., Zhang, J., 2008. A remotely sensed approach on waterline ex- traction of silty tidal flat for DEM construction, a case study in Jiuduansha Shoal of Yangtze River. Acta Geodaetica et Cartographica Sinica, 37(1), 102–107.

Shimabukuro, Y.E., Batista, G.T., Melio, E.M.K., Moreira, J.C., Duarte, V., 1998. Using shade fraction image segmentation to evaluate deforestation in Landsat Thematic Mapper images of the Amazon region. International Journal of Remote Sensing, 19(3), pp. 535–541. https://doi.org/10.1080/014311698216152

Singh, S., Talwar, R., 2013. Review on different change vector analysis algorithms based change detection techniques. In: 2013 IEEE Second International Conference on Image Information Processing (ICIIP-2013) (pp. 136-141). IEEE. https://doi.org/10.1109/ICIIP.2013.6707570

Small, C., 2004. The Landsat ETM+ spectral mixing space. Remote sensing of Environment, 93(1-2), 1-17. https://doi.org/10.1016/j.rse.2004.06.007

Steele, B.M., 2000. Combining multiple classifiers: an application using spatial and remotely sensed information for land cover type mapping. Remote Sensing of Environment, 74(3), 545–556. https://doi.org/10.1016/S0034-4257(00)00145-0

Stouthamer, E., 2001. Sedimentary products of avulsions in the Holocene Rhine–Meuse Delta, the Netherlands. Sedimentary Geology, 145(1-2), 73-92. https://doi.org/10.1016/S0037-0738(01)00117-8

Sun, N., Zhu, W., Cheng, Q., 2018. GF-1 and Landsat observed a 40-year wetland spatiotemporal variation and its coupled environmental factors in Yangtze River estuary. Estuarine, Coastal and Shelf Science, 207, 30-39. https://doi.org/10.1016/j.ecss.2018.03.022

Suresh, M., Jain, K., 2018. Subpixel level mapping of remotely sensed image using colorimetry. The Egyptian Journal of Remote Sensing and Space Science, 21(1), 65-72. https://doi.org/10.1016/j.ejrs.2017.02.004

Syvitski, J. P., Saito, Y., 2007. Morphodynamics of deltas under the influence of humans. Global and Planetary Change, 57(3-4), 261-282. https://doi.org/10.1016/j.gloplacha.2006.12.001

Syvitski, J. P., Kettner, A. J., Overeem, I., Hutton, E.W., Hannon, M.T., Brakenridge, G.R., Day, J., Vörösmarty, C., Saito, Y., Giosan, L., Nicholls, R.J., 2009. Sinking deltas due to human activities. Nature Geoscience, 2(10), 681. https://doi.org/10.1038/ngeo629

Syvitski, J.P., Overeem, I., Brakenridge, G.R., Hannon, M., 2012. Floods, floodplains, delta plains—a satellite imaging approach. Sedimentary Geology, 267, 1-14. https://doi.org/10.1016/j.sedgeo.2012.05.014

Tarboton, D.G., Idaszak, R., Horsburgh, J. S., Heard, J., Ames, D., Goodall, J.L., Merwade, V., Couch, A., Arrigo, J. and Hooper, R., 2014. HydroShare: advancing collaboration through hydrologic data and model sharing.

Thanh Noi, P., Kappas, M., 2018. Comparison of random forest, k-nearest neighbor, and support vector machine classifiers for land cover classification using Sentinel-2 imagery. Sensors, 18(1), 18. https://doi.org/10.3390/s18010018

Theseira, M.A., Thomas, G., Taylor, J.C., Gemmell, F., Varjo, J., 2003. Sensitivity of mixture modelling to end-member selection. International Journal of Remote Sensing, 24(7), 1559-1575. https://doi.org/10.1080/01431160210146631

Tso, B., Mather, P.M., 2001. Classification Methods for Remotely Sensed Data, CRC Press.

Ulrich, M., Grosse, G., Chabrillat, S., Schirrmeister, L., 2009. Spectral characterization of periglacial surfaces and geomorphological units in the Arctic Lena Delta using field spectrometry and remote sensing. Remote Sensing of Environment, 113(6), 1220-1235. https://doi.org/10.1016/j.rse.2009.02.009

Van Maren, D.S., 2005. Barrier formation on an actively prograding delta system: The Red River Delta, Vietnam. Marine Geology, 224(1-4), 123-143. https://doi.org/10.1016/j.margeo.2005.07.008

Viaña-Borja, S. P., Ortega-Sánchez, M., 2019. Automatic Methodology to Detect the Coastline from Landsat Images with a New Water Index Assessed on Three Different Spanish Mediterranean Deltas. Remote Sensing, 11(18), 2186. https://doi.org/10.3390/rs11182186

Walker, N. D., Hammack, A. B., 2000. Impacts of winter storms on circulation and sediment transport: Atchafalaya-Vermilion Bay region, Louisiana, USA. Journal of Coastal Research, 996-1010.

Wang, F., Zhang, R., Zhao, H., Chen, X., 2019. Dynamic Evolution of the Yellow River Delta coastline Based on Multi-Source Remote Sensing. Ekoloji, 28(107), 615-627.

Warrender, C.E., Augusteihn, M.F., 1999. Fusion of image classification using Bayesian techniques with Markov random fields. International Journal of Remote Sensing, 20(10), 1987–2002. https://doi.org/10.1080/014311699212308

Wei, W., Zhang, X., Chen, X., Tang, J., Jiang, M., 2008. Wetland mapping using subpixel analysis and decision tree classification in the Yellow River delta area. ISPRS Archives, 38(B7), 667-670.

White, K., El Asmar, H.M., 1999. Monitoring changing position of coastlines using Thematic Mapper imagery, an example from the Nile Delta. Geomorphology, 29(1-2), 93-105. https://doi.org/10.1016/S0169-555X(99)00008-2

Wilson, P.A., 1997. Rule-based classification of water in Landsat MSS images using the variance filter. Photogrammetric Engineering & Remote Sensing, 63(5), 485491.

Woodroffe, C.D., Nicholls, R.J., Saito, Y., Chen, Z., Goodbred, S.L., 2006. Landscape variability and the response of Asian megadeltas to environmental change. In: Harvey, N. (Ed.), Global Change and Integrated Coastal Management, 10, 277-314. Dordrecht, The Netherlands: Springer. https://doi.org/10.1007/1-4020-3628-0_10

Wu, C., 2009. Quantifying high-resolution impervious surfaces using spectral mixture analysis. International Journal of Remote Sensing, 30(11), 2915-2932. https://doi.org/10.1080/01431160802558634

Xia, L., 1998. Measurement of rapid agricultural land loss in the Pearl River Delta with the integration of remote sensing and GIS. Environment and Planning B: Planning and Design, 25(3), 447-461. https://doi.org/10.1068/b250447

Xie, Y., Sha, Z., Yu, M., 2008. Remote sensing imagery in vegetation mapping: a review. Journal of Plant Ecology, 1(1), 9-23. https://doi.org/10.1093/jpe/rtm005

Xu, H. 2006. "Modification of Normalised Difference Water Index (NDWI) to Enhance Open Water Features in Remotely Sensed Imagery." International Journal of Remote Sensing 27 (14): 3025–33. https://doi.org/10.1080/01431160600589179.

Xu, J., Li, Z., Lei, L., Tian, B., Shan, Z., 2012. Land Cover Classification of Polarimetric SAR Images for the Yellow River Delta Based on Support Vector Machine. In: 2012 International Conference on Computer Vision in Remote Sensing (pp. 256-261). IEEE. https://doi.org/10.1109/CVRS.2012.6421271

Yang, X., 1996. Satellite Monitoring of the Dynamic Environmental Change of the Active Yellow River Delta, China. International Archives of Photogrammetry and Remote Sensing, 31, 801-806.

Yang, X., Damen, M.C.J., Van Zuidam, R.A., 1999. Satellite remote sensing and GIS for the analysis of channel migration changes in the active Yellow River Delta, China. International Journal of Applied Earth Observation and Geoinformation, 1(2), 146-157. https://doi.org/10.1016/S0303-2434(99)85007-7

Yates, M.L., Cozannet, G.L., 2012. Brief communication: Evaluating European Coastal Evolution using Bayesian Networks. Natural Hazards and Earth System Sciences, 12(4), 1173-1177. https://doi.org/10.5194/nhess-12-1173-2012

Yeh, A.G.O., Li, X., 1997. An integrated remote sensing and GIS approach in the monitoring and evaluation of rapid urban growth for sustainable development in the Pearl River Delta, China. International Planning Studies, 2(2), 193-210. https://doi.org/10.1080/13563479708721678

Yoshino, K., Kawaguchi, S., Kanda, F., Kushida, K., Tsai, F., 2014. Very high resolution plant community mapping at High Moor, Kushiro Wetland. Photogrammetric Engineering & Remote Sensing, 80(9), 895-905. https://doi.org/10.14358/PERS.80.9.895

Zhang, W., Xu, Y., Hoitink, A.J.F., Sassi, M.G., Zheng, J., Chen, X., Zhang, C., 2015. Morphological change in the Pearl River Delta, China. Marine Geology, 363, 202-219. https://doi.org/10.1016/j.margeo.2015.02.012

Zhang, X., Treitz, P.M., Chen, D., Quan, C., Shi, L., Li, X., 2017. Mapping mangrove forests using multi-tidal remotely-sensed data and a decision-tree-based procedure. International Journal of Applied Earth Observation And Geoinformation, 62, 201-214. https://doi.org/10.1016/j.jag.2017.06.010

Zhang, X., Lu, Z., Jiang, S., Chi, W., Zhu, L., Wang, H., Lv, K., Wang, B., Yang, Z. (2018). The progradation and retrogradation of two newborn Huanghe (Yellow River) Delta lobes and its influencing factors. Marine Geology, 400, 38-48. https://doi.org/10.1016/j.margeo.2018.03.006

Zhang, B., 2009. A CART Based Sub-pixel Method to Map Spatial and Temporal Patterns of Prairie Pothole Lakes with Climatic Variability. Unpublished manuscript, Ohio State University, Columbus, Ohio.

Zhang, J., Foody, G.M., 1998. A fuzzy classification of sub-urban land cover from remotely sensed imagery. International Journal of Remote Sensing, 19(14), 2721-2738. https://doi.org/10.1080/014311698214479

Zhao, B., Guo, H., Yan, Y., Wang, Q., Li, B., 2008. A simple waterline approach for tidelands using multi-temporal satellite images: a case study in the Yangtze Delta. Estuarine, Coastal and Shelf Science, 77(1), 134-142. https://doi.org/10.1016/j.ecss.2007.09.022

Zhu, X., 2001. Remote sensing monitoring of coastline change in Pearl River Estuary. In: 22nd Asian Conference on Remote Sensing (Vol. 5, p. 9).

Zhu, C., Zhang, X., Huang, Q., 2018. Four decades of estuarine wetland changes in the Yellow River delta based on Landsat observations between 1973 and 2013. Water, 10(7), 933. https://doi.org/10.3390/w10070933

CHAPTER 3

SUITABILITY ANALYSIS OF REMOTE SENSING TECHNIQUES FOR SHORELINE EXTRACTION OF GLOBAL RIVER DELTAS

Abstract

High frequency flooding, sea level rise and changes to riverine sediment fluxes have threatened the habitable land area of river deltas, where close to half a billion people live, globally. Understanding shoreline positions is important for overall sustainable planning of deltaic communities and delta evolution predictive modeling. However, a gap in literature is recognized where there is a) no understanding of the most effective shoreline extraction method for a delta, and b) comparisons across techniques to infer on the performance metrics of techniques across deltas in different climate regions. This makes it difficult to apply existing knowledge to lesser studied, data sparse deltaic regions worldwide. In addressing these gaps, we evaluated the performance of 5 different remote sensing techniques against a hand-digitized shoreline vector of 44 river deltas globally, representing the 3 different morphological types of deltas (river-, tide- and wave-dominated), across 4 Köppen Climate Classes using Landsat 8 imagery. We propose a new metric (Robustness: R) to evaluate the performance of a given technique. The results show that 1) the best performing method for the majority of the deltas (35/44) was Unsupervised Classification, 2) there is no geographical significance in the performance of the tested techniques, and 3) wave dominated deltas showed the highest classification robustness while tide dominated deltas showed the lowest. Recommendations are

made for the application of techniques in different types of deltas and unknown deltaic territories worldwide.

1. Introduction

River deltas, home to almost half a billion people around the world, are important coastal depositional systems. They not only act as central locations for agricultural production and hydrocarbon extraction, but are also biodiversity hotspots, and carry a vast cultural heritage (Hutchings and Campbell, 2005; Lentz et al., 2016). Over the past half century, changes to storm frequency and intensity, eustatic sea level rise, and natural-human driven delta morphology evolution (e.g. changes in sedimentation patterns in deltas over time; (Syvitski et al., 2009; Tessler et al., 2015) have added growing pressures to the effective deltaic land area available for human habituation, and consequently, has attracted enhanced scientific interest to studying temporal shifts in the land-sea boundary of deltas (i.e. shoreline). Understanding river delta shoreline positions are important for sustainable planning of deltaic communities. They are important in the construction of engineering structures (e.g. breakwaters, weirs), for flood mitigation, dam construction, erosion-accretion studies, regional sediment budget calculations, and for predictive modeling of coastal morphodynamics (Al Bakri, 1996; Cenci et al., 2018).

Remote Sensing provides a useful diagnostic technology to monitor large scale changes in river delta shoreline positions over time (Besset et al., 2019). Although there exist a number of studies in the literature on identifying shoreline positions and their temporal evolution, in a recent literature review, Munasinghe et al. (2021) revealed that there was no consensus as to which remote sensing technique(s) would be the most suitable to extract shorelines with satisfactory accuracy, emulating close-to-real-world shoreline positions. Challenges in shoreline

identification were attributed to shoreline dynamics that are driven by many other location/climate related factors (e.g. inherent variability in rainfall, soil minerals, growing cycle phases of vegetation). They also revealed that a) studies in the literature focused mostly on a few major river deltas globally, b) there were not enough studies which compared multiple techniques at a given river delta, and c) no comparisons of techniques across multiple deltas in different climatic regions or delta types, making it challenging to apply shoreline extraction methodologies to lesser studied deltas worldwide. A comparison of remote sensing techniques on an array of delta types (river-, tide-, wave-dominated) across the globe could provide insights into the performance of techniques under varying fluvial and marine conditions. Elucidating which technique(s) would be the most appropriate for a given climatic region and delta type would allow us to infer why particular techniques underperform in different regions of the world. This will highlight some of the inherent problems of particular techniques and will offer a pathway for improving existing algorithms (e.g. to compensate for environmental noise) and development of new ones.

2. Methodology

In this study, we evaluate five traditional remote sensing techniques on 44 large river deltas worldwide (variety of river-, tide- and wave-dominated deltas (Galloway, 1975); characteristics of these types discussed later), curated to represent 4 major and 13 sub-Köppen Climate classes. The Köppen Climate Classification is based on air temperature and precipitation and represents biome distributions around the world: different regions in a similar class share common vegetation characteristics (Beck et al., 2018). Five remote sensing techniques are compared: 1) Modified Normalized Difference Water Index (MNDWI), 2) Normalized

Difference Vegetation Index (NDVI), 3) PCA analysis 4) Unsupervised Classification 5) Supervised Classification. Shorelines were extracted for deltas using Landsat imagery from the year 2018. The shoreline is highly dynamic and is the position of the land-sea interface at one instant in time (Gens, 2010). For the purposes of this study, the shoreline is defined as the land-sea interface derived at the moment of satellite image capture. This can be anywhere between the high and low water lines. The robustness of each method in shoreline extraction was assessed against a hand-digitized shoreline vector created using high resolution Google Earth imagery of the same year. A performance comparison was made between techniques and different deltaic environmental settings.

Machine learning (ML) techniques were not considered in this study. While Munasinghe et al. (2021) found that ML can outperform traditional methods in some river deltas, ML techniques are 1) more challenging to apply as they rely on training data which might not be available in all regions, and 2) cannot be readily transitioned between case studies.

2.1 Digitization of Reference Shoreline

High resolution Google Earth imagery was used to manually digitize the shorelines of river deltas (termed 'real shoreline' hereafter). Digitization of the land-water boundary was performed at an altitude of 2000 m from a nadir view, with general spacing of around 2 meters between vertices, on Google Earth Pro, on imagery from 2018. The digitized line files were saved as .kml files and subsequently converted to shapefiles in ArcMap 10.6.

2.2 Preparation of Satellite Imagery

Polygon shapefiles were created for each river delta based on river delta extents provided by Tessler et al. (2015). Image Search was carried out on Google Earth Engine (GEE), an open source Geospatial Solution by Google LLC. The Landsat 8 - OLI Surface Reflectance Product (cataloged within the GEE) for the year 2018 for each delta were used in the study. Search parameters were governed by cloud freeness and low discharge seasons of the feeder river of the delta (high river discharge increases water turbidity which hinders shoreline identification). Constrained by the above two governing factors, generally, creating a composite mosaic to cover an entire delta coastline required imagery within a consecutive 3-month period of the year. Imagery making up the composite are captured during different days within the 3-month period and thus are subject different magnitudes of tidal variations at different segments of the river delta. However, since the objective of this study is not to accurately extract shorelines of deltas at instants in time to depict real world conditions, but to assess the performance of techniques that can be used to extract the land-sea interface from a remotely sensed image the use of a composite is justified.

2.3 Extraction of shorelines using Remote Sensing Techniques

The following techniques were used in this analysis:

Modified Normalized Difference Water Index (MNDWI; Xu, 2006):

An enhancement of the Normalized Difference Water Index (NDWI; McFeeters, 1996). Uses Landsat 8 shortwave infrared band (SWIR; Band 5) [MNDWI = (Green-SWIR)/(Green+SWIR)] to enhance open water features while efficiently eliminating built-up land noise and suppressing vegetation and soil noise.

Supervised Classification:

A classification technique based on user-identified sample pixels (training areas) as representatives of a specific spectral signature class (e.g., water). In this study, training areas were identified based on high resolution google earth imagery of 2018. Four different types of land use/feature classes were used in training the classifier (i.e. water bodies, vegetated land, urban land, agricultural land). In addition, for deltas with visible sediment plumes at feeder river mouths, a separate class was added to the classifier.

Unsupervised Classification (K-Means Classification):

A classification technique based on an automated differentiation of the pixel's spectral signature to a user-defined number of groups (Jensen, 2015). The identification of the nature of each group (e.g. water) is made by the user. In this study, after preliminary testing for 4-7 land use classes, a uniform number of 5 land use classes were selected and specified for all deltas (fifth class ideally to represent the sediment plume). However, it must be noted that for deltas with no visible sediment plumes classes were concatenated during final raster processing.

Normalized Difference Vegetation Index (NDVI; Rouse et al., 1974):

A technique based on band ratioing [NDVI = (NIR-Red)/(NIR+Red)] to usually monitor vegetation growth/plant biomass. The strong absorbance by water and reflection by the terrestrial vegetation and dry soil by the near-infrared (NIR) band, is leveraged in this study to distinguish the land-sea boundary (Sun et al., 2012).

Principal Component Analysis (PCA):

A technique based on transforming the data to a new set of variables (principal components) which are uncorrelated and ordered, so that the first few retain most of the variation present in all the multispectral imagery (Deng et al., 2008). The variance of the first four Principal components were used in this study.

Images were processed in batches for each technique (using Python scripts) to generate rasters with Land/Water classification. These rasters were then converted into Polygon layers representative of land/water areas. The Polygon layers were then converted into polylines. The water-land boundary (shoreline) was extracted from these polylines. First, in order to mask out polylines which covered the land area of the delta and separate the ones which only extended from the land towards the sea, a 5-km seaward buffer was created to the manually digitized shoreline. Then, to find out which out of these polylines represented the real (manually digitized) shoreline at best, the real shoreline was used as a baseline to find out the closest polylines to it from within the buffered area. This was done by creating points every 50 meters on the real shoreline and by selecting the nearest polyline segments to these points (euclidean distance to real shoreline) using GIS methods (Figure 1: Inset-1). Subsequent to this selection these selected polyline segments were merged in order to obtain a single continuous shoreline representation. However, if no polyline segment was present to the euclidean line (due to poor performance of technique), gaps are created in the extracted shoreline. This process was repeated for the different techniques to obtain 5 shoreline representations for a given delta.

2.4 Evaluation of the Remote Sensing Techniques

Two metrices were used to compare the robustness of the extracted shorelines: 1) the percentage length of the shoreline that was extracted in comparison to that of the real shoreline, and 2) the average distance of the shoreline from the real shoreline. A new robustness index (*R*) was developed which joins both metrices:

$$R = \frac{L_E * 100 / L_R}{D_{EA}} \qquad (1)$$

where L_E is the length of the extracted shoreline, L_R is the length of the real shoreline, and D_{EA} is the perpendicular distance between the extracted and real shorelines (Fig. 1: inset 1). The *R* index value increases as the shoreline extracted by a given method is closer to the real shoreline in length, whereas robustness decreases as the real shoreline is farther away from the extracted shoreline. It must be noted that the potential maximum L_E for a given technique can go beyond L_R. This is because the extracted shoreline can have undulations that are absent in the real shoreline. Better the shoreline extraction higher the possibility that $L_E > L_R$ (evident for Unsupervised and Supervised values for L_E in Table 1). Also, D_{EA} is an average only calculated where both extracted and real shoreline exist. Gaps in the extracted shoreline are not considered (i.e. $D_{EA} = 0$ are omitted).

Non-parametric ANOVA tests (Kruskall Wallis one-way ANOVA) with pairwise comparisons of robustness values across techniques were carried out to infer 1) which technique(s) performs significantly better in shoreline delineation across all the deltas, and 2) if a given technique(s) was performing better in certain regions in the world.

We also evaluated how the robustness values of the best performing technique clustered based on the type of delta and attempted to provide guidelines for the usage of these techniques in different deltaic environments.

3. Results and Discussion

Unsupervised classification yielded the best performance for the majority of the deltas (35 of 44) whilst supervised classification yielded the best for the remainders (9 of 44) (Table 1). For the two best performing techniques, the median percentage extractions were 94% and 89%, while the median average distances from the actual shoreline were 46 m and 67 m (Table 1). The

least successful method in shoreline delineation was PCA. The length extractions were very low (4%-84%), with a median of 26%, and the average distances were very large (as much as 2.6 km; median=405 m; Table 1).

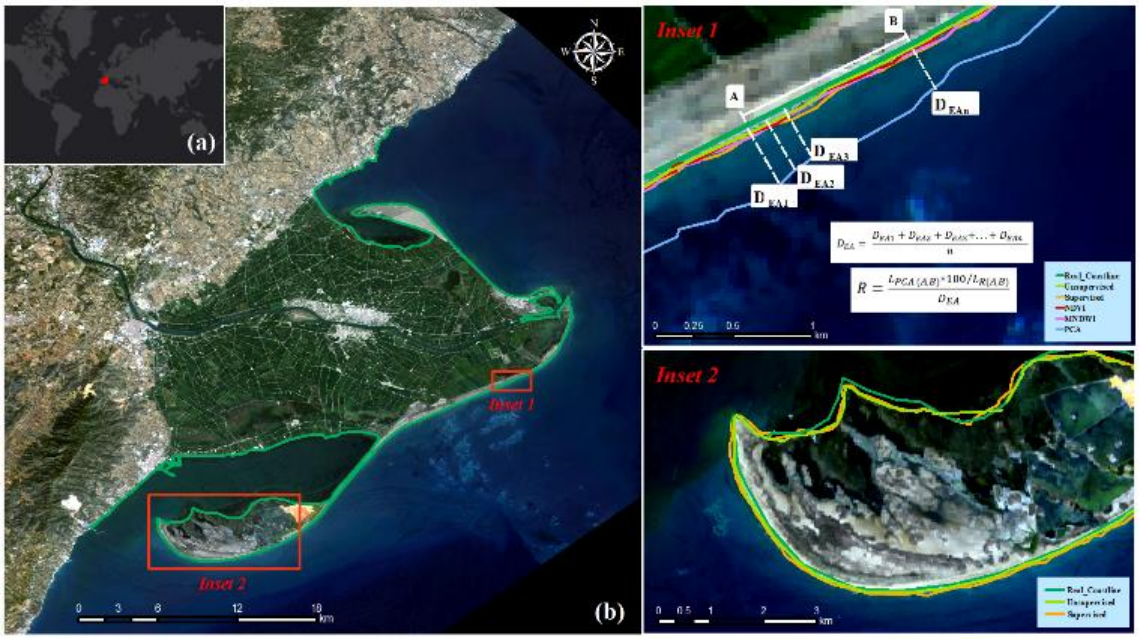

Figure 3.1. (a) Ebro river delta, Spain. (b) A natural color Landsat 8 image of the Ebro delta. The real shoreline is shown by the green line. (Inset 1) Illustration of Calculation of the Robustness index for a shoreline extracted using the PCA technique. A shoreline segment between points A and B are used. (Inset 2) Highly satisfactory performance of Unsupervised and Supervised classification-derived shoreline along the beach spit.

The nonparametric ANOVA showed that when all river deltas were considered, *R* values of Unsupervised and Supervised were significantly outperforming all the other techniques but did not show a significant difference (P=0.087; α = 0.05) between each other. The two ratioing techniques' performance also did not have a significant difference between each other (P=0.49; α = 0.05). All other techniques had significant differences with PCA (Table 1).

However, a comparison of techniques based on climate classes showed that deltas located in tropical and arid steppe climates (Amazon, Fly, Mahakam, Danube, Dnieper, Ebro) did not show significant differences in the performance of the five shoreline extractions techniques. Also, even though all techniques performed significantly better than PCA in general, NDVI performed comparably with PCA, in 6 climatic classes (Tropical Rainforests, Tropical Monsoons, Tropical Savannahs, Arid desert, Arid Steppes, and Temperate regions with no dry seasons).

The reason that the Unsupervised clustering methods performed well across a range of river deltas can be attributed to the automatic clustering of image pixels into *n* spectral classes based on fine differences in spectral reflectance with minimum user interference. The strength in this technique is that the assignment of pixels to a spectral class is based on the sampling of the entirety of image pixels. The intra-image pixel bias (the ambiguity of allocating a class to a certain pixel resulting from sampling only a portion of an image) is at a minimum. The analyst only attempts to assign or transform the spectral classes into thematic information classes of interest (e.g., forest, agriculture) after spectral classes have been identified. Unsupervised and Supervised not only captured straight shoreline segments, but also features such as beach spits, tombolos, bay mouth bars and cuspate forelands which are parts of shorelines (Fig. 1). In general, four of the five techniques (except PCA) performed well in capturing straight shoreline segments (Fig. 1).

Table 3.1. The ranges of the percentage lengths of extracted shorelines, their average distances from the real shoreline and mean robustness values for each technique, for the entire suit of deltas analyzed.

Technique	*Range of L_E (%) (Median in parenthesis)*	*Range of D_{EA} (m) (Median in parenthesis)*	*R* mean

Unsupervised	69-102 (94)	19-239 (46)	2.03
Supervised	36-101 (89)	30-365 (67)	1.34
MNDWI	7-84 (48)	52-2448 (226)	0.32
NDVI	5-80 (42)	57-1250 (246)	0.28
PCA	4-84 (26)	75-2668 (405)	0.13

This average performance of ratioing techniques is attributed to the usage of two different bands, and their compounding errors. For example, the Band 2/Band 5 ratio (basis of the MNDWI index) has a value greater than one for water and less than one for land in large areas of the coastal zone. This ratio works well in coastal zones covered by soil, but not in land with vegetative cover (Alesheikh et al., 2007). This can lead to mistakenly classifying other land use types as water, especially along the land-sea boundary, which seemed to be happening in most of the deltaic environments studied herein.

The working principle of a PCA is such that is reduces the dimensionality of a dataset consisting of many interrelated variables, while retaining as much variation present in the dataset as possible. This is achieved by transforming the data to a new set of variables (principal components) which are uncorrelated and ordered so that the first few retain most of the variation present in all the original variables (Deng et al., 2008). However, during the reduction in dimensionality, a loss of data can also be expected. Although usually, the first four principal components account for over 95% of the variation of the data, for the deltaic environments in this study, the variation only ranged between 60%-90% which created land/water rasters with diminished accuracies, and consequently yielded low robustness values.

Analysis was also carried out to infer if a given technique was performing significantly better in certain Köppen Climate classes. Non-parametric ANOVAs conducted separately on $L_{E,}$ D_{EA} and R values of a given technique across different classes showed that there was no

statistical significance in either of the 3 categories. If a technique performs well in length/distance/robustness, it performs well across all regions, uniformly, and vice versa.

Hierarchical Clustering (Ward's method was used to find links between points and cluster them around centroids; (Ward Jr, 1963)) of the robustness of the best performing technique of each delta produced a dendrogram (Fig. 2b). Reasonable clustering is where the ratio between the largest and smallest cluster sizes are close to 3. Thus, different cluster configurations (3-8) were tested, for which a best ratio of 3.40 was obtained for a forcing of 4 clusters (see horizontal axis of dendrogram (Fig. 2b) representing the dissimilarity at 2.5% scaled distance). By correlating the clusters with robustness values, we identified that river deltas with high robustness values (above 2.17, clusters 3 and 4) are mostly wave-dominated.

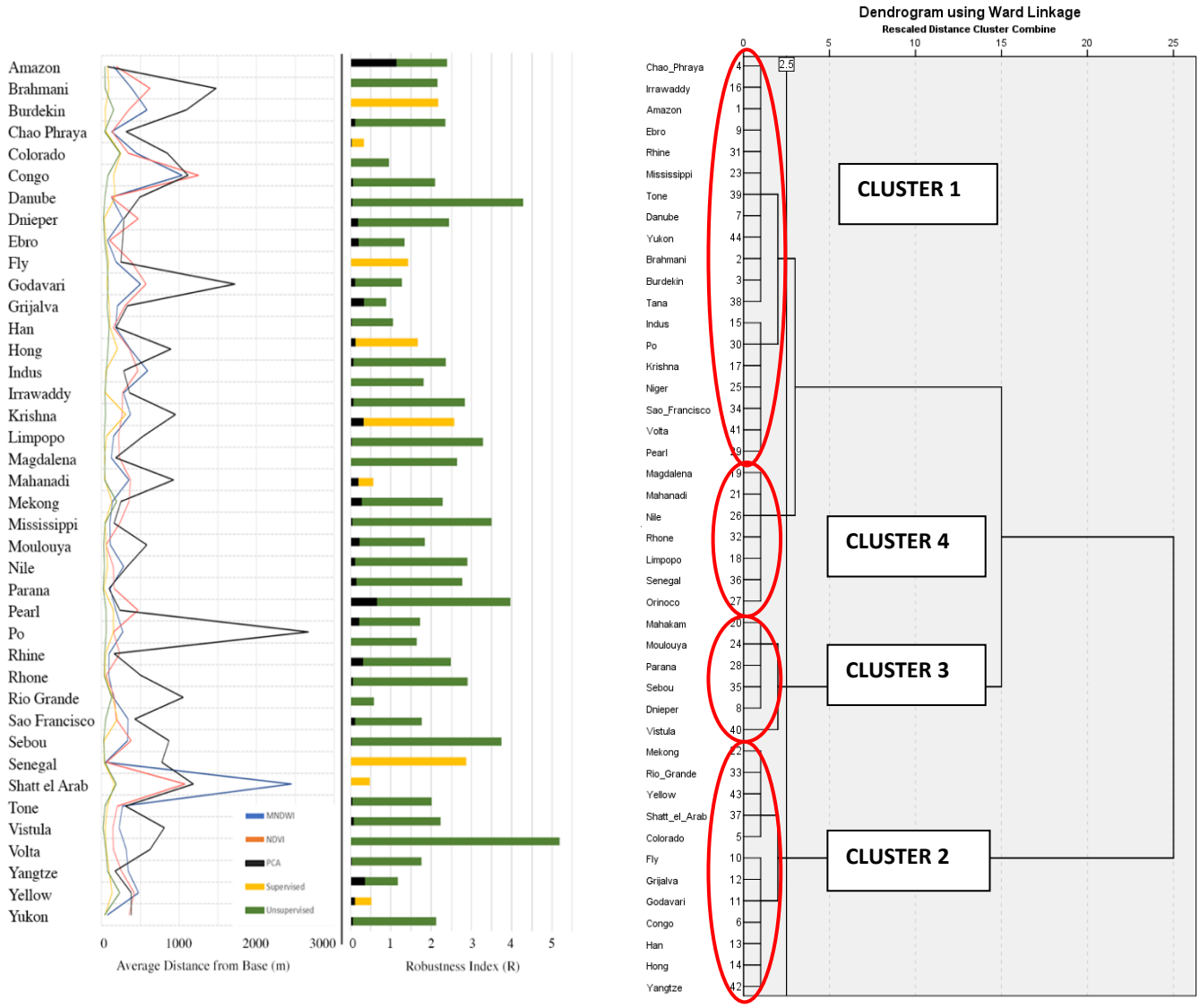

Figure 3.2. (a) A comparison of average distances from the actual to extracted shorelines of each technique (line graph) and best and worst performing techniques for each delta (overlapping bar graph); (b) dendrogram of clusters of robustness of best performing technique at each delta.

A delta is considered wave-dominated when the maximum amount of sediment that the waves can transport along both flanks of the delta is greater than the coarse-grained fluvial sediments supplied to the river mouth (Nienhuis et al., 2015). River deltas with robustness values at the lower end of the spectrum (below 1.42; Cluster 1) are mostly tide-dominated. These deltas

occur in locations of large tidal ranges or high tidal current speeds in which sediment is carried seaward during the low tide and is brought ashore during high tides. Cluster 2 had an equal mix of river-, wave- and tide-dominated deltas.

Wave domination limits the accumulation of fine-grained sediment at the delta mouth by transporting river-borne sediments offshore and away from the littoral zone (the area between high and low tide), and muddy sediments are generally below the shoreface toe (where the slope of the delta ends and smoothens out with the sea floor). This in turn sculpts delta shorelines into a cuspate shape consisting of sandy shorelines (Fig. 3a). Sandy shorelines which are typical of wave dominated deltas, provide great contrast in pixel values with their neighboring water pixels and provide clear land-water boundaries and successful shoreline extractions.

Tide-dominated/tidally influenced deltas, on the other hand, accumulate sediment at the shoreface by the continuous oscillatory reworking and resuspension of sediment by ocean waves and fluvial energies. As a consequence of these varying transport energies, the sedimentary facies formed in tide-dominated deltaic settings tend to be heterolithic, with interbedded sands, silts, and clays giving it a muddy texture. This muddy-ness extends for many kilometers over land in large deltas and is also visible as plumes in the water making distinguishing between land/water pixels challenging (Fig. 3b).

Figure 3.3. (a) a natural color Landsat 8 image of the wave-dominated Nile river delta, where a clear distinction between land and water exists (c) a natural color Landsat 8 image of the tide-dominated Colorado river delta. The muddy intertidal flats and sediment plumes surrounding the mouth bars at the river mouth make high-accuracy shoreline extractions challenging.

In addition to the inferences on the robustness of techniques on different types of deltas, as a general guideline, we advocate assigning the sediment plume in the delta nearshore environment to a separate class when conducting Supervised or Unsupervised Classifications. This is especially important in the low-robustness, tide-dominated deltas or low/mid-robustness river dominated deltas with high sediment concentrations from feeder rivers. In most cases, when not actively assigned, deltaic land and sediment plume features clustered together, heavily affecting D_{EA} values and erroneous extractions.

4. Conclusion

This global analysis conducted to infer on the suitability of remote sensing techniques in delta shoreline extraction shows Unsupervised Classification as generally the best among the five techniques, whilst PCA yielded the poorest results. No significant differences in the performance of a given technique was found across different climate classes. Based on the results, we recommend the use of Unsupervised Classification as a first order extraction technique for previously unstudied deltaic regions. Special attention is drawn to deltaic environments with high sediment-laden intertidal conditions. We also elucidate that wave-dominated deltas show the best performance in shoreline extraction while tide-dominated deltas were most challenging for the techniques employed. This is envisioned to provide prior understanding of the range of robustness values that one could expect for an unknown deltaic region, given the type of delta, and make advanced decisions on the necessity of advanced algorithms, and/or high resolution data for better shoreline extractions at these locations.

5. References for Chapter 3

R. M. Hutchings, and S. K. Campbell, "The Importance of Deltaic Wetland Resources: A Perspective from the Nooksack River Delta, Washington State," *Journal of Wetland Archaeology*, vol. 5, no. 1, pp. 17–34, Jun. 2005.

E. E. Lentz *et al.*, "Evaluation of dynamic coastal response to sea-level rise modifies inundation likelihood Sea-level rise (SLR) poses a range of threats to natural and built environments," *Nature Climate Change*, vol. 6, no. 7, pp. 696-700, Jul. 2016.

J. P. M. Syvitski *et al.*, "Sinking deltas due to human activities*," Nature Geoscience*, vol. 2, no. 10, pp. 681-686, Oct. 2009.

Z. D. Tessler *et al.*, "Profiling risk and sustainability in coastal deltas of the world," *Science*, vol. 349, no. 6248, pp. 638-643, Aug. 2015.

D. Al Bakri, "A geomorphological approach to sustainable planning and management of the coastal zone of Kuwait," *Geomorphology*, vol. 17, no. 4, pp. 323-337, Oct. 1996.

L. Cenci *et al.*, "Integrating remote sensing and GIS techniques for monitoring and modeling shoreline evolution to support coastal risk management," *GIScience & Remote Sensing*, vol. 17, no. 4, pp. 355-375, May. 2018.

M. Besset *et al.*, "Multi-decadal variations in delta shorelines and their relationship to river sediment supply: An assessment and review," *Earth-science reviews*, vol. 193, pp. 199-219, Jun. 2019.

D. S. N. Munasinghe, and S. Cohen, "A Review of Satellite Remote Sensing Techniques of River Delta Morphology Change," (under review).

W. E. Galloway, "Process framework for describing the morphologic and stratigraphic evolution of deltaic depositional systems, in *Deltas: Models for Exploration*. Houston Geological Society, Houston, TX, USA, 1975, pp. 87-98.

H. E. Beck *et al.*, "Present and future Köppen-Geiger climate classification maps at 1-km resolution," *Scientific Data*, vol. 5, Oct. 2018, Art. no. 180314

R. Gens, "Remote sensing of coastlines: detection, extraction and monitoring," *International Journal of Remote Sensing*, vol 31, no. 7, pp 1819-1836. Apr 2010.

H. Xu, "Modification of Normalised Difference Water Index (NDWI) to Enhance Open Water Features in Remotely Sensed Imagery," *International Journal of Remote Sensing*, vol. 27, no. 14, pp. 3025–33, Jul. 2006.

S. K. McFeeters, "The Use of the Normalized Difference Water Index (NDWI) in the Delineation of Open Water Features," *International Journal of Remote Sensing*, vol. 27, no. 7, pp. 1425–1432, May. 1996.

J. R. Jensen, *Introductory Digital Image Processing: A Remote Sensing Perspective*. Upper Saddle River, NJ, USA: Prentice Hall, 2015, pp. 197-256.

J. W. Rouse *et al.*, "Monitoring Vegetation Systems in the Great Plains with ERTS," in *Proc. 3rd Earth Resource Technology Satellite (ERTS) Symposium*, vol. 1, pp. 48-62, Jan 1974.

F. Sun *et al.*, "Comparison and improvement of methods for identifying waterbodies in remotely sensed imagery," *International Journal of Remote Sensing*, vol. 33, no. 21, pp. 6854-6875, Nov. 2012.

J. S. Deng *et al.*, "PCA-based land-use change detection and analysis using multitemporal and multisensor satellite data," *International Journal of Remote Sensing*, vol. 29, no. 16, pp. 4823-4838, Aug. 2008.

A. A. Alesheikh *et al.*, "Coastline change detection using remote sensing," *International Journal of Environmental Science & Technology*, vol. 4, no. 1, pp. 61-66, Dec. 2007.

J. H. Ward Jr, "Hierarchical Grouping to Optimize an Objective Function," *Journal of the American Statistical Association*, vol. 58, no. 301, pp. 236–244, Mar. 1963.

J. H. Nienhuis, *et al.*, "What makes a delta wave-dominated?," *Geology*, vol. 43, no. 6, pp. 511-514, Jun. 2015.

CHAPTER 4

HUMAN MODIFICATIONS OF RIVER DELTA PLAINS AND THEIR IMPACT ON SEDIMENT FLUXES IN DELTAIC CHANNEL NETWORKS

Abstract

River delta distributary networks distribute water, sediment, and nutrients across a river delta and provide fertile floodplains to humans, and a nutrient-rich habitat for a diverse and biologically valuable ecosystem. Quantifying the sediment loaded into these channels from the river delta plain explicitly is important in terms of assessing total fluxes from land to the ocean, assessing river delta morphology change and planning engineering developments such as flood control and channel modifications.

Anthropogenic modifications of river delta plains owing largely to agricultural activities, clearance of land for settlements and economic activity related to urbanization have dramatically changes sediment mobilization and erosion from the river delta plains into these channels, but have largely left unquantified. In this study we investigate the following in 44 major global river deltas: (a) How much sediment is eroding into the distributary network originating from the delta plain? (b) What is the distribution of sediment within the channel orders of the network? and (c)What are the intensities and key human drivers of river delta plain modification and their relationship to sediment loading into distributary channel networks?

We show that (a) that most of the sediment eroded from the plain is concentrated in mid-size channels located in agriculturally dominated areas (b) in total, 56.71% of total deltaic land are highly or very highly modified by humans; only 17.75% of deltaic land that is minimally

disturbed. The most anthropogenically influenced river deltas are Chao Phraya, Yangtze, Hong, Po, and Nile, while the Yukon and Amazon deltas are the most likely to have pristine land, (c) Population, Cropland and Night-Time Lights are identified as the most dominant stressors on deltaic land, and (d) 27% of global variability in sediment loading into deltaic distributary networks is recognized as a result of anthropogenic stress on the river delta plains.

1. Introduction

River deltas are coastal landforms that are iconic examples of economic and social hotspots. The ever-growing human footprint on deltas through urbanization, economic development, and land conversions for agriculture has had significant impacts on sediment transport dynamics on the river delta plain (Walling and Fang, 2003; Syvitski and Kettner, 2011; Du et al., 2016; Best, 2019). Delta plains typically contain networks of bifurcating channels that distribute water, sediment, and nutrients from upstream sources to downstream wetlands and coastlines (Syvitski & Saito, 2007). The distribution of this material not only nourishes coastal-deltaic environments with a nutrient rich habitat facilitating diverse ecosystems (Olson and Dinerstein, 1998; see Edmonds and Slingerland 2008; Vörösmarty et al., 2009), but also, overtime, contributes to the construction of stratigraphy, preserving a unique fingerprint of the hydrology and sediment dynamics of past environmental conditions (Vörösmarty et al., 2009, Jarriel et al., 2020).

Estimates of sediment flux from the land to the ocean through deltaic distributary networks demand an understanding of the sediment contribution from the delta plain. Human activities on the delta plain alter sediment delivery by modifying the quantity of sediment entering channel networks through soil and bank erosion (Best and Darby, 2020; Pelletier, 2012).

Activities related to urbanization, agriculture, economic development, and land conversions, are leading dramatic alterations in sediment transport dynamics (Best, 2019; Syvitski and Kettner, 2011; Syvitski and Milliman, 2007; Walling and Fang, 2003). Furthermore, increased industrial activity and exploitation of natural resources, such as through sand mining, building construction and infrastructure development, lead to land disturbance that increases the likelihood of high sediment yields (Li et al., 2020; Syvitski and Kettner, 2011; Walling and Fang, 2003). Unless eroding from the delta plain is explicitly quantified, reasonable estimates of cumulative fluxes of sediment from land to ocean is difficult to ascertain.

Despite the importance of deltaic environments and the key role of distributary branches in their morphological functioning, there are no comprehensive studies quantifying intra-deltaic sediment fluxes (Syvistski et al. 2005a). Current literature only provides examples of studies performed at individual bifurcation scale, analyzing partitioning of water and sediment utilizing field surveys, and numerical and physical experiments (Bolla Pittaluga et al., 2003; Kleinhans et al., 2008; Redolfi et al., 2019; Dong et al. 2020), and a few studies on basin-scale influence of landuse change and human activities on sediment fluxes in the feeder river of the delta. Quantification of sediment in the distributary network of large river deltas is key for studying delta/coastal morphodynamics (variations in the 3-D morphology of deltas and the coastal shelf) (Syvitski et al., 2005b), alongshore sediment transport, delta pragradation, predicting impacts of relative sea level rise on deltaic land subsidence (Syvitski et al., 2009), channel migration within the delta plain (Nienhuis et al., 2016), and engineering developments such as making recommendations on flood control structures, artificial channel modifications and navigation.

In this study, we use two recently released global datasets to provide, for the first time, an assessment of the impact of human modifications on river delta plains on the sediment loading

into delta distributary networks. Using 44 case studies we quantify (a) sediment eroding into the distributary network originating from the delta plain, (b) the distribution of sediment within the channel orders of the distributary network, and (c) the key human drivers of river delta plain modification their intensities, and the relationship to sediment loading into distributary channel networks.

2. Methods

2.1 Case Studies

The study was performed on 44 major Global River Deltas (Figure 1) curated to represent 4 major and 13 sub-Köppen Climate Classes (climate, biome, and socioeconomic contexts). They cover a range of geographic, fluvial and socioeconomic contexts, and the 3 main delta morphology types; river-, tide- and wave-dominated deltas. The Köppen Climate Classification is based on air temperature and precipitation and represents biome distributions around the world: different regions in a similar class share common vegetation characteristics (Beck et al., 2018). The choice of deltas was based on the availability of data from databases and scientific literature, delta size (large deltas were chosen to accommodate fluvial sediment simulations to deltas performed in a companion study), and the geographical distribution.

Table 4.1. River deltas and their characteristics

River Delta	Continent	Major Köppen Climate Class	Delta Area (km2)	Long-Term Average Suspended Sediment Flux to the Delta (kg/s)	Distributary Channel Length (km)	Total Sediment loading into Distributary Channels	Average Human Modification of Delta Plain	Most Dominant Stressor on Delta Plain
Amazon	SA	Tropical	108,950	99,695	4,810	1,693,219	0.099	Population
Brahmani	AS	Tropical	7,088	143	1,283	5,480,825	0.648	Population
Burdekin	OC	Tropical	1,398	200	50	26,360	0.257	Cropland
Chao_Phraya	AS	Tropical	25,225	616	1,897	8,046,975	0.785	Cropland
Colorado	NA	Arid	11,992	2,023	960	184,949	0.229	Livestock
Congo	AF	Tropical	2,243	36,883	516	990,453	0.335	Population
Danube	EU	Arid	9,955	1,649	596	74,035	0.324	Livestock
Dnieper	EU	Continental	1,715	41	200	14,237	0.439	Population
Ebro	EU	Temperate	939	45	94	72,885	0.434	Night-time lights
Ganges	AS	Tropical	109,528	46,328	12,512	33,272,112	0.702	Cropland
Godavari	AS	Tropical	4,355	2,921	317	1,112,969	0.694	Population
Grijalva	NA	Tropical	12,769	1,985	1,963	3,619,163	0.462	Cropland
Han	AS	Temperate	4,056	199	151	598,965	0.714	Night-time lights
Hong	AS	Temperate	6,497	2,345	357	2,104,110	0.724	Cropland
Indus	AS	Arid	6,991	6,953	242	274,241	0.325	Population
Irrawaddy	AS	Tropical	36,242	25,424	2,340	4,429,419	0.510	Population
Krishna	AS	Tropical	2,635	511	163	551,431	0.638	Cropland

Limpopo	AF	Tropical	4,140	337	909	1,194,071	0.337	Population
Magdalena	SA	Tropical	4,278	9,679	502	285,407	0.407	Livestock
Mahakam	AS	Tropical	5,570	3,998	799	1,680,975	0.454	Night-time lights
Mahanadi	AS	Tropical	7,779	1,431	521	1,984,934	0.661	Population
Mekong	AS	Tropical	52,405	28,260	3,624	11,124,091	0.541	Population
Mississippi	NA	Temperate	38,747	3,974	1,030	1,002,693	0.323	Night-time lights
Moulouya	AF	Arid	791	40	123	41,412	0.572	Cropland
Niger	AF	Tropical	18,819	20,286	889	317,282	0.430	Population
Nile	AF	Arid	37,790	406	1,143	18,921	0.720	Cropland
Orinoco	SA	Tropical	27,529	18,780	980	210,094	0.127	Population
Parana	SA	Temperate	21,977	43,476	2,640	1,023,324	0.365	Livestock
Pearl	AS	Temperate	13,618	12,315	1,360	4,762,955	0.727	Night-time lights
Po	EU	Temperate	1,894	358	162	135,282	0.682	Cropland
Rhine	EU	Temperate	12,483	739	263	10,272	0.750	Night-time lights
Rhone	EU	Temperate	3,205	321	136	37,111	0.553	Night-time lights
Rio_Grande	NA	Temperate	19,653	82	1,013	1,094,448	0.456	Cropland
Sao_Francisco	SA	Tropical	1,355	310	346	486,791	0.308	Night-time lights
Sebou	AF	Temperate	359	666	107	58,719	0.640	Population
Senegal	AF	Arid	4,947	371	833	286,059	0.264	Population
Shatt_el_Arab	AS	Arid	6,341	15,665	342	11,514	0.326	Population
Tana	AF	Tropical	921	2,513	161	163,681	0.260	Population
Tone	AS	Temperate	1,565	44	277	572,424	0.732	Night-time lights

Vistula	EU	Temperate	7,697	406	113	13,957	0.687	Cropland
Volta	AF	Tropical	2,948	1,406	277	344,910	0.547	Population
Yangtze	AS	Temperate	50,751	12,107	946	2,533,618	0.778	Night-time lights
Yellow	AS	Temperate	10,230	2,391	235	342,199	0.531	Cropland
Yukon	NA	Polar	26,115	3,046	917	7,658	0.004	Livestock

**These are simulated fluxes from the WBMsed global hydro-geomorphic model. Model calibration, validation and simulation settings are available from Cohen et al. (2013, 2014).*

Figure 4.1. Map showing the 44 deltas used in this study.

2.2 Extraction of Distributary Channel Networks on River Delta Plains

The hydrographic dataset published as supplementary to the research article by Grill et al. (2019) (hereafter referred to as the Grill dataset) is used to extract distributary channel networks for each of the river deltas. The Grill dataset is a geometric network of the global river system consisting of hydro-geometric properties (e.g. sediment flux, water discharge) for each individual river reach (see Figure 2 for the definition of a 'river reach'). The Grill dataset is temporally static and the values of hydro-geomorphic attributes of reaches are mostly long-term averages. It is available for download at https://doi.org/10.6084/m9.figshare.7688801. Figure 2 below shows how rivers, river reaches, and reach catchments are conceptually defined in the dataset.

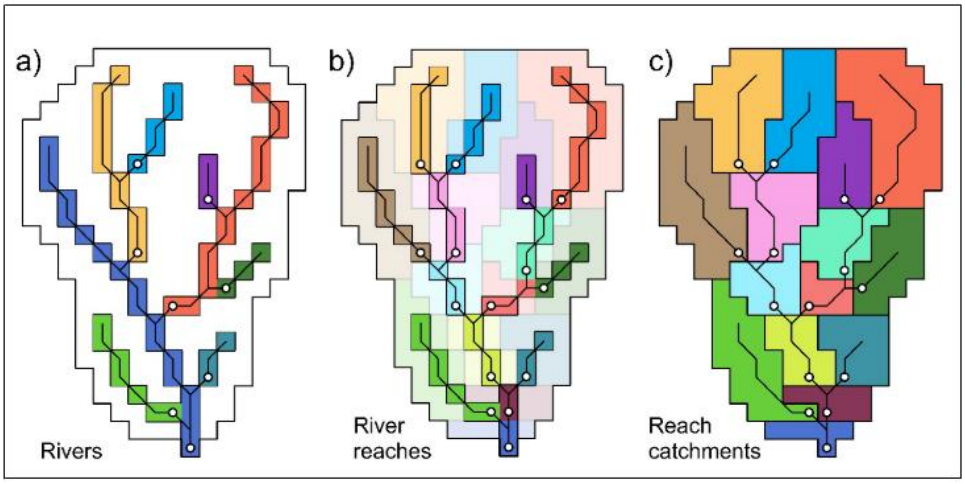

Figure 4.2. The panels show the grid cell delineation into (a) rivers; (b) river reaches; and (c) spatial zones that represent the contributing area of each river reach, i.e. reach catchments. Individual rivers, river reaches, and reach catchments are identified by different solid colors. Black river or river reach lines show the corresponding vector representation. The white dots represent the pour point of each river or river reach. (Source: Grill and Lehner., 2019)

The Backbone River Identifier (BB_ID; an attribute of the dataset) represents the contiguous river unit (the flow path from source/headwater to sink/terminus). All river reaches connected to the feeder river responsible for the construction of the river delta is identified using the BB_ID. To explicitly identify distributaries on the river delta plain, river delta extents (shapefile polygon representation of the plan view of the river delta plain) of these 44 deltas provided by Tessler et al. (2016) are used as cookie-cutters to extract the delta plain channel network.

2.3 Analysis of Sediment Transported in the Distributary Channel Network

One of the attributes in the Grill dataset is the ‘sum of erosion in tons per year’ (ERO_YLD_TON). This is a long-term average of the sediment erosion within the river reach catchment (Figure 2 (c)). Using the previously extracted delta plain channel network, analysis

was performed to quantify (a) the total amount of sediment that moves through the network and (b) the distribution of sediment among the different channel orders for each delta. We make note that this sediment is a function of erosion in the river reach catchment only, apropos to the study goal (i.e. analysis of how modifications on the delta plain influence the sediment loading into channels). It does not account for sediment that is already transported in the system from upstream catchments. It is only the sediment generated from within the delta plain, eroded into the distributary channel network, and sequestered in lowland wetlands or drained into the ocean. It is noted that in the Grill dataset, the sediment that is transported in the given reach is equal to the sediment eroded from governing reach catchment. Typically, what is transported in a reach segment is not the same as what is loaded into the channel from erosion in the governing catchment, as deposition on floodplains, deposition on channel beds, bed scouring, and riverbank erosion can alter fluxes in the channel. This shortcoming is addressed in Grill et al., 2019 during dataset production.

The sediment that is concentrated in the entire channel network for a given delta is calculated by accumulating the per-reach segment sediment values. We also calculate length-averaged sediment delivery (sediment transport per km of river reach) which is envisioned to have more more pragmatic applications in river science.

Next, we calculate how the loaded sediment is distributed in the different delta network channel orders. Sediment values of each river reach are concatenated separately for a given channel order (e.g. total sediment of reach segments of order 7; total sediment of reach segments of order 8 etc.). Channel orders in the Grill dataset are not based on the Strahler stream order. Although they show a certain degree of similarity, the channels in the Grill Dataset are based on

long-term average discharge (CMS; cubic meters per second) of each river order (Table 1), unlike explicitly on the hierarchy of tributaries in the Strahler system.

Table 4.2. Discharge categories of Channel Orders

Channel Order	Long-Term Average Discharge (CMS)
1	>100000
2	10000 – 100000
3	1000 – 10000
4	100 – 1000
5	10 – 100
6	1 – 10
7	0.1 - 1
8	0.01 - 0.1
9	0.001 - 0.01
10	< 0.001

2.4 Quantifying Anthropogenic Modification of Delta Plains

The Global Human Modification Dataset (gHM) developed by Kennedy et al. (2019; available on Google Earth Engine) is used to provide a cumulative measure of human modification of terrestrial lands globally at 1 square-kilometer resolution (Kennedy et al., 2019). The cumulative Human Modification (HMc) values range from 0.0-1.0 and are calculated by estimating the proportion of a given location (pixel) that is modified based on a given type(s) of human modification or "stressor" acting on that location. 13 such stressors are identified (i.e. population, settlements/built-up areas, cropland, livestock, major/minor roads, tracks, railways, powerlines, mining, oil wells, wind turbines, night-time lights). A detailed description of the human stressors is explained in Keneddy et al. (2018). The modification intensities are categorized into four modification classes: “low” ($0.00 \leq HMc \leq 0.10$), “moderate” ($0.10 < HMc$

≤ 0.40), “high” (0.40 < HMc ≤ 0.70), and “very high” (0.70 < HMc ≤ 1.0). These values are measured on a ratioscale with meaningful differences: 0.00 indicating no impact, and 0.25 indicating half the intensity of impact of 0.50 (Kennedy et al. (2019) Supplemental Info). A threshold of 0.4 is used to demarcate a transition from a moderate to a highly modified state, because it corresponds to low-intensity agriculture, thus, approximating to a transition to a human-dominated state. Tessler et al. (2016) river delta extents are used to extract the delta plain areas from the gHM dataset. The Irrawaddy Delta is used in Figure 3 to illustrate the intensities of human modification (panel a), intensity classes (panel b), the number of stressors acting on a given pixel (panel c), and the most dominant stressor on a pixel (panel d).

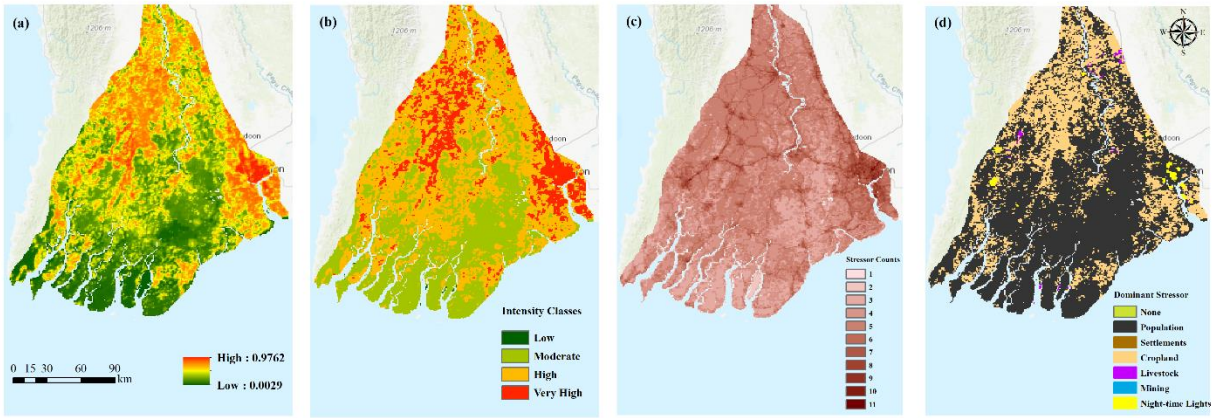

Figure 4.3. Overview of human modification of Irrawaddy Delta; (a) Human modification intensities across the delta (b) modification intensity classes (c) the number of human stressors acting on a given location (pixel) (d) the most dominant type of stressor at a given location

For each of the 44 delta plains, the following calculations were conducted: (1) average modification, calculated by summing up intensity values of pixels within a delta plain and dividing it by the pixel count, (2) total areas of each of the 4 intensity categories within the delta plain, (3) the number of stressors and the most dominant stressor(s) acting on each delta plain.

Next, we investigate potential differences of human modification in the coastal zone, which tend to include more intense economic activities (Wang et al., 2012; Yu et al., 2014), and the rest of the delta plain. A 5 km buffer was created to the shoreline (shorelines for the 44 river deltas were generated in Munasinghe et al. (under review)) to demarcate the coastal zone. Although it is understood that the exact extents of coastal zones of river deltas vary by biomes/ climate region, vegetation zonation, and type of river delta (Munasinghe et al. 2021), a 5 km was chosen for all deltas for uniformity and to be commensurate with the resolution of the other data layers (this approach has precedence in literature (Lo and Gunasiri, 2014)). This buffer was used on the human modifications of the river delta plain to extract the modifications exclusively of the coastal zone (hereinafter coastal zone layer). All analyses done for the entire delta plain were also conducted within these the coastal zones.

2.5 Relationship between Delta Plain Human Modification and Sediment loading into Distributary Channels

We use five statistical approaches to understand relationships between human modification and sediment in the channel network:

(1) Correlation analysis between the average modification on the delta plain and the total sediment eroded into the channels.

(2) Correlation analysis between the average modification on the delta plain and the delta plain area-normalized sediment erosion.

    Correlation analysis between average modification on the delta plain and the average sediment per sub-basin (summation of all sediment from the sub basins and dividing by the number of sub basins).

(3) The sub-basin used is the level 12 basin (smallest basin) of the Pfafstetter system (Lehner, 2019; Grill and Lehner, 2019; Pfafstetter, 1989). Basin and sub-basin delineations are pre-processed during the creation of the Grill dataset and available at https://www.hydrosheds.org/page/hydrobasins . These delineations offer a suite of 12 layers, each containing nested sub-basins that are subdivided and coded using the topological concept of the Pfafstetter system.

(4) Correlation analysis for each of the 44 deltas based on the average modification and average sediment generated within each sub-basin.

(5) Regression analysis to understand the effect of different categories of human modification (i.e. the 4 different intensity classes) of land have on sediment erosion.

3. Results and Discussion

3.1 Sediment Distribution in the Deltaic Channel Network

3.1.1 The Total Sediment in the Network

An overview of the total sediment that is dispersed in the channel network and amounts per unit length of channel in each delta is presented in Figure 4.

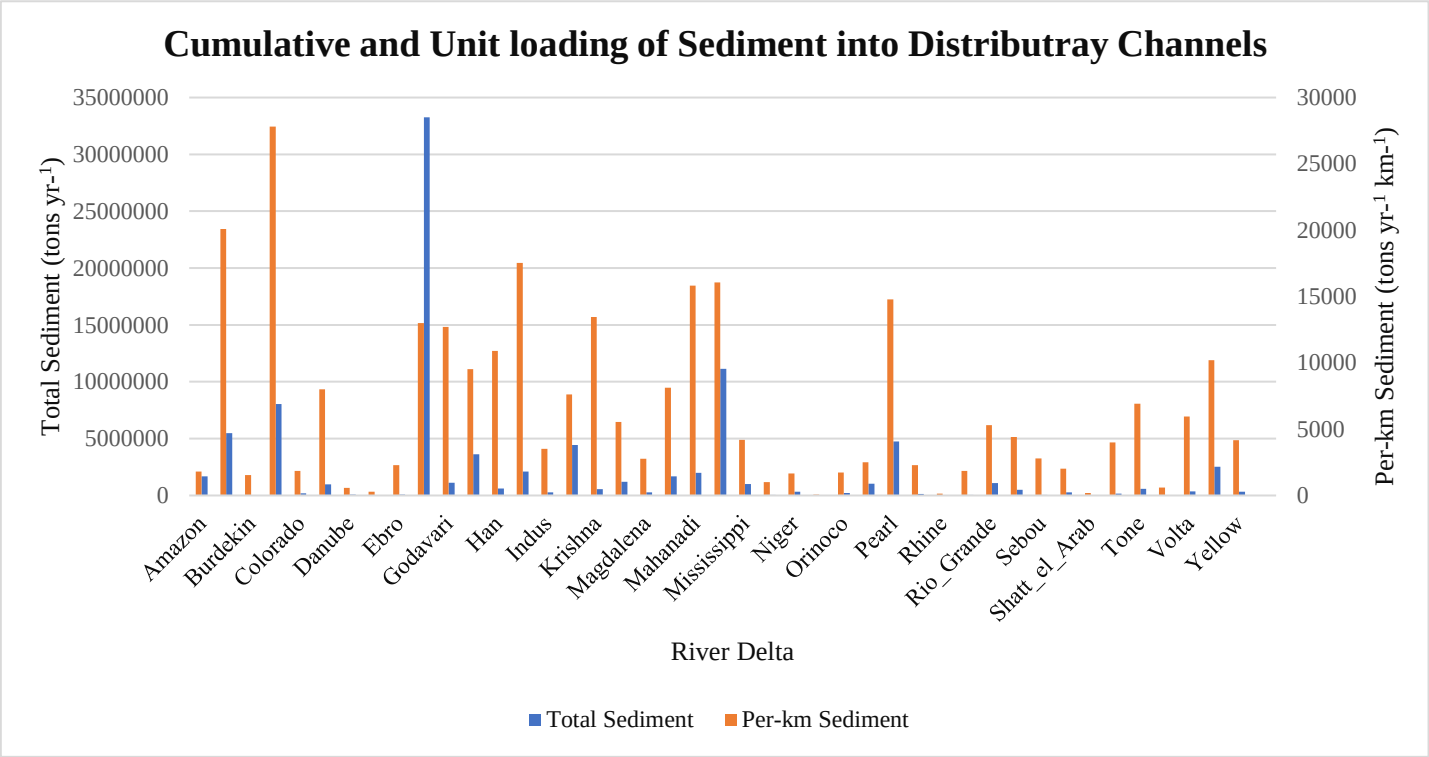

Figure 4.4. A comparison between the total (tons yr^{-1}) and length-averaged sediment (tons $yr^{-1}km^{-1}$) in channel networks resulting exclusively from delta plain erosion.

Of the river delta plains analyzed, the Ganges delta plain recorded the highest total sediment input (33,272,111 tons/year) while the Yukon recorded the lowest (7,658 tons/year). A mean of 2,097,526 tons yr^{-1} with a standard deviation of 5,319,365 tons yr^{-1} across deltas are observed. The length-normalized calculations show that the Chao Phraya delta plain has the highest value with 27,801 tons yr^{-1} km^{-1} while Yukon generates the lowest value with 29 tons yr^{-1} km^{-1}. We see relatively high per-km values when compared to the trend of total sediment in Burdekin, Ebro, Sebou, Moulouya deltas suggesting higher concentration of sediment in their distributary networks. Interestingly, Ganges' per km sediment value does not follow the trend of

the total sediment yield. Low per-km erosion values could be due to a) high density of distributary channels (effectively increasing the channel network length), 2) higher proportion of lower order channels (8-10) which transport relatively less sediment, and/or 3) low rates of soil mobilization on the delta plain. In comparison, high per-km sediment yield values in afore-mentioned deltas could be due to the reverse of said phenomena, or more importantly, increased erosion on the plain due to human modifications. The variability even for normalized values across deltas was orders of magnitude apart with a mean of 6,307 tons yr^{-1} and a standard deviation of 6,387 tons yr^{-1} across deltas.

3.1.2 Distribution of Sediment in the River orders

Understanding how the cumulative sediment quantities are partitioned between different channel orders may be useful to generalized trends such as hotspots of sediment depletion on the delta plain, where nutrient delivery and uptake are located, estimation of delta responses to environmental and anthropogenic stresses (sea level rise, modification and subsequent erosive areas of the delta plain), and assisting in management decisions on coastal restoration (Passalaqua , 2017; Dong et al., 2020). Figure 5 provides a summary of how the total sediment that were analyzed in the earlier section, are dispersed among the different river orders of the channel network.

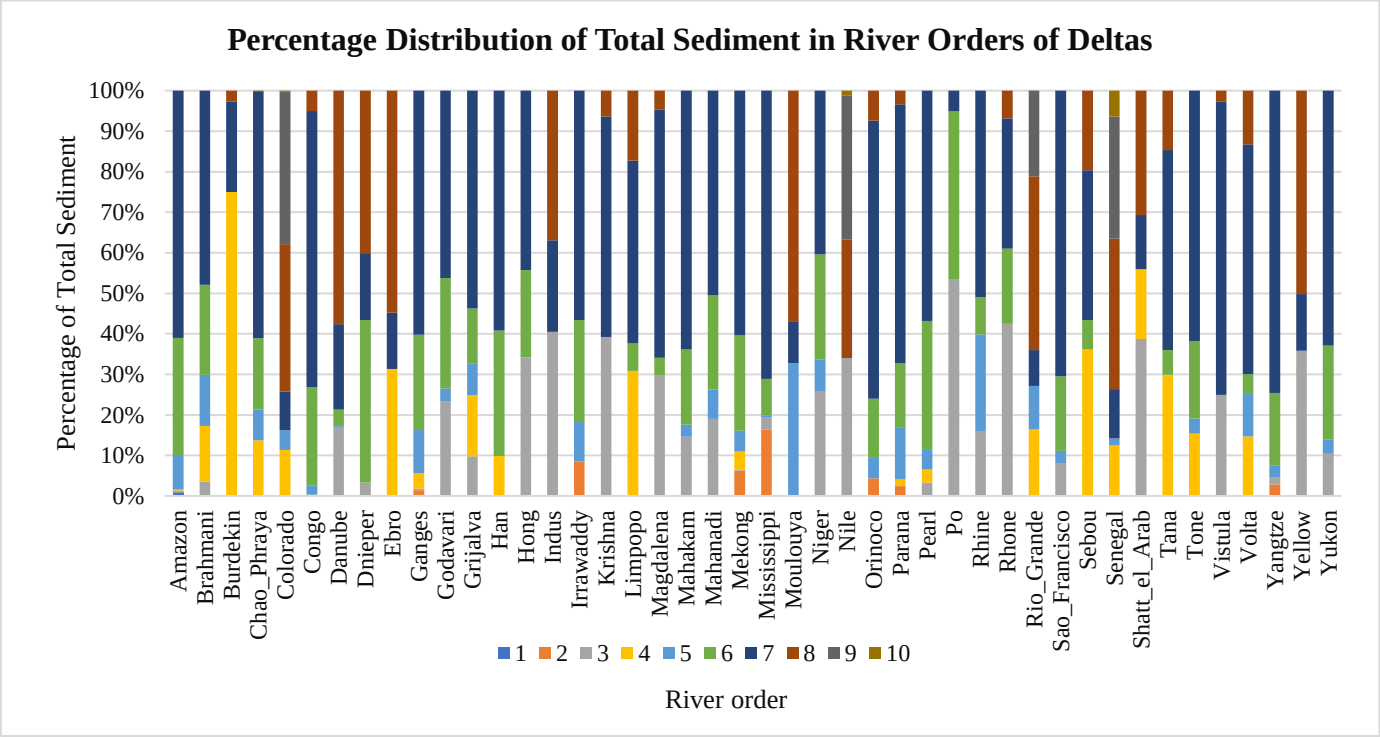

Figure 4.5. Comparison between the percentage distribution of the total sediment transported across the channel orders.

It can be elucidated from Figure 5 that most of the sediment is concentrated in orders 6, 7 or 8 in river deltas. Further investigation shows that this is mainly because most delta plains are dominated by the mid-order channels and are limited in channels belonging to orders that are high (1-3) or at the lower end (9-10). We summarize the length-normalized sediment of a particular order for a given delta by averaging sediment values of all such orders across deltas with the intention of creating transferable results to lesser studied regions (Table 2).

Table 4.3. The ranges of sediment in distributary channel orders

Channel Order	Length-averaged Sediment in channel order (tons yr^{-1} km^{-1})
2	921.759
3	1300.03
4	1462.364
5	1474.045
6	1556.361
7	1683.201
8	1652.899
9	405.3747

River orders 7 and 8 were where the most amount of sediment was found to be per unit distance (1683.201 and 1652.899 tons yr^{-1} km^{-1} respectively). These results bring out a few interesting notions. In a typical watershed, you would expect to see high sediment accumulation in high discharge orders: not in this case. The sub catchments governing the reach segments of higher discharge orders (2-4) in this study lay close to the coast, were extremely low/almost non-existent slope prevails. Low slope culminates in low amounts of plain erosion. On the other hand, high values in lower discharge channels (6-9) could mean either a) there is significant erosion going on in delta plain catchments of lower order reaches than higher order ones or b) anthropogenic-driven soil erosion in upstream areas of the deltas is, on average, greater. The reasons for mid-order channels to show dominance can be attributed to intense agricultural activities in mid-delta plain regions. Soil mobilization and sediment erosion due clearing of land (and associated excess runoff), ploughing, and tilling are major drivers. These will be investigated below.

3.2 Human Modifications of River Delta Plains

3.2.1 Intensities of human modifications across delta plains

Humans modifications of delta plains and stream networks are highly heterogenous, both between global and within individual deltas. Figure 6 shows the average cumulative Human Modification (HMc) index, a comparative reflection of human modifications across deltas. Figure 7 is a summary of the distribution of the percentage of delta plain land of different intensity categories.

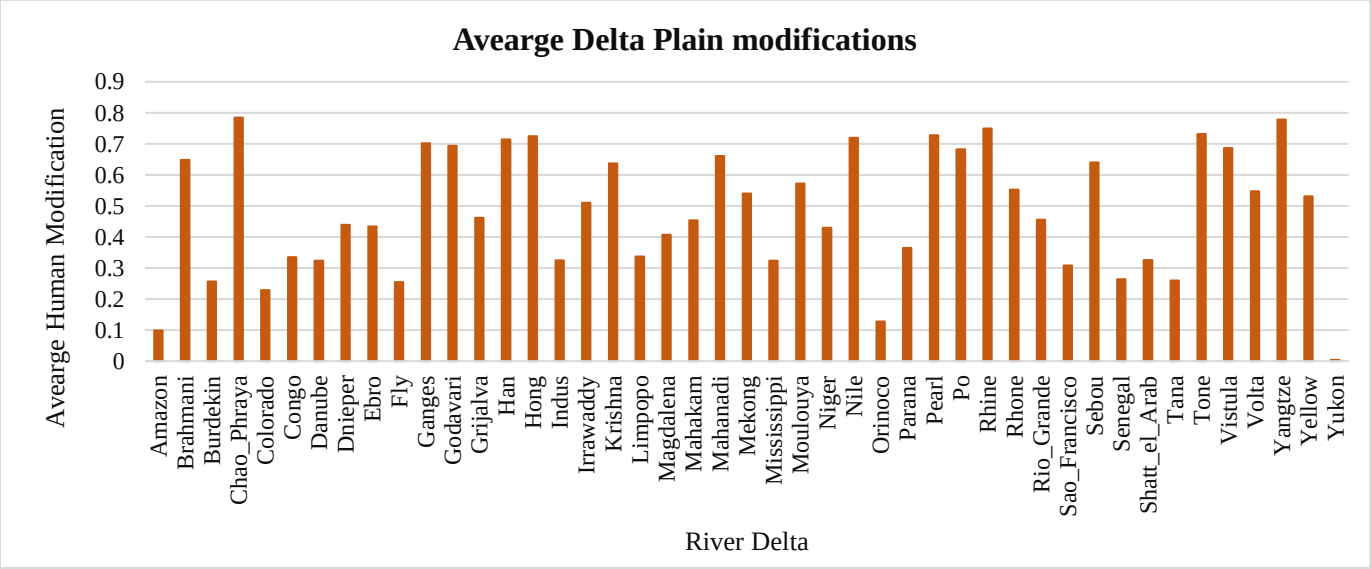

Figure 4.6. Average human cumulative Human Modification (HMc) intensities on river delta plains. Higher the value, higher the level of modification.

Top 5 lowest modified delta plains are Yukon (0.0044), Amazon (0.09), Orinoco (0.127), Colorado (0.229) and Fly (0.255). These river deltas in turn contain the highest pristine areas. Top 5 highest modified deltas are Chao Phraya (0.784), Yangtze (0.778), Rhine (0.749), Tone (0.732) and Pearl (0.727) (see Table 1 for more details). The most anthropogenically influenced river deltas (percentage of category 4 land area) are Chao Phraya (97.09%), Yangtze (89.47%), Hong (79.74%), Po (77.22%) and Nile (75.12%). The highest percentages of pristine lands

(percentage of category 1 land area) are at Yukon river delta (98.49%), followed by the Amazon (69.52%), Colorado (50.21%), Orinoco (46.18%) and Fly (44.8%). 19 of the deltas have no pristine areas available (it has to be noted that there can be sub-pixel areas that are pristine; a 1 x 1 km grid pixel in the dataset records an average modification of land within that pixel).

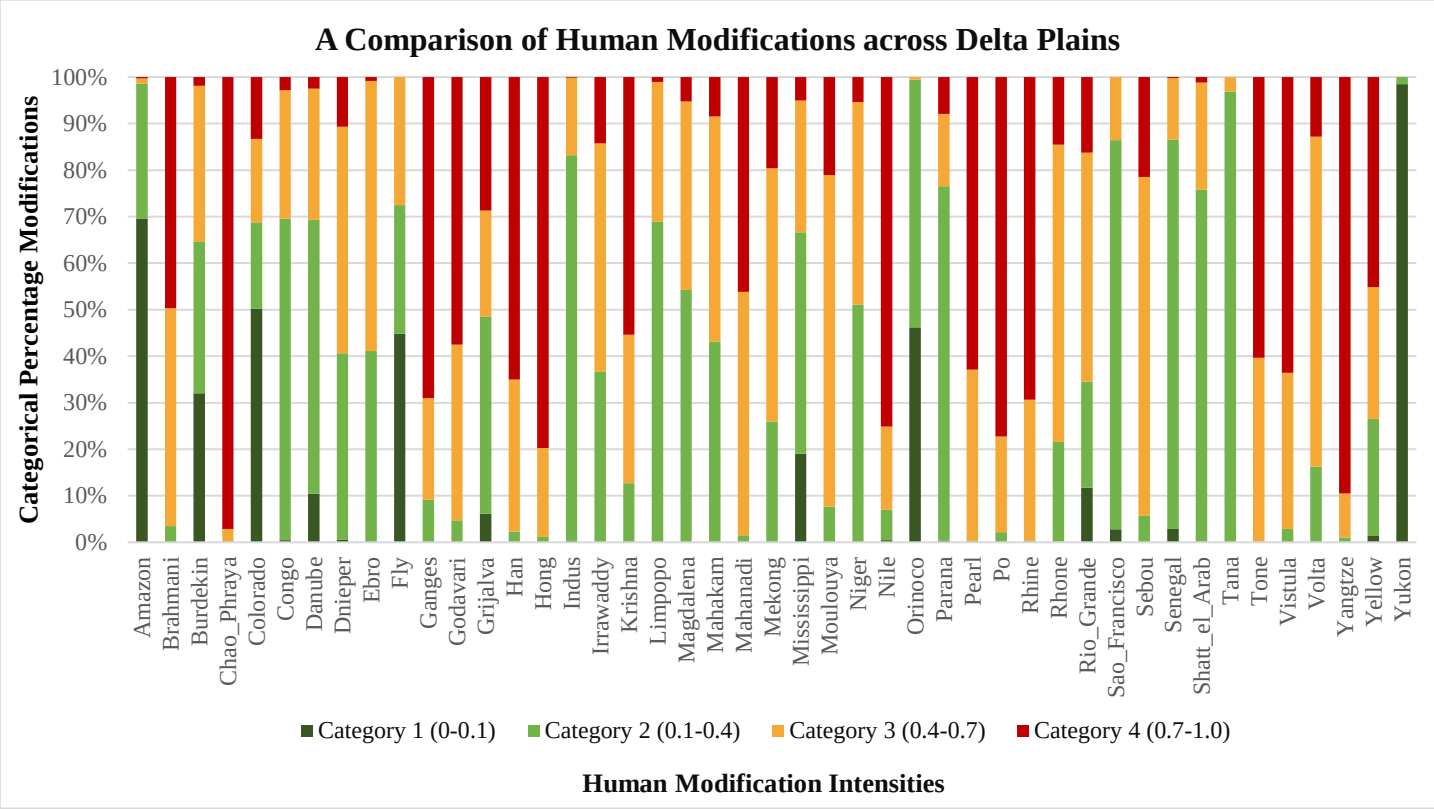

Figure 4.7. Stacked bars representing the percentage of deltaic land belonging to each intensity category of modification

When the percentage of land belonging to each intensity category was ranked for each delta, Category 1 land was recorded as the highest in 4 deltas, Category 2 in 14 deltas, Category 3 in 12 deltas, and Category 4 in 15 deltas, resulting in 27 of the 44 delta plains land area being subject to high/very high human modification (Categories 3 and 4). There are no deltas with only 1 type of intensity category covering the entire delta plain suggesting that none of the deltas are fully pristine; deltas are modified across the plain at different rates, and the modifications are

highly diversified between deltas. When land area of a particular category across all deltas are analyzed, the following area percentages results: Category 1: 17.75%; Category 2: 25.54%; Category 3: 23.19%; Category 4: 33.52%. A cumulative of 56.71% of total deltaic land are highly or very highly modified by humans.

3.2.2 Drivers of Delta Plain Modifications

To understand driving factors/anthropogenic stressors governing delta plain land modifications, we summarize the results of percentages of 13 anthropogenic stressors found to be acting on deltaic land (Figure 8). It should be noted that these might not be the only driving forces, but analyses are constrained by the attributes of the dataset (see Supplement 1 of Kennedy et al. 2019 for details).

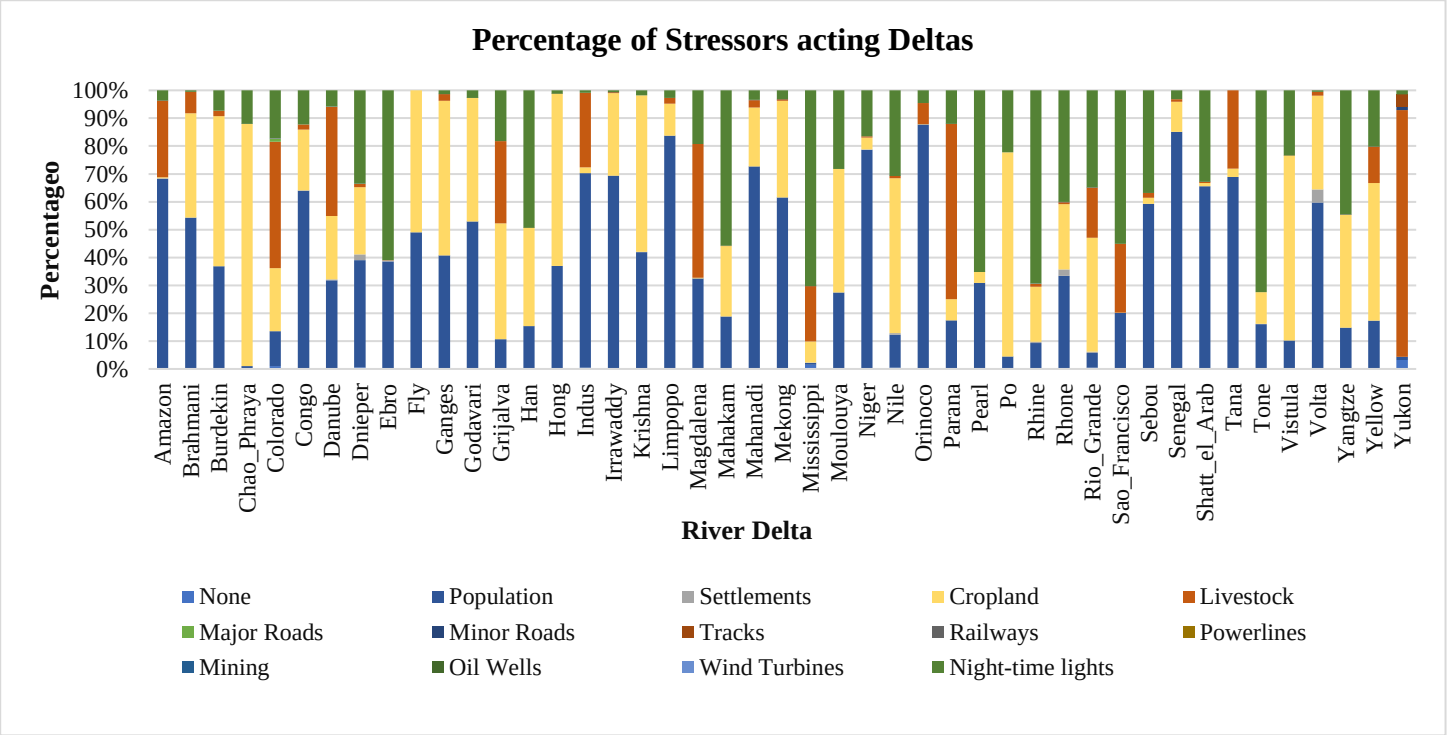

Figure 4.8. Stacked bars representing the percentage of each stressor acting on the entire delta plain. Note: 'None' in the legend represent no-stressor activity on a given land pixel. Results show that there were 0 'none' pixels in all deltaic land.

The results show that Human settlements (population), Agriculture (Cropland) and Night-Time Lights are identified as the most dominant stressors on deltaic land. The most dominant human stressors on each delta are summarized in Table 4. No deltas had less than 6 stressors. There were no deltas for which all 13 stressors present. The highest number of stressors for given delta are 12 and can be found in 4 deltas (Danube, Ganges, Mississippi, Parana). We generally see that a higher number of stressors acted on relatively larger deltas.

Table 4.4. River deltas governed by a stressor category. Frequency is the number of deltas that are governed by that particular human stressor.

Dominant Stressor	Frequency	Case Study Examples
Population Density	17	Volta, Tana, Shatt-el-Arab, Senegal, Sebou, Amazon, Brahmani, Congo, Dnieper, Godavari, Indus, Irrawaddy, Limpopo, Mahanadi, Mekong, Niger, Orinoco
Built-up areas/ Settlements	0	
Cropland	13	Yellow, Vistula, Burdekin, Chao Phraya, Fly, Ganges, Grijalva, Hong, Moulouya, Nile, Po, Rio Grande, Krishna,
Livestock	5	Yukon, Colorado, Danube, Magdalena, Parana
Major Roads	0	
Minor Roads	0	
Tracks	0	
Railway	0	
Powerlines	0	
Mining	0	
Oil Wells	0	
Wind-Turbines	0	
Night-time lights	10	Yangtze, Tone, Ebro, Han, Mahakam, Mississippi, Pearl, Rhine, Rhone, Sao Francisco

A comparison between drivers affecting the entire delta plain and deltaic coastal zones shows that although for Population density (17 deltas) and Cropland (13 deltas) rank as the most dominant when the entire delta plains are considered, in the coastal zone, the dominance of

cropland decreases to 4 (Chao Phraya, Fly, Moulouya, Po). However, the dominance of population density (25 deltas) and Night-time lights (14 deltas) increases. The differences between coastal and delta plains can be explained by human migration towards the coast to build megacities (over 1 billion people live in megacities) and increase use of inland deltaic land for agriculture (due to soil salinity in coastal regions) and livestock. This may also explain the higher sediment yield in mid-order channels as agricultural land use tend to yield greater soil erosion than built environments.

3.3 Relationship between Delta Plain Modification and Sediment Transport in the Distributary Channel Network

To elucidate a generalized relationship between human modifications on the delta plain and the sediment loading into the channel network, regression analysis was performed between average modification of delta plains (average HMc values; Figure 6) and the area-normalized total sediment from each delta plain. Area-normalization (dividing the total sediment loaded into the channel network from the delta plain by the area of the delta) was thought of as a good indicator as it provides the capability to transfer results to other river deltas, globally. We observe an R^2 of 0.26 for the afore-described relationship (Figure 10); in other words, 27% of the variability of sediment that is loaded into the distributary channels is explained by anthropogenic stress on the river delta plains. This we think is a significant outcome, especially considering the global distribution of the deltas. The remainder (73%) is attributed to naturally driven soil erosion due to factors such as river delta gradient, temperature and precipitation regime in the deltaic region.

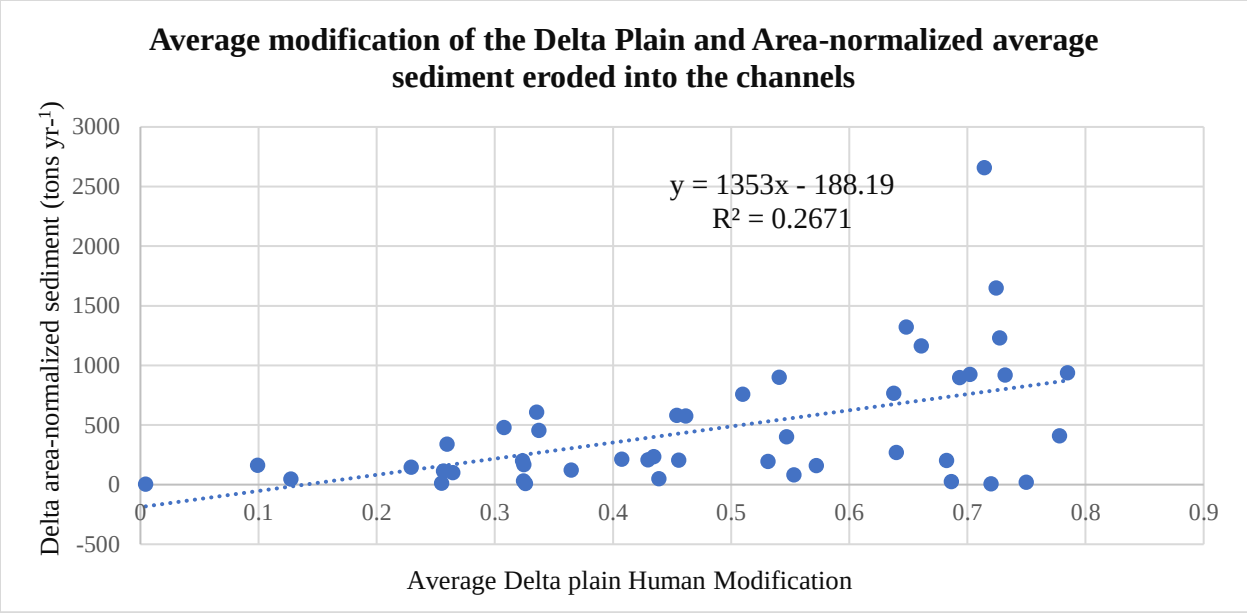

Figure 4.9. Relationship between anthropogenic stress on the delta plain sediment loading into distributary channels

We also inferred on any standout relationships between average modification *within a sub-basin* of a river delta (this is the level 12 Pfafstetter basin) and the total sediment generated *within that sub-basin* to explain individual dynamics of river deltas. Average modification and average sediment generated within sub-basins of each delta were regressed. 44 such relationships were tested. The Regressions were generally low with the lowest being 0.0005 (Rhone delta), and the highest, 0.52 (Krishna). The highest correlations were Krishna (0.53), Po (0.38), Mahakam (0.33), Parana (0.32), Yellow (0.31), Brahmani (0.30), Grijalva (0.26), Niger (0.23). The lowest were Rhone (0.0005), Nile (0.001), Yukon (0.001) and Pearl (0.006). Although, in general, the relationships were moderate, five of the top 8 highest correlated deltas are found to be in the tropical region (main Köppen Climate Class), and 3 of the top 4 lowest were in Temperate or cold Regions. We attribute the relatively high correlations in the tropical regions to the soil mobilization and rapid urbanization due to delta plain agricultural activities of mostly developing countries in the equatorial belt. Intense monsoonal precipitations and faster soil

weathering due to temperatures may also be an explanatory factor. On the other hand, colder climates decrease soil weathering and agricultural soil mobilization.

4. Conclusions

This study investigated the human impact of delta plain modifications on the sediment loading into the distributary channel networks of 44 global river deltas. The results show that (a) most of the sediment is concentrated in orders mid-order distributary channels, with about 75% of average sediment fluxes carried in orders 4 and 7. Agricultural activities in mid-delta plain regions are speculated to this dominance. The averages of sediment in each channel order are summarized envisioning potential applications in other deltaic regions. (b) the most anthropogenically influenced river deltas (above 75% land in the “very high” modification category) are Chao Phraya, Yangtze, Hong, Po, and Nile. The Yukon and Amazon are the least modified. In total 56.71% of total deltaic land are highly or very highly modified by humans. There is only 17.75% of deltaic land that is of very low alteration. (c) Population, Cropland and Night-Time Lights are identified as the most dominant stressors on deltaic land. The population stress increases towards the coastal zones. (d) Human modifications on the delta plain accounts for 27% of the variability of sediment that is loaded into the deltaic distributary channel network. We envision outcomes of this study helping better understand anthropogenic presence in river delta systems and complement sustainable delta management efforts.

References for Chapter 4

Beck, H. E., Zimmermann, N. E., McVicar, T. R., Vergopolan, N., Berg, A., and Wood, E. F. (2018). Present and future Köppen-Geiger climate classification maps at 1-km resolution. Scientific data, 5(1), 1-12.Best, J., 2019. Anthropogenic stresses on the world's big rivers. *Nature Geoscience*, *12*(1), pp.7-21.

Best, J. and Darby, S.E. (2020). The Pace of Human-Induced Change in Large Rivers: Stresses, Resilience, and Vulnerability to Extreme Events. *One Earth*, *2*(6), pp.510-514.

Bolla Pittaluga, M., Repetto, R., and Tubino, M. (2003). Channel bifurcation in braided rivers: Equilibrium configurations and stability. *Water Resources Research*, *39*(3).

Cohen, S., Kettner, A. J., Syvitski, J. P., & Fekete, B. M. (2013). WBMsed, a distributed global-scale riverine sediment flux model: Model description and validation. *Computers & Geosciences*, *53*, 80-93.

Cohen, S., Kettner, A. J., & Syvitski, J. P. (2014). Global suspended sediment and water discharge dynamics between 1960 and 2010: Continental trends and intra-basin sensitivity. *global and planetary change*, *115*, 44-58.

Dong, T.Y., Nittrouer, J.A., McElroy, B., Il'icheva, E., Pavlov, M., Ma, H., Moodie, A.J. and Moreido, V.M. (2020). Predicting Water and Sediment Partitioning in a Delta Channel Network Under Varying Discharge Conditions. *Water Resources Research*, *56*(11), p.e2020WR027199.

Du, J. L., Yang, S. L., and Feng, H. (2016). Recent human impacts on the morphological evolution of the Yangtze River delta foreland: A review and new perspectives. *Estuarine, Coastal and Shelf Science*, *181*, pp.160-169.

Edmonds, D. A., and Slingerland, R. L. (2008). Stability of delta distributary networks and their bifurcations. *Water Resources Research*, *44*(9).

Grill, G., Lehner, B., Thieme, M., Geenen, B., Tickner, D., Antonelli, F., Babu, S., Borrelli, P., Cheng, L., Crochetiere, H. and Macedo, H.E., 2019. Mapping the world's free-flowing rivers. *Nature*, *569*(7755), pp.215-221.

Grill and Lehner, 2019: Mapping the world's free-flowing rivers-Dataset and attributes-Technical Documentation Version 1.0 available at https://figshare.com/articles/dataset/Mapping_the_world_s_free-flowing_rivers_data_set_and_technical_documentation/7688801

Jarriel, T., Isikdogan, L. F., Bovik, A., and Passalacqua, P. (2020). System wide channel network analysis reveals hotspots of morphological change in anthropogenically modified regions of the Ganges Delta. *Scientific Reports*, *10*(1), pp.1-12.

Kennedy, C. M., Oakleaf, J. R., Theobald, D. M., Baruch-Mordo, S., and Kiesecker, J. (2019). Managing the middle: A shift in conservation priorities based on the global human modification gradient. *Global Change Biology*, *25*(3), pp.811-826.

Kleinhans, M. G., Jagers, H. R. A., Mosselman, E., and Sloff, C. J. (2008). Bifurcation dynamics and avulsion duration in meandering rivers by one-dimensional and three-dimensional models. *Water resources research*, *44*(8).

Lehner, 2019: Hydroatlas Technical Documentation Version 1.0 available at https://hydrosheds.org/images/inpages/HydroATLAS_TechDoc_v10.pdf

Li, Z., Saito, Y., Matsumoto, E., Wang, Y., Tanabe, S., and Vu, Q. L. (2006). Climate change and human impact on the Song Hong (Red River) Delta, Vietnam, during the Holocene. *Quaternary International*, *144*(1), pp.4-28.

Lo, K. F. A., and Gunasiri, C. W. (2014). Impact of coastal land use change on shoreline dynamics in Yunlin County, Taiwan. *Environments*, *1*(2), pp.124-136.

Munasinghe et al. (under review) Suitability Analysis of Remote Sensing Techniques for Shoreline Extraction of Global River Deltas. *Pre-Print available through EarthArXiv at: https://www.researchgate.net/publication/342289110_Suitability_Analysis_of_Remote_Sensing_Techniques_for_Shoreline_Extraction_of_Global_River_Deltas*

Nienhuis, J. H., Ashton, A. D., and Giosan, L. (2016). Littoral steering of deltaic channels. *Earth and Planetary Science Letters*, *453*, pp.204-214.

Munasinghe, D., Cohen, S., & Gadiraju, K. (2021). A Review of Satellite Remote Sensing Techniques of River Delta Morphology Change. *Remote Sensing in Earth Systems Sciences*, pp.1-32.

Passalacqua, P. (2017). The Delta Connectome: A network-based framework for studying connectivity in river deltas. *Geomorphology*, *277*, pp.50-62.

Pfafstetter, O. (1989). Classification of hydrographic basins: coding methodology. *unpublished manuscript, Departamento Nacional de Obras de Saneamento, August*, 18(1989), pp.1-2.

Redolfi, M., Zolezzi, G., and Tubino, M. (2019). Free and forced morphodynamics of river bifurcations. *Earth Surface Processes and Landforms*, *44*(4), pp.973-987.

Syvitski, J.P., Vörösmarty, C.J., Kettner, A.J. and Green, P., 2005a. Impact of humans on the flux of terrestrial sediment to the global coastal ocean. science, 308(5720), pp.376-380.

Syvitski, J. P. M., Kettner, A. J., Correggiari, A. and Nelson, B. W. (2005b). Distributary channels and their impact on sediment dispersal. *Mar. Geol.* 222–223, pp.75–94.

Syvitski, J.P. and Kettner, A. (2011). Sediment flux and the Anthropocene. *Philosophical Transactions of the Royal Society A: Mathematical, Physical and Engineering Sciences*, *369*(1938), pp.957-975.

Syvitski, J.P., and Milliman, J.D. (2007). Geology, geography, and humans battle for dominance over the delivery of fluvial sediment to the coastal ocean. *J. Geol.115* (1), pp.1–19.

Syvitski, J.P., Kettner, A.J., Overeem, I., Hutton, E.W., Hannon, M.T., Brakenridge, G.R., Day, J., Vörösmarty, C., Saito, Y., Giosan, L. and Nicholls, R.J. (2009). Sinking deltas due to human activities. *Nature Geoscience*, *2*(10), pp.681-686

Syvitski, J. P., and Saito, Y. (2007). Morphodynamics of deltas under the influence of humans. *Global and Planetary Change*, *57*(3-4), pp.261-282.

Tessler, Z. D., Vörösmarty, C. J., Grossberg, M., Gladkova, I., Aizenman, H., Syvitski, J. P., and Foufoula-Georgiou, E. (2015). Profiling risk and sustainability in coastal deltas of the world. *Science*, *349*(6248), pp.638-643.

Vörösmarty, C. J., Syvitski, J., Day, J., De Sherbinin, A., Giosan, L., and Paola, C. (2009). Battling to save the world's river deltas. *Bulletin of the Atomic Scientists*, *65*(2), pp.31-43.

Walling, D. E. and Fang, D. (2003). Recent trends in the suspended sediment loads of the world's rivers. *Global Planet. Change*, *39*, pp.111–126.

Wang, H., Wright, T. J., Yu, Y., Lin, H., Jiang, L., Li, C., and Qiu, G. (2012). InSAR reveals coastal subsidence in the Pearl River Delta, China. *Geophysical Journal International*, *191*(3), pp.1119-1128.

Yu, J., Li, Y., Han, G., Zhou, D., Fu, Y., Guan, B., Wang, G., Ning, K., Wu, H. and Wang, J. (2014). The spatial distribution characteristics of soil salinity in coastal zone of the Yellow River Delta. *Environmental Earth Sciences*, *72*(2), pp.589-599.

CHAPTER 5

SATELLITE REMOTE SENSING OF GLOBAL RIVER DELTA SHORELINE MOBILITY AND THEIR RELATIONSHIP TO FLUVIAL SEDIMENT FLUXES

Abstract

Anthropogenic activities in river basins (e.g. land use changes, mining, damming), have significantly altered riverine sediment flux resulting in shifts in river delta shorelines, and subsequent changes to deltaic land mass. Understanding changes to the river deltaic shoreline is important to identify vulnerable areas on the delta and install coastal defense structures, plan engineering structures for transport, and land reclamation/zoning works in accordance with sustainable deltaic land management.

The overarching goal of this study was to identify temporal trends of sediment fluxes (i.e. suspended, bedload and suspended bed-material) to river deltas, and their effects on shoreline movement of 30 global river deltas between 1978-2018. We use a global-scale riverine modeling framework (WBMsed) to investigate sediment fluxes to river deltas over time. Landsat satellite imagery are used to extract shorelines of river deltas during 5 historical time steps to derive shoreline positions. Rates of shoreline migration and other accretion/erosion statistics are calculated using the Digital Shoreline Analysis System (USGS).

We provide (a) for the first time in literature, quantitative understandings and long-term trends of sediment fluxes to river deltas, (b) quantitative understandings of historical migration rates and ancillary shoreline migration statistics of well-curated shorelines of global deltas, and (c) link relationships between sediment fluxes and shoreline mobility provides useful baselines and directions to researchers regarding comparative studies that will further solidify our understanding of sediment-driven shoreline migration.

The outcomes of this study yield several novel insights into decadal relationships between sediment fluxes and shoreline mobility, transform our analytical capabilities for studying human influences on river deltas, globally, and also provide a platform to better estimating incoming fluxes to river deltas, large scale flux modeling endeavors, erosion/accretion in different parts of the deltaic land-sea interface, and zonal planning operations for long-term sustainability of deltas.

1. Introduction

River deltas are important coastal depositional systems. They not only act as central locations for agricultural production and hydrocarbon extraction, but are also biodiversity hotspots, and carry a vast cultural heritage (Hutchings & Campbell, 2005; Lentz et al., 2016). Many of the world's major river deltas are undergoing rapid changes in response to alterations in riverine fluxes of sediment (Ericson et al., 2006; Syvitski et al., 2009; Minderhoud et al., 2018). Fluvial fluxes into deltas have altered dramatically in the last several decades due to river engineering (e.g. dams), land use changes (Dunn et al., 2019), and soil erosion and conservation measures (Syvitski et al., 2005, Wang et al. 2011; Best and Darby, 2020).

Increasing impacts of human activities on deltas have placed attention on global river deltas, and have shown the importance to necessitate the need to identify and quantify fluvial sediment fluxes and their impacts on river delta morphology change (Yang et al. 2015; Besset et al., 2019; Nienhuis et al. 2020). Identifying the relationships between riverine sediment fluxes, and the changes in river delta areas and their future behavior is important for constructing engineering structures (e.g. breakwaters, weirs) to mitigate flooding, construction of dams, erosion-accretion studies, and conceptual or predictive modeling of coastal morphodynamics (Al Bakri, 1996, Masria et al., 2015, Cenci et al., 2018). More importantly these dynamics can be used to identify tipping points to undesirable system configurations of deltas, which recognize future threats (Kwadijk et al., 2010) or unacceptable changes (Werners et al., 2013) that can be used in setting 'adaptation turning points' in sustainable deltaic environment planning, and focus and accelerate a comprehensive research agenda toward understanding and modeling these complex environmental systems.

In this study, we use 30 major river deltas globally, to identify relationships between temporal changes in incoming sediment flux and the river delta shoreline migration responses to flux alterations. We envision that the quantitative understandings of historical and future predictions of shoreline change rates and their fluvial sediment drivers will be used not only to identify individual trajectories of vulnerability of river deltas, but also as aids in decision making for future coastal management. They are also envisioned to provide useful baselines and directions to researchers regarding comparative studies that will further advance our understanding of different shoreline extraction techniques and allow transfer of that knowledge to lesser studied deltaic systems.

2. Methodology

2.1 Case Studies

Thirty large river deltas across the globe were selected for the study. The selection of these deltas was based on representation of the different Köppen Climate Classes (global biome distribution based on air temperature and precipitation), different river delta morphologies (i.e. river, wave and tide-dominance), availability of cloud-free Landsat satellite imagery at delta locations at pre-determined temporal time scales, and the capability of the *WBMsed* fluvial hydro-geomorphic model (discussed in part 2.3) to simulate incoming sediment fluxes to a river delta with high confidence. Figure 5.1 shows the geographical distribution and Table 5.1 lists the study-related characteristics of the deltas.

Figure 5.1. Global distribution of river deltas used in the study

Table 5.1. River deltas and study-related characteristics

River Delta	Continent	Major Köppen Climate Class	[1]Delta Area (km^2)	[2]Long-Term Average Suspended Sediment Flux to the Delta (kg/s)
Amazon	SA	Tropical	108,950	99,695
Brahmani	AS	Tropical	7,088	143
Burdekin	OC	Tropical	1,398	200
Chao	AS	Tropical	25,225	616
Colorado, TX	NA	Arid	11,992	2,023
Danube	EU	Arid	9,955	1,649
Dnieper	EU	Boreal/Continental	1,715	41
Ebro	EU	Temperate	939	45
Godavari	AS	Tropical	4,355	2,921
Grijalva	NA	Tropical	12,769	1,985
Irrawaddy	AS	Tropical	36,242	25,424
Krishna	AS	Tropical	2,635	511
Limpopo	AF	Tropical	4,140	337
Magdalena	SA	Tropical	4,278	9,679
Mahakam	AS	Tropical	5,570	3,998
Mahanadi	AS	Tropical	7,779	1,431
Mekong	AS	Tropical	52,405	28,260
Mississippi	NA	Temperate	38,747	3,974
Moulouya	AF	Arid	791	40
Nile	AF	Arid	37,790	406
Parana	SA	Temperate	21,977	43,476
Rhine-Meuse	EU	Temperate	12,483	739
Rhone	EU	Temperate	3,205	321
Sao Francisco	SA	Tropical	1,355	310
Sebou	AF	Temperate	359	666
Senegal	AF	Arid	4,947	371

Shatt-el-Arab	AS	Arid	6,341	15,665
Tone	AS	Temperate	1,565	44
Vistula	EU	Temperate	7,697	406
Volta	AF	Tropical	2,948	1,406

Note: [1]*This is the sub-aqueous area of a delta during a point in time. Values are based on River Delta areas from Tessler et al. (2016). It has to be noted that the sub-aqueous area of a delta changes temporally based on migration of shoreline.*

[2]*These are simulated fluxes from the WBMsed global hydro-geomorphic model. Model calibration, validation and simulation settings are available from Cohen et al. (2013, 2014).*

In this study, the synoptic capability of Satellite Remote Sensing is used to extract the shorelines of river deltas. Landsat satellite imagery of 5 historical time-steps of deltaic locations are used to calculate the annual rate of shoreline migration for each delta. A global-hydrogeomorphic model is used to simulate annual suspended, bedload and suspended bed material influxes to the river deltas over the past 30 years. Relationships are constructed between the rates of change of river delta shorelines and the influx of sediment over time.

2.2 Shoreline Migration of the Deltas

In a recent study, Munasinghe et al., (2021) showed that there was no clear understanding in the literature as to which Remote Sensing technique would be the most optimum to extract the shoreline of a particular river delta, as shoreline dynamics are driven by many other location/climate related factors (e.g. inherent variability in rainfall, growing cycle phases of vegetation, river delta type) which make the identification of shorelines difficult.

The performance of 5 different remote sensing techniques for shoreline extraction were evaluated against a hand-digitized shoreline vector (used as a reference baseline) on Landsat imagery for the year 2018 (Munasinghe et al. (under review)). Best performing algorithms for each delta identified through that study was used to derive historical temporal shoreline positions from Landsat imagery for 5 historical time steps (1978, 1988, 1998, 2008, 2018) herein. Five time steps were used as smaller gaps between time steps did not show sufficient shoreline movement, and larger gaps yielded not too many shoreline positions for migration rate calculations. Each automatically derived shoreline was manually curated to reduce artifacts (unrealistic curves and angles) and to reflect the best representation of the shoreline for each time step.

The Tessler et al. (2016) dataset, static polygons of major global river deltas, was used to identify the extent of the delta landmass. In certain deltas, the position of a shoreline is heavily influenced by tides and thus the location of the shoreline can fluctuate considerably on a daily basis. To reduce error of shoreline identification within the inter-tidal zones (zone between the high-water level and low-water level) we use a global dataset generated by Murray et al. (2019). This dataset consists of large, low-sloping tidal flats and tide-dominated subaerial portions of river deltas from 1984-2016 with averaged tidal range data for every two years. We use tidal ranges from 1984-1986 to make corrections to the 1978 shoreline, 1986-1988 to the 1988 shoreline, 1996-1998 to the 1998 shoreline, 2006-2008 to the 2008 shoreline and 2014-2016 to the 2018 shoreline. The error correction is illustrated using part of the Mekong delta in Figure 5.2.

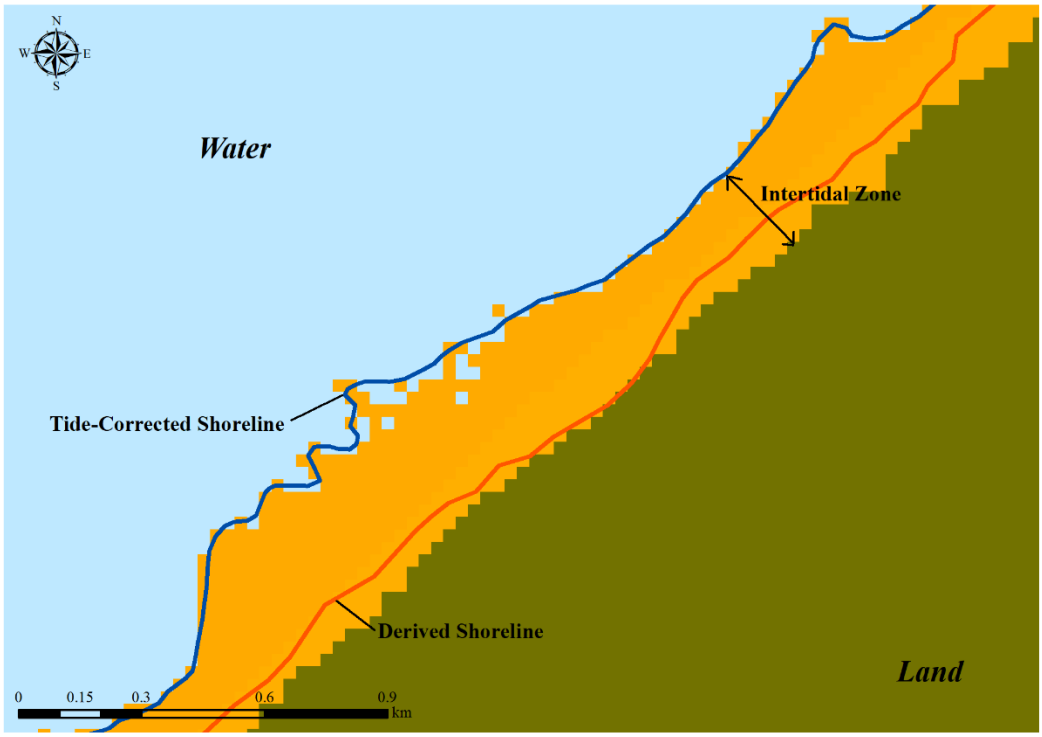

Figure 5.2. Tidal correction to a shoreline. A ‘derived’ shoreline is the resultant of automatic shoreline extraction algorithm application to satellite imagery.

The shoreline is a delta's Land-Water Interface (LWI; Boak and Turner, 2005). However, in complex systems such as river deltas, a large fraction of LWI includes channel banks and sheltered back sides of islands that are not directly exposed to open water. This complicates shoreline demarcation. The Opening-Angle Method (Shaw et al., 2008) builds on the idea that the shoreline is a direct measure of exposure to open-water. The quantitative measure used to approximate the degree of exposure at a point is the angle Q of open water the point can see, or ''opening angle'' (Figure 5.3). A point on the LWI that does not have a direct line of sight to open water (point A) is not part of the shoreline, but a beach that sees 180° of open ocean clearly is (point B). As recommended by Shaw et al. (2008), we use the standard value of Θ = 45° across all deltas to determine how far inland the shoreline extended. The COGO tool in ArcMap was used to measure the angle, and manual corrections were made to the tide-corrected shorelines.

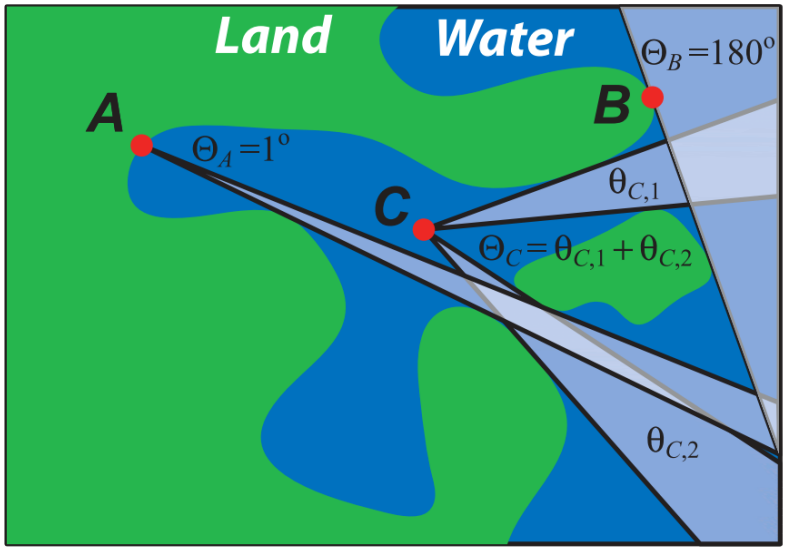

Figure 5.3. The opening angle

Subsequent to finalization of shorelines for the different time steps, the Digital Shoreline analysis system (DSAS) extension for ArcGIS is used to calculate:

a) Average End-point-Rate (EPR) (m/yr) - the rate of average shoreline migration for the delta.

b) Percent of all transects that are erosional – equidistant transects are created between shorelines to calculate EPR. Using the percentage of these transects that are erosional, the percentage of eroding shoreline can be calculated.

c) Average of all erosional rates (m/yr) – rate at which the erosional transects erode/rate of eroding sections of the shoreline.

d) Percent of all transects that are accretional - percentage of accreding shoreline

e) Average of all accretional rates (m/yr) - rate of accreding sections of the shoreline. Landsat Image search and delta extent demarcations were carried out on Google Earth Engine, while shoreline derivation was performed in ArcGIS v10.7.

2.3. Simulation of Sediment, Bedload and Suspended Bed-Material Fluxes

2.3.1 Model Description

A global scale Hydro-geomorphic model (WBMsed; Cohen et al., 2013, 2014) is used to quantify the suspended, bedload and suspended bed-material fluxes to the river delta. The Suspended Sediment load is the portion of sediment that is carried within the water column as fine-grained particles (i.e. fine sand, silt and clay-sized grains). Bedload is the portion of coarser sediment particles that travels along the riverbed. As the bed shear stress increases, beyond some critical value for particle motion on the bed, certain particles can enter the water column (Syvistski et al., 2019). This is the suspended bed-material load. The WBMsed modeling framework (Cohen et al., 2013, 2014) was developed and has been used extensively to investigate global riverine sediment dynamics (Dunn et al., 2019; Nienhuis et al., 2020; Syvitski et al., 2014, 2019; Taylor et al., 2015). The model incorporates climatic (precipitation,

temperature, solar radiation), surface (lithology, topography, riverine) and anthropogenic (dams, irrigation, land use) parameters, making it an ideal framework for investigating complex human-environmental dynamics and scenarios. A comprehensive description of the model infrastructure and input parameters can be found in Cohen et al. (2013 and 2014). Annual Suspended, Bed and Bed-material sediment flux simulations were performed from 1978 to 2018.

WBMsed employs the BQART equation (Syvitski and Milliman, 2007) as its governing equation for calculating relationships between long-term (> 30 years) average suspended sediment loads ($Qs = \omega BQ^{0.31}A^{-0.5}RT$) and basin-average contributing *A*rea, maximum *R*elief, *T*emperature, average water discharge (Q) and a B parameter ($B = IL(1–Te)Eh$) that incorporates a *L*ithology factor, trapping efficiency of reservoirs and dams (Te), glacial erosion factor (I) and a human-influenced erosion factor (Eh). ω is the coefficient of proportionality in units of kg/s which equals to 0.02. The WBMsed model is proven to be successful in predicting suspended sediment loads in global rivers and studying different mechanisms and drivers associated with these processes (e.g. Cohen et al., 2013, 2014; Taylor et al., 2015; Syvitski et al., 2019).

WBMsed bedload flux module uses the modified Bagnold (1966) equation:

$$Qb_{[i]} = \left(\frac{\rho_s}{\rho_s - \rho}\right)\frac{\rho g Q_{[i]}^{p} Se_b}{g \tan\lambda} \quad \text{when } u \geqslant u_{cr}$$

where ($Qb[i]$; kg/s) daily bedload flux at river delta outlets, ρ_s is sediment density (constant 2560 kg/m^3), ρ is fluid density (constant 1000 kg/m^3), $Q[i]$ is daily mean water discharge (m^3/s), S is Slope (m/m), e_b is the bedload efficiency (-), β is a dimensionless bedload rating term (-), λ is the limiting angle of repose of sediment grains lying on the river bed (constant 32.4^o), g is acceleration due to gravity (constant 9.67 m/s^2), u is stream velocity (m/s), and u_{cr} is the critical velocity needed to initiate bedload transport (m/s). Daily bedload outputs were averaged to generate annual bedload flux values for the river delta outlets.

WBMsed suspended bed-material use an equation proposed in Syvistski et al. (2019) that is applicable to fully turbulent flows and larger transport rates (Bagnold, 1966). The available power of the flow is transformed into kinetic energy required for sediment transport, such that

$$Q_{sbm} = \left(\frac{\rho_s}{\rho_s - \rho_f}\right) \rho_f Q^{-\beta} S \left(0.01 \frac{\overline{\mu}}{\omega}\right)$$

where Q_{sbm} is the bed-material (kg/s), Q is river discharge (m^3/s) averaged over turbulence, β is a load rating term (−) and set to 1 for this study, S is the energy slope (m/m) that powers the discharge, u is the transport velocity of suspended particles and approximated by average river velocity (m/s), and ω is the settling velocity (m/s) of the bulk suspended particles, or for each size fraction being separately tracked (Syvitski et al. 2019).

2.3.2 Simulation Settings

The WBMsed simulations were conducted for the historical period under the 'disturbed' mode where parameters related to anthropogenic activities (i.e. irrigation, ground and surface water uptake, agriculture-affected evapotranspiration, dam operations, and water retention in man-made reservoirs) are activated in the simulations. The simulations were performed to mimic real-world settings between the period from 1978 to 2018 to obtain outputs of suspended sediment, bed and bed-material. The simulations were set up at a daily time step and 6 arc-min (~11 km) spatial resolution, later averaged to an annual output. The simulations were performed on the University of Alabama High Performance Computing Cluster.

3. Results and Discussion

3.1 Model Validation

WBMsed long-term averaged suspended sediment flux predictions for 95 global sites (pre-damming) and 11 USGS sites resulted in correlations with R^2 of 0.66 and 0.94 respectively, against observed data (Cohen et al. (2013, 2014). A comprehensive analysis of WBMsed bedload and suspended bad material have not yet been conducted due to acute limitation in observational data for these parameters in large rivers. Islam (2018) compiled an observational bedload dataset (n=30) for the WBMsed module development based on reported values. Comparison of the model results to this dataset is challenging given the very limited spatial and temporal representation of the observations and the instantaneous nature of bedload sediment transport. WBMsed average bedload yields an R^2 of 0.2. Correlation between the observed bedload and WBMsed suspended bad material yields an R^2 of 0.45.

3.2 Analysis of Historical Sediment Fluxes

Table 5.2 gives a summary of the long-term averages of the different types of sediment fluxes and their annual rates of change for the 30 deltas.

Table 5.2. The long-term averages of suspended load, bed load, suspended bed material, total load and their annual rates of change. The percentage proportions of fluxes against the total are given within brackets.

		Suspended Flux (kg/s)		Bedload Flux (kg/s)		Bed-material Flux (kg/s)		Total Sediment Flux (kg/s)	Suspended Sediment Flux Annual Rate of Change (kg/s/yr)	Bedload Flux Annual Rate of Change (kg/s/yr)	Bed-material Flux Annual Rate of Change (kg/s/yr)	Total Sediment Annual Rate of Change (kg/s/yr)
1	Amazon	99695.43	(73.48)	35198.22	(25.94)	783.79	(0.58)	135677.44	-152.49	132.10	2.42	-17.97
2	Brahmani	142.91	(84.90)	22.45	(13.34)	2.98	(1.77)	168.34	0.03	0.06	0.01	0.11
3	Burdekin	199.96	(95.09)	8.73	(4.15)	1.59	(0.76)	210.28	-0.53	0.36	0.06	-0.11
4	Chao Phraya	615.56	(96.56)	17.92	(2.81)	4.00	(0.63)	637.48	2.06	0.26	0.05	2.37
5	Colorado	2023.41	(97.20)	51.04	(2.45)	7.33	(0.35)	2081.79	-113.59	-0.38	-0.09	-114.06
6	Danube	1649.35	(96.06)	4.10	(0.24)	63.58	(3.70)	1717.04	-30.21	0.00	-0.22	-30.43
7	Dnieper	40.63	(99.03)	0.06	(0.15)	0.34	(0.82)	41.03	-0.46	0.00	-0.01	-0.47
8	Ebro	45.05	(91.97)	2.06	(4.20)	1.87	(3.83)	48.98	-1.27	0.00	-0.07	-1.34
9	Godavari	2921.20	(97.99)	47.94	(1.61)	12.13	(0.41)	2981.27	10.19	0.28	0.09	10.56
10	Grijalva	1985.29	(63.30)	1110.69	(35.41)	40.57	(1.29)	3136.55	-6.28	0.72	0.00	-5.56
11	Irrawaddy	25423.58	(98.18)	432.28	(1.67)	40.03	(0.15)	25895.89	5.58	1.17	0.09	6.84
12	Krishna	510.85	(92.83)	27.37	(4.97)	12.10	(2.20)	550.31	-2.64	0.17	0.03	-2.45
13	Limpopo	336.85	(97.50)	6.73	(1.95)	1.89	(0.55)	345.47	-6.88	0.02	-0.02	-6.88
14	Magdalena	9679.31	(98.83)	93.99	(0.96)	20.55	(0.21)	9793.86	-17.50	-0.19	-0.06	-17.74
15	Mahakam	3998.09	(96.43)	133.71	(3.22)	14.42	(0.35)	4146.22	30.49	0.50	0.04	31.03
16	Mahanadi	1431.24	(92.43)	106.01	(6.85)	11.17	(0.72)	1548.42	-6.82	0.30	0.06	-6.46
17	Mekong	28259.97	(94.31)	1622.68	(5.42)	83.31	(0.28)	29965.96	-109.29	0.44	0.06	-108.78
18	Mississippi	3973.56	(94.86)	181.66	(4.34)	33.72	(0.80)	4188.93	-72.04	1.27	0.32	-70.45
19	Moulouya	39.67	(98.45)	0.08	(0.19)	0.55	(1.36)	40.30	1.35	0.00	0.01	1.37
20	Nile	406.43	(94.29)	18.49	(4.29)	6.12	(1.42)	431.04	-3.65	0.16	0.01	-3.48
21	Parana	43476.07	(99.68)	81.13	(0.19)	57.64	(0.13)	43614.84	-656.95	0.29	0.01	-656.65
22	Rhine	738.95	(93.67)	43.27	(5.49)	6.67	(0.85)	788.89	-16.01	-0.42	-0.07	-16.49

23	Rhone	320.97	(42.01)	428.50	(56.09)	14.49	(1.90)	763.95	-8.83	-3.36	-0.12	-12.31
24	Sao Francisco	309.79	(91.99)	19.54	(5.80)	7.44	(2.21)	336.76	-11.62	-0.27	-0.37	-12.27
25	Sebou	666.18	(95.37)	29.09	(4.16)	3.25	(0.46)	698.52	1.90	0.60	0.04	2.55
26	Senegal	370.58	(98.02)	3.02	(0.80)	4.49	(1.19)	378.09	-1.34	0.05	0.01	-1.28
27	Shatt-el-Arab	15664.54	(99.63)	7.40	(0.05)	50.04	(0.32)	15721.99	-757.58	-0.04	-1.28	-758.90
28	Tone	44.41	(60.05)	27.36	(37.00)	2.18	(2.95)	73.95	-0.69	0.02	0.00	-0.68
29	Vistula	405.77	(97.48)	2.27	(0.54)	8.23	(1.98)	416.27	-11.05	0.01	-0.08	-11.12
30	Volta	1406.10	(55.73)	1087.84	(43.11)	29.34	(1.16)	2523.28	-14.89	12.35	0.18	-2.36

Among the analyzed deltas, the top 3 total fluxes were recorded in the Amazon (135, 677 kg/s), Parana (43, 614 kg/s) and Mekong (29, 965 kg/s) while the lowest fluxes were recorded Moulouya (40 kg/s), Dnieper (41 kg/s), and Ebro (48 kg/s). We present, for the first time in literature, first order estimates of total sediment fluxes (suspended, bedload and suspended bed material) to river deltas and the percentage distribution of these flux components among each delta (Figure 5.4).

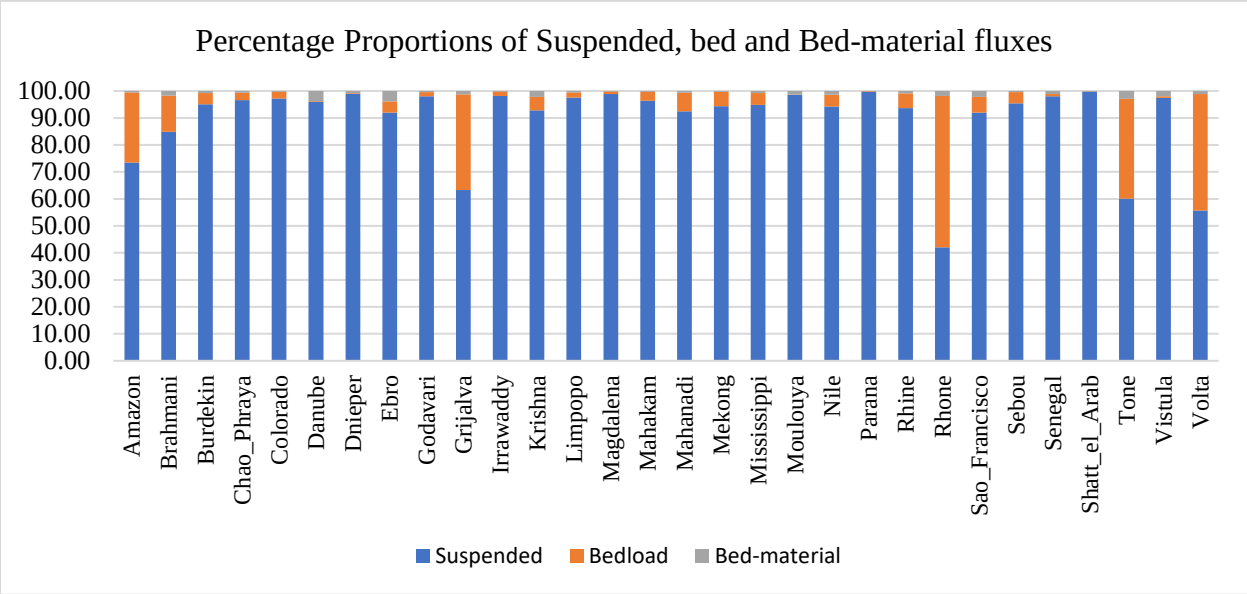

Figure 5.4. The distribution of component fluxes of sediment among deltas

The mean fluxes of suspended, bedload and suspended bed-material were 8226 (± 20035), 1361 (±6403) and 44 (±141) kg/s respectively. The ranges in fluxes (kg/s) were 99,655 for Suspended sediment, 35,198 for Bedload and 783 for suspended Bed-material. Suspended and bedload show a much greater range than bed-material. Highest suspended flux proportions were observed in Parana (99.68%), Shatt-et-Arab (99.63%), Dnieper (99.03%), Magdalena (98.83%). Certain suspended sediment flux plumes even visible to earth observing satellites are illustrated in Figure 5.5. Although generally, suspended sediment flux is said to dominate the

total sediment load of sediment we see bedload flux domination at a few case studies (e.g. Rhone, Volta, Tone, Amazon). Although we attribute possible reasoning to greater delta slope gradient and relatively higher discharge in these systems, further investigation is needed to find causation. These relative proportions once validated through secondary means are envisioned to be used in delta progradation studies, and engineering applications such as constructions of dams and levees, channel dredging.

Figure 5.5. The sediment plumes emanating from the Parana and Shatt-el-Arab rivers at their deltas visible through Landsat 8-OLI imagery (images captured in 2018).

We also compare the annual rates of change (this is the slope of the annual time series for a given type of flux) at deltas. Highest annual rates in suspended, bedload, suspended bed-material and total fluxes are at Mahakam (30 kg/s/yr), Amazon (132 kg/s/yr), Amazon (2.4 kg/s/y) and Mahakam (31 kg/s/yr) while the lowest rates in the respective categories are for Shatt-el-Arab (-758 kg/s/yr), Rhone (-3.4 kg/s/yr), Shatt-el-Arb (-1.3 kg/s/y) and Shatt-el-Arab (-

759 kg/s/y). Heavy deforestation in river basins associated with tropical monsoonal rains are speculated to be driving factors of high rates of flux changes in these tropical deltas.

We observe that the driving component of total sediment is the suspended load in the vast majority of deltas (also observed in Figure 5.4). The decreases in total load (or vice versa) is mainly driven by the suspended load. We also observe of instances were a delta can gain in certain components and lose in other component fluxes. A classic example to illustrate both said observations is the Amazon delta, where the suspended rate is decreasing (-152 kg/s/yr) while bedload is increasing (132.10), bed material increasing (2.42) and the Total is decreasing: (-18 kg/s/yr).

3.3 Shoreline Migration and Relationship to Fluvial Sediment Fluxes

The 5 different types of shoreline migration statistics calculated are summarized in Table 5.3.

Table 5.3. Shoreline migration statistics of river deltas

River Delta	Average EPR (m/yr)	Proportion of eroding shoreline	Average of all erosional rates (m/yr)	Maximum value erosion (m)	Proportion of accreding shoreline	Average of all accretional rates (m/yr)	Maximum value accretion (m)
Amazon	-0.98	56.77%	-5.23	-130.15	43.23%	4.61	139.07
Brahmani	1.79	54.06%	-6.04	-21.11	45.94%	11.01	39.12
Burdekin	5.97	31.78%	-4.11	-29.11	68.22%	10.66	37.63
Chao Phraya	-3.31	66.36%	-7.37	-22.7	33.64%	4.69	20.55
Colorado	-4.76	89.84%	-50.7	-238.8	10.16%	17.56	168.02
Danube	1.44	44.87%	-10.55	-78.58	55.13%	11.2	69.75
Dnieper	-0.74	66.52%	-1.92	-8.99	33.48%	1.62	15.05
Ebro	0.36	43.53%	-4.78	-38.06	56.47%	4.33	27.53
Godavari	-0.36	55.12%	-8.49	-33.8	44.88%	9.61	84.58
Grijalva	-3.79	65.49%	-7.21	-41.33	34.51%	2.68	11.13
Irrawaddy	-0.59	57.03%	-9.63	-194.21	42.97%	11.42	139.39
Krishna	-5.97	77.60%	-14.33	-39.39	22.40%	9.61	44.31
Limpopo	1.68	22.25%	-5.59	-28.2	77.75%	3.76	22.5
Magdalena	-1.79	71.75%	-3.81	-16.96	28.25%	3.36	21.18
Mahakam	-3.3	82.11%	-4.38	-24.75	17.89%	1.67	5.66
Mahanadi	-2.29	52.80%	-7.81	-39.63	47.20%	3.88	28.62
Mekong	-1.72	56.45%	-17.02	-113.77	43.55%	18.11	72.37
Mississippi	-2.72	76.69%	-5.38	-89.85	23.31%	6.04	102.73
Moulouya	0.14	41.11%	-2.55	-10.3	58.89%	2.02	8.52
Nile	-2.5	53.67%	-8.36	-116.78	46.33%	4.29	77.82
Parana	2.73	69.31%	-4.43	-97.73	30.69%	18.91	69.92
Rhine	3.07	48.68%	-6.67	-181.81	51.32%	12.3	111.69
Rhone	-2.23	74.40%	-4.98	-43.53	25.60%	5.75	31.23
Sao Francisco	-0.06	36.99%	-5.75	-37.02	63.01%	3.28	13.62
Sebou	0.71	30.40%	-0.77	-2.49	69.60%	1.35	6.98

Senegal	1.12	15.78%	-6.6	-29.26	84.22%	2.56	9
Shatt-el-Arab	2.48	12.76%	-23.83	-132.96	87.24%	17.79	148.1
Tone	5.7	3.74%	-4.29	-46.36	96.26%	6.08	66.92
Vistula	1.15	32.06%	-1.11	-15.02	67.94%	2.21	39.93
Volta	-0.99	74.51%	-1.72	-8.58	25.49%	1.13	3.94

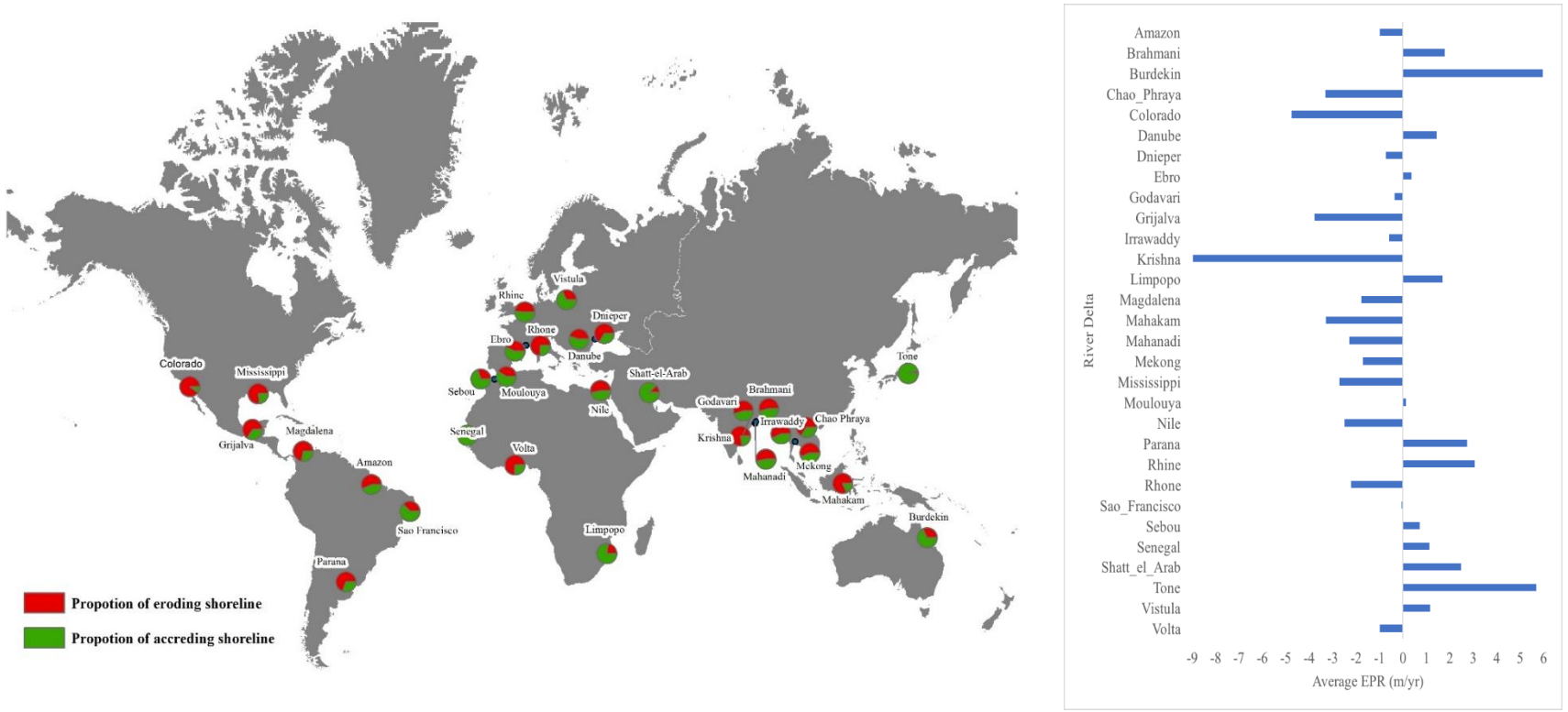

Figure 5.6. (left) The relative proportion of accretion and erosion of a given delta shoreline. (right) The average annual shoreline migration rate

Highest accretion rates (Figure 5.6 *right*) can be seen at Burdekin (~6 m/yr), Tone (~6 m/yr) and Rhine (~3 m/yr) while highest erosions persisting at Krishna (~6 m/yr), (Colorado ~5 m/yr), and Grijalva (~4 m/yr). Of the 30 sample deltas tested, 13 were accreding while 17 were eroding. A shoreline, however, even it was accreding (positive average EPR rate), can have portions of it eroding. This is true for the reverse as well (an eroding shoreline can have accreding segments). We calculate the percentage that eroded and accreded for each shoreline (Figure 5.6 *left*) and observe that the mean percentage of erosion of accreding deltas was roughly similar to the mean percentage of accretion in eroding deltas (35%). Although similar values are coincidental, we can use these as baseline references to validate geologic modeling endeavors of river delta area change.

Attempts to cluster river deltas to infer the influence of the size of deltas on shoreline migration parameters and Fluvial Dominance Ratio (an indication of how much river dominated a delta is: (Nienhuis et al., 2015, Nienhuis et al., 2020) yielded non-significant results necessitating the incorporation of other local drivers (delta subsidence, sea level change) in analyses. We also inform the readers that this compendium of shorelines from an array of deltas only reflect average rates. For example, some river deltas that showed progradation during the early 1980s and 1990s might now be showing aggressive erosion that are not reflective in these statistics. Therefore, we suggest careful consideration before application of results taking into account not only long-term trends, but also decadal variations.

To elucidate relationships between the different flux components and the migration statistics we perform correlation analyses. The rate of change (slope of the time series) of each sediment type (i.e. suspended, bedload, suspended bed material and total) are regressed against the 5 different migration statistics. Results are summarized in Table 5.4.

Table 5.4. R^2 values of relationships between individual sediment flux components and migration statistics

Flux component \ Migration Statistic	Average EPR (m/yr)	Proportion of eroding shoreline (%)	Average of all erosional rates (m/yr)	Proportion of accreding shoreline (%)	Average of all accretional rates (m/yr)
Suspended sediment annual rate of change (kg/s/yr)	0.0347	0.0116	0.0872	0.0116	**0.3799**
Bedload annual rate of change (kg/s/yr)	0.0002	0.0031	0.0054	0.0031	0.0108
Bed-material annual rate of change (kg/s/yr)	0.0118	0.0556	0.0493	0.0556	0.0579
Total flux annual rate of change (kg/s/yr)	0.0343	0.0135	0.0938	0.0135	**0.3995**

(a)

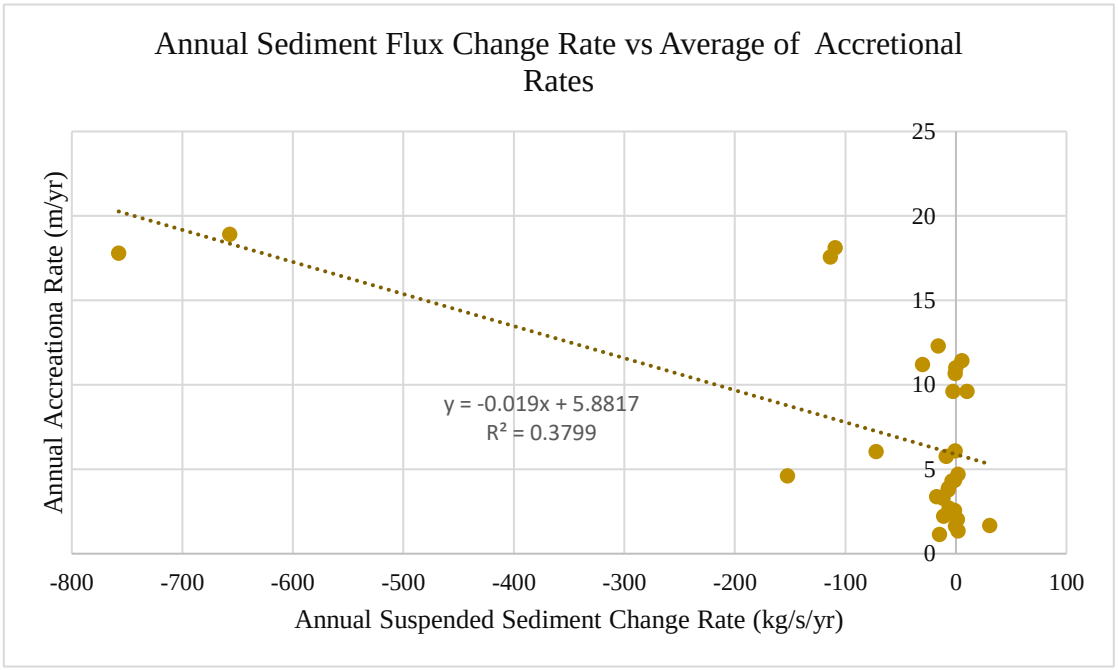

(b)

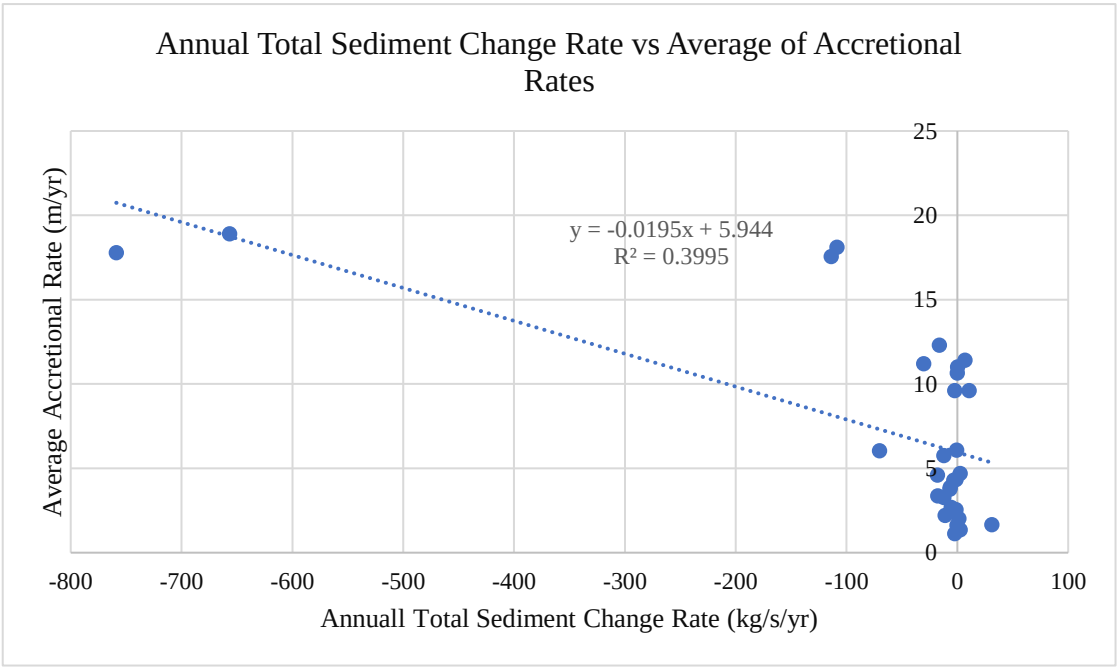

Figure 5.7. Relationships between delta shoreline change and fluvial fluxes (a) Suspended Sediment Flux (b) Total Flux

A standout relationship is observed where the annual change in suspended flux rate to a delta is moderately well correlated ($R^2 = 0.38$) with the average rate of accretion of a river delta. In other words, suspended flux explains ~38% of the propagation of the river delta shoreline. We also find that total sediment fluxes explains ~40% of the accretion of deltas. This is a significant percentage when the geographic and climatic variability of the river deltas are considered. We expect future synergistic research attempting to understand the holistic dynamics of deltaic environment to immensely benefit from this isolation as results are also readily transferable to other deltaic regions. In a synergistic study (Chapter 4) we quantify the anthropogenic stress on river deltas as a whole, and within a 5-km buffered region of the coastal zone of deltas. Although an attempt to attribute a certain percentage of the remaining ~60% of the variability to the average human stress on the delta plain (and the coastline) to shoreline mobility, it yielded below par significance. However, we find that the major human stress factors driving shoreline change are Population pressure/ Night-time lights (27 deltas) Cropland Livestock (3 deltas) of the 13 other stress factors (see Chapter 4 for full description of these). Near-future work will include incorporating other dominating processes, such as primarily sea-level rise, wave/tide-transported sediment fluxes, and delta subsidence-driven inundation and testing the sensitivity of each delta's shoreline response to alteration in fluvial sediment to increase the robustness of this relationship.

4.0 Conclusion

A sample of 30 large global river deltas are used to elucidate relationships between fluvial sediment fluxes and decadal changes in river delta shorelines. For the first time in literature we provide first order estimates of spatially and temporally explicit bedload and suspended bed-

material proportions flowing into major river deltas worldwide. We also provide a well-curated database of river delta shorelines with derived shoreline statistics as attributes. We find that deviating from the classical suspended flux dominance of total sediment fluxes, bedload fluxes dominate in certain river deltas. We find that the annual change in suspended flux rate to a delta explains 38% of the accretion of the delta shoreline while the total flux explains ~40%. The importance of incorporating other driving factors of shoreline change in analyses is highlighted. We envision, combined with model simulations, that these results will allow the scientific community to develop and test concepts and hypotheses not previously feasible and transform our analytical capabilities.

4. References for Chapter 3

Aerts, J.C.J.H., Renssen, H., Ward, P.J., De Moel, H., Odada, E., Bouwer, L.M., Goosse, H., 2006. Sensitivity of global river discharges under Holocene and future climate conditions. Geophys. Res. Lett. 33 (19).

Bagnold, R.A., 1966. An approach to the sediment transport problem from general physics. In: United States Geological Survey Professional Paper 4221, (37 p).

Besset, M., Anthony, E. J., & Bouchette, F. (2019). Multi-decadal variations in delta shorelines and their relationship to river sediment supply: An assessment and review. Earth-science reviews, 193, 199-219.

Best, J. and Darby, S.E., 2020. The Pace of Human-Induced Change in Large Rivers: Stresses, Resilience, and Vulnerability to Extreme Events. One Earth, 2(6), pp.510-514.

Cohen, S., Kettner, A.J., Syvitski, J.P., Fekete, B.M., 2013. WBMsed, a distributed global- scale riverine sediment flux model: model description and validation. Comput. Geosci. 53, 80–93.

Cohen, S., Kettner, A.J., Syvitski, J.P., 2014. Global suspended sediment and water dis- charge dynamics between 1960 and 2010: Continental trends and intra-basin sensitivity. Glob. Planet. Chang. 115, 44–58.

Dunn, F.E., Darby, S.E., Nicholls, R.J., Cohen, S., Zarfl, C., Fekete, B.M., 2019. Projections of declining fluvial sediment delivery to major deltas worldwide in response to cli- mate change and anthropogenic stress. Environ. Res. Lett. 14 (8), 084034.

Ericson J.P., C.J. V r smarty, S.L. Dingman, L.G. Ward, and M. Meybeck (2006), Effective sea-level rise and deltas: causes of change and human dimension implications. Global and Planetary Change, 50:63–82

Haddeland, I., Heinke, J., Biemans, H., Eisner, S., Flörke, M., Hanasaki, N., Konzmann, M., Ludwig, F., Masaki, Y., Schewe, J., Stacke, T., 2014. Global water resources affected by human interventions and climate change. Proc. Natl. Acad. Sci. 111 (9), 3251–3256.

Hutchings, R. M., and S.K. Campbell (2005), The Importance of Deltaic Wetland Resources: A Perspective from the Nooksack River Delta, Washington State. Journal of Wetland Archaeology, 5(1): 17-34.

Lentz, E. E., E.R. Thieler, N.G. Plant, S.R. Stippa, R.M. Horton, and D.B. Gesch (2016), Evaluation of dynamic coastal response to sea-level rise modifies inundation likelihood Sea-level rise (SLR) poses a range of threats to natural and built environments. Nature Climate Change, 6(7): 696.

IPCC, 2014. Climate Change 2014: Synthesis Report. Contribution of Working Groups I, II and III to the Fifth Assessment Report of the Intergovernmental Panel on Climate Change [Core Writing Team, R.K. Pachauri and L.A. Meyer (Eds.)]. IPCC, Geneva, Switzerland, pp. 151.

Karila, K., Nevalainen, O., Krooks, A., Karjalainen, M., Kaasalainen, S., 2014. Monitoringchanges in rice cultivated area from SAR and optical satellite images in Ben Tre andTra Vinh provinces in mekong delta, Vietnam. Remote Sens. 6:4090–4108.https://doi.org/10.3390/rs6054090.725P.S.J. Minderhoud et al. / Science of the Total Environment 634 (2018) 715–726

Knox, J.C., 1993. Large increases in flood magnitude in response to modest changes in climate. Nature 361 (6411), 430–432.

Lu, X.X., Ran, L.S., Liu, S., Jiang, T., Zhang, S.R., Wang, J.J., 2013. Sediment loads response to climate change: a preliminary study of eight large Chinese rivers. Int. J. Sed. Res. 28 (1), 1–14.

Minderhoud, P. S. J., Coumou, L., Erban, L. E., Middelkoop, H., Stouthamer, E., & Addink, E. A. (2018). The relation between land use and subsidence in the Vietnamese Mekong delta. Science of The Total Environment, 634, 715-726.

Munasinghe et al. (under review) Suitability Analysis of Remote Sensing Techniques for Shoreline Extraction of Global River Deltas. Pre-Print available through EarthArXiv at:

https://www.researchgate.net/publication/342289110_Suitability_Analysis_of_Remote_Sensing_Techniques_for_Shoreline_Extraction_of_Global_River_Deltas

Munasinghe, D., Cohen, S., & Gadiraju, K. (2021). A Review of Satellite Remote Sensing Techniques of River Delta Morphology Change. Remote Sensing in Earth Systems Sciences, pp.1-32.

Nienhuis, J. H., Ashton, A. D. & Giosan, L. What makes a delta wave-dominated? Geology 43, 511–514 (2015).

Nienhuis, J.H., Ashton, A.D., Edmonds, D.A., Hoitink, A.J.F., Kettner, A.J., Rowland, J.C., Törnqvist, T.E., 2020. Global-scale human impact on delta morphology has led to net land area gain. Nature 577 (7791), 514–518.

Oki, T., Kanae, S., 2006. Global hydrological cycles and world water resources. Science 313 (5790), 1068–1072.

Pelletier, J.D., 2012. A spatially distributed model for the long-term suspended sediment discharge and delivery ratio of drainage basins. Journal of Geophysical Research: Earth Surface, 117(F2).

Pendergrass, A.G., Knutti, R., Lehner, F., Deser, C., Sanderson, B.M., 2017. Precipitation variability increases in a warmer climate. Sci. Rep. 7 (1), 17966. Rodríguez-Blanco, M.L., Arias, R., Taboada-Castro, M.M., Nunes, J.P., Keizer, J.J., Taboada-Castro, M.T., 2016. Potential impact of climate change on suspended sedi- ment yield in NW Spain: a case study on the Corbeira catchment. Water 8 (10), 444.

Syvitski, J.P., 2003a. The influence of climate on the flux of sediment to the coastal ocean. In: OCEANS 2003. Proceedings. Vol. 2. IEEE, pp. 981–985 September.

Syvitski, J.P., 2003b. Supply and flux of sediment along hydrological pathways: research for the 21st century. Glob. Planet. Chang. 39 (1), 1–11.

Syvitski, J.P., Kettner, A.J., Overeem, I., Hutton, E.W., Hannon, M.T., Brakenridge, G.R., Day, J., Vörösmarty, C., Saito, Y., Giosan, L. and Nicholls, R.J. (2009). Sinking deltas due to human activities. Nature Geoscience, 2(10), pp.681-686

Syvitski, J.P., Vörösmarty, C.J., Kettner, A.J. and Green, P., 2005. Impact of humans on the flux of terrestrial sediment to the global coastal ocean. science, 308(5720), pp.376-380.

Syvitski, J.P., and Milliman, J.D. (2007). Geology, geography, and humans battle for dominance over the delivery of fluvial sediment to the coastal ocean. J. Geol.115 (1), pp.1–19.

Syvitski, J.P., Cohen, S., Kettner, A.J., Brakenridge, G.R., 2014. How important and dif- ferent are tropical rivers?—an overview. Geomorphology 227, 5–17.

Syvitski, J., Cohen, S., Miara, A., Best, J., 2019. River temperature and the thermal-dy- namic transport of sediment. Glob. Planet. Chang. 178, 168–183.

Taylor, P.G., Wieder, W.R., Weintraub, S., Cohen, S., Cleveland, C.C., Townsend, A.R., 2015. Organic forms dominate hydrologic nitrogen export from a lowland tropical watershed. Ecology 96 (5), 1229–1241.

Tessler, Z. D., Vörösmarty, C. J., Grossberg, M., Gladkova, I., Aizenman, H., Syvitski, J. P., and Foufoula-Georgiou, E. (2015). Profiling risk and sustainability in coastal deltas of the world. Science, 349(6248), pp.638-643.

Tran, H., Tran, T., Kervyn, M., 2015. Dynamics of land cover/land use changes in the Me-kong Delta, 1973–2011: a remote sensing analysis of the Tran Van Thoi District, CaMau Province, Vietnam. Remote Sens. 7:2899–2925.https://doi.org/10.3390/rs70302899

Wang, H., Saito, Y., Zhang, Y., Bi, N., Sun, X., Yang, Z., 2011. Recent changes of sediment flux to the western Pacific Ocean from major rivers in East and Southeast Asia. Earth Sci. Rev. 108 (1–2), 80–100.

Yang, S.L., Xu, K.H., Milliman, J.D., Yang, H.F., Wu, C.S., 2015. Decline of Yangtze River water and sediment discharge: Impact from natural and anthropogenic changes. Sci. Rep. 5, 12581.

CHAPTER 6

OVERALL CONCLUSION

River deltas are important landforms that serve many societal and ecological functions. Assessing changes to delta morphology is important to identify vulnerable areas and sustainably manage deltaic land. Satellite remote sensing and riverine sediment flux modeling provides an effective way of detecting delta morphology change over time.

In this dissertation we show that conventional remote sensing techniques outperform machine learning methods in river delta shoreline extraction. We recommend the use of Unsupervised Classification as a first order extraction technique for previously unstudied deltaic regions. We also elucidate that wave-dominated deltas show the best performance in shoreline extraction while tide-dominated deltas were most challenging for the techniques employed.

We find that in total ~57% of deltaic land is highly modified by humans. There is only ~18% of deltaic land that is in its pristine state. We find that human modifications on the delta plain accounts for ~27% of the variability of river delta plain erosion. Population, Cropland, and Night-Time Lights are identified as the key drivers on deltaic land causing erosion. The population stress is found to increase towards the coastal zones.

As a first in literature, we provide first order estimates of spatially and temporally explicit bedload and suspended bed-material proportions flowing into major river deltas worldwide. We find that deviating from the classical suspended flux dominance of total sediment fluxes, bedload fluxes dominate in certain river deltas. We also elucidate as a preliminary finding that the total

fluvial fluxes explain ~40% of the accretion of a river delta. The importance of incorporating other driving factors for increased robustness of shoreline change in analyses is highlighted.

REFERENCES

Elliott T (1986) Deltas. In: Reading HG (ed) Sedimentary environments and facies. Blackwell Scientific Publications, Oxford, pp 113–154

Al Bakri, D. (1996). A geomorphological approach to sustainable planning and management of the coastal zone of Kuwait. Geomorphology, 17(4), 323-337.

Cenci, L., Disperati, L., Persichillo, M. G., Oliveira, E. R., Alves, F. L., & Phillips, M. (2018). Integrating remote sensing and GIS techniques for monitoring and modeling shoreline evolution to support coastal risk management. GIScience & remote sensing, 55(3), 355-375.

Dunn, F.E., Darby, S.E., Nicholls, R.J., Cohen, S., Zarfl, C., Fekete, B.M., 2019. Projections of declining fluvial sediment delivery to major deltas worldwide in response to cli- mate change and anthropogenic stress. Environ. Res. Lett. 14 (8), 084034.

Ericson J.P., C.J. V r smarty, S.L. Dingman, L.G. Ward, and M. Meybeck (2006), Effective sea-level rise and deltas: causes of change and human dimension implications. Global and Planetary Change, 50:63–82

Hutchings, R. M., and S.K. Campbell (2005), The Importance of Deltaic Wetland Resources: A Perspective from the Nooksack River Delta, Washington State. Journal of Wetland Archaeology, 5(1): 17-34.

Lentz, E. E., E.R. Thieler, N.G. Plant, S.R. Stippa, R.M. Horton, and D.B. Gesch (2016), Evaluation of dynamic coastal response to sea-level rise modifies inundation likelihood Sea-level rise (SLR) poses a range of threats to natural and built environments. Nature Climate Change, 6(7): 696.

Maiti, S., Bhattacharya, A.K., 2009. Shoreline change analysis and its application to prediction: A remote sensing and statistics based approach. Marine Geology, 257(1-4), 11-23.

Masria, A., Nadaoka, K., Negm, A., Iskander, M., 2015. Detection of shoreline and land cover changes around Rosetta promontory, Egypt, based on remote sensing analysis. Land, 4(1), 216-230.

Mathers, S., Zalasiewicz, J., 1999. Holocene sedimentary architecture of the Red River delta, Vietnam. Journal of coastal research, 314-325

Munasinghe D, Cohen S, Huang YF, Tsang YP, Zhang J, Fang Z (2018) Intercomparison of satellite remote sensing-based flood inundation mapping techniques. JAWRA Journal of the American Water Resources Association 54(4):834–846.

Syvitski, J.P., Kettner, A.J., Overeem, I., Hutton, E.W., Hannon, M.T., Brakenridge, G.R., Day, J., Vörösmarty, C., Saito, Y., Giosan, L. and Nicholls, R.J. (2009). Sinking deltas due to human activities. Nature Geoscience, 2(10), pp.681-686

Syvitski, J.P., Vörösmarty, C.J., Kettner, A.J. and Green, P., 2005. Impact of humans on the flux of terrestrial sediment to the global coastal ocean. science, 308(5720), pp.376-380.

Syvitski, J. P., and Saito, Y. (2007). Morphodynamics of deltas under the influence of humans. *Global and Planetary Change*, *57*(3-4), pp.261-282.

Wang, H., Saito, Y., Zhang, Y., Bi, N., Sun, X., Yang, Z., 2011. Recent changes of sediment flux to the western Pacific Ocean from major rivers in East and Southeast Asia. Earth Sci. Rev. 108 (1–2), 80–100.

Woodroffe, C. D., R.J. Nicholls, Y. Saito, Z. Chen, and S.L. Goodbred (2006), Landscape variability and the response of Asian megadeltas to environmental change. In N. Harvey (Eds.), Global Change and Integrated Coastal Management, 10: 277-314. Dordrecht, The Netherlands: Springer.

Yang, S.L., Xu, K.H., Milliman, J.D., Yang, H.F., Wu, C.S., 2015. Decline of Yangtze River water and sediment discharge: Impact from natural and anthropogenic changes. Sci. Rep. 5, 12581.

ZhangW, Xu Y,Hoitink AJF, SassiMG, Zheng J, ChenX, Zhang C (2015) Morphological change in the Pearl River Delta, China. Mar Geol 363:202–219.

Zhao B, Guo H, Yan Y,Wang Q, Li B (2008) A simple waterline approach for tidelands using multi-temporal satellite images: a case study in the Yangtze Delta. Estuar Coast Shelf Sci 77(1): 134–142.